Functional correlates of immediate early gene expression in visual cortex and hippocampus

Inauguraldissertation

zur

Erlangung der Würde eines Doktors der Philosophie

vorgelegt der

Phliosophisch-Naturwissenschaftlichen Fakultät

der Universität Basel

von

David Mahringer

aus Linz, Österreich

Basel, 2018

Genehmigt von der Philosophisch-Naturwissenschaftlichen Fakultät
auf Antrag von:

Dr. Georg Keller (Dissertationsleiter)

Prof. Dr. Rainer W. Friedrich (Fakultätsvertreter)

Dr. Wulf Haubensak (Korreferent)

Basel, den 26.06.2018

Prof. Dr. Matin Spiess (Dekan)

Acknowledgements

I would like to thank Georg Keller for being a great mentor, I could not have asked for more support and intellectual guidance during my PhD from a supervisor. I'm grateful for the time Anders Petersen and I shared in the lab, our collaboration and endeavor of exploring new paths in the lab was an exciting experience for both our curious minds. I'm thankful for the fruitful collaborations with Pawel Zmarz, Aris Fiser and Hassana Oyibo throughout my PhD, teamwork was really the key driver that made our projects so successful. Being in the Keller lab is an experience that goes beyond science, so thanks to all past and current lab members for wonderful moments of joy during discussions, athletic challenges and fondue/BBQ evenings.

I would like to thank my PhD committee members Thomas Mrsic-Flogel and Wulf Haubensak for helpful scientific advice. The success of any project relies on input from outside, their insightful comments helped to define strategies throughout my PhD.

I would like to thank my whole family for letting me explore my ideas and always being there for me in times when needed.

To Verena, this PhD would have not been possible without our shared experiences, your constant support and presence in my mind and heart.

Contents

Prologue

Any biological, cellular system needs to integrate information from the outside environment to function within its cellular regime. This is true for single cell systems in the domains of bacteria, archaea and eukaryotes, as well as for any multicellular systems of the latter. Nature is probabilistic and so is the information that can be acquired about the environment, cellular systems faced with such challenges adopted by changing their responses after integrating over all available information. Multicellular systems are facing a double challenge: Not only do they need to integrate information, they also need to coordinate the changes across all cells. From the molecular level upwards, the process of changing can be called learning, which is a fundamental part of life. Some of these multicellular systems created a special class of cells, neurons, building up a nervous system that is specialized in dealing with this challenge. It is their task to integrate information about the external world and coordinate a multitude of other cellular regimes within the multicellular system to react appropriately to the environment. Neurons do this by transmitting electric signals across its interconnected web, thereby spreading the information throughout the system (Kandel, 2013). Interestingly, the spread of information, does not only impact non-nervous system cells, but also with time the nervous systems itself. This manifests in changes of how external signals are integrated by neurons (McCool and Britten, 2008) and goes even further by changing the expression of genes inside neurons (Curran and Morgan, 1995). Alterations of gene expression give a cell the possibility to change its molecular composition and show a plastic adoption to the environment. This process is the essence of learning and impacts not only the molecular composition of neurons, but also the response to incoming information (Okuno, 2011). Intriguingly, such a change in the response to information within the nervous system shapes the future processing of information and thus alters its quality, which we will see in a later chapter of this thesis.

Feature detection versus predictive coding

Information processing in the nervous system has classically been viewed as the detection of features of the external world. This idea originates from studies of Charles Scott Sherrington, who coined the term “receptive field”, by mapping body parts from which a scratching reflex of a dog could be elicited (Sherrington, 1906). Haldan Keffer Hartline made used of this term later in 1938 for the visual system to

describe responses in the frog retina (Hartline, 1938). Further studies by Horace Barlow in the 50's lead to the conclusion that neurons in the brain code for specific features of the outside world (Barlow, 1953). David Hubel and Torsten Wiesel then went on to show that neuronal signals in the cat's visual cortex can be explained by hierarchical processing of such features (Hubel and Wiesel, 1962).

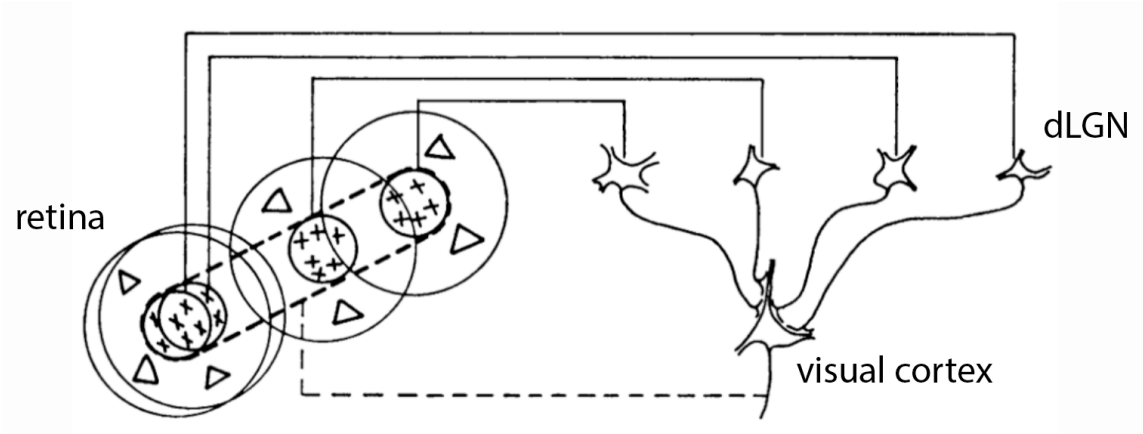

Figure 1: A hierarchical processing stream for feature detection in the visual system of our brain. Features of the environment are detected within the receptive fields of neurons in the retina, which send their information to individual neurons in the dorsal lateral nucleus of the thalamus (dLGN), from where these neurons project onto a single neuron in primary visual cortex. Since the information of neurons with overlapping receptive fields, aligned in one direction converge onto one single neurons, it response to a stimulus in the shape of a bar. Modified from: (Hubel and Wiesel, 1962)

This brief history of visual neuroscience is not a complete list of all the contributions to this field of neuroscience, many more labs have shown in elegant work, how sensory brain areas decode information about the environment based on such a hierarchical processing stream. However, this model does not account for one visual experience we are all familiar with: visual illusions. How is it possible that we see something, although the necessary features are not present? A famous example for such an illusion is the Kanizsa triangle (Kanizsa, 1976).

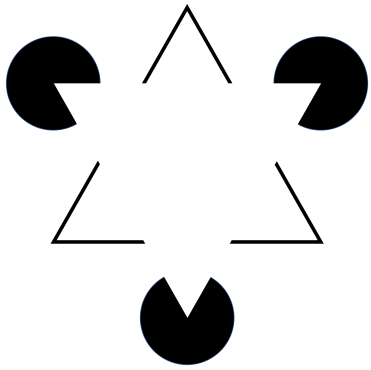

Figure 2: Kanizsa triangle.

Note the perception of a white triangle in the foreground, although lines like for the triangle in the background are not present. Image can be found on: https://en.wikipedia.org/wiki/Illusory_contours (CC BY-SA 3.0 license).

This striking perception of something featureless illustrates the point that sensory brain areas likely code for more than pure features of the outside world. What else do our sensory system code for? In recent years scientist have look for answers to this puzzling questions and realized that the old, but historically rather unappreciated hypothesis of predictive coding might be a good candidate to put to the test. Predictive coding states that our sensory experience are influenced by our experience, hence our expectation of the immediate future. The theory of predictive coding originates from ideas and studies of Hermann von Helmholtz, who postulated that our sensory perception is influenced by an internal representation of the world (Von Helmholtz, 1867). When looking at patients that suffered from a paralysis of the lateral rectus muscle of the right eye, he noticed that when patients were asked to look to the right, they perceived objects moving to the right, although the eye was stationary and the image on the retina did not change (Von Helmholtz, 1867). He explained this perception by assuming that our brain makes unconscious inferences and therefore constructs reality. Erich von Holst and Horst Mittelstaedt were among the first ones to provide indirect evidence for such unconscious inferences. They rotated the head of a fly by 180 degrees and coupled it's lateral movement to visual flow either to the right or left on a surrounding cylinder with a stripped pattern (von Holst and Mittelstaedt, 1950). Stationary flies react to visual flow of such a cylinder by moving to the same direction, thereby stabilizing their visual field. However under conditions of self-generated visual flow, whenever the movement of the fly itself would lead to a shift of the pattern on the cylinder, the fly would stabilize its visual field, by initiating a movement into the opposite direction. What happens during self-generated visual flow in the case of a fly with its head turned 180 degrees? Interestingly, flies fail to stabilize their visual field, as they

move in the same direction as the visual flow. Under normal condition movements to the right, cause images on the retina to move to the left, leading to a corrective movement of the fly to the left. With eyes rotated by 180 degrees, flies experience movement of images on their retina into the opposite direction. When now turning right, flies experience visual flow as if the turned left and initiate a movement to the right, causing more destabilizing visual flow. Such behavior can be easiest explained by the assumption that the fly's brain knows about the visual flow generated by its movement and therefore the authors concluded that flies predict the direction of visual flow by internally processing their movement commands. Such internal movement commands were afterwards named efference copy. It has become clear over last decades that efference copies exist and a multitude of organisms use it to process information (Bell, 1982; Eliades and Wang, 2008; Keller et al., 2012; Keller and Hahnloser, 2009; Kim et al., 2017, 2015; Poulet and Hedwig, 2006; Saleem et al., 2013). Scientist gained deeper insight into the processing of efference copies from studies in visual cortex of mice. It has been shown that motor command–related brain areas project to visual cortex, sending information about visual flow predictions (Leinweber et al., 2017). Such predictions are used to form a comparison of predicted visual flow and actual visual input (Attinger et al., 2017), which signals a deviation of expectations from reality.

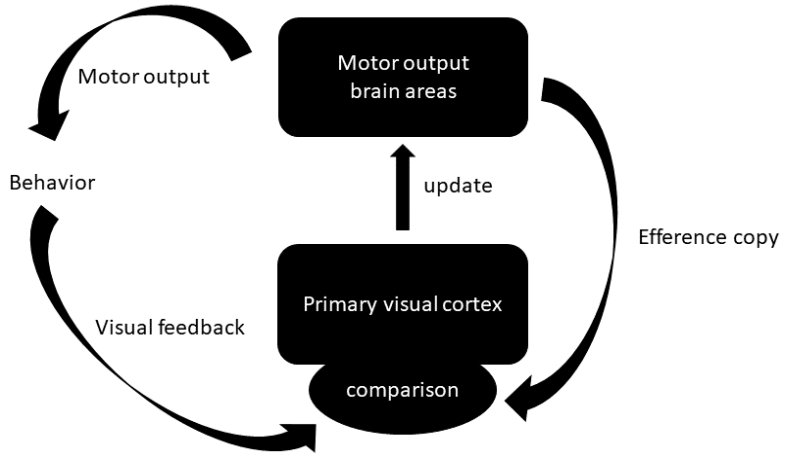

Figure 3: A simplified schematic for predictive coding in the visual system

Movement of an animal generates visual flow, which is sensed by its visual organs and sent to visual cortex. At the same time a copy of the motor command that initiated the movement is sent in addition to visual cortex for a comparison of predicted visual flow (efference copy) and actual sensory input. It has been speculated that such a comparison could be used to update future motor output.

Animals, including humans, are not born with prior knowledge about the stochastic quality of nature. Brains acquire knowledge with time and experiences shape their processing. It takes time until kids are able to walk and deal with immediate consequences of their movements. For this reason it wasn't surprising to see that mismatch signals, computed by the above mentioned comparison, undergo a development and are subject to learning (Attinger et al., 2017). If brains are required to undergo a plastic change with experience in order to facilitate predictive coding, what are the molecular players that enable learning? Which genes might influence processing of information in visual cortex within a predictive coding framework?

Neuronal activity and gene expression

Many genes that play a role in learning and neuronal plasticity have been discovered more than 20 years ago and where named immediate early genes (IEGs) (Okuno, 2011). This name was initially borrowed from the field of cellular growth regulation as eloquently explained by Tom Curran and James Morgan:

> *"The concept of the cellular immediate-early response arose from observations made in the field of growth regulation. It was noted that growing cells could be rendered quiescent by deprivation of growth factors. Entry into the cell cycle could be triggered by resupplying a cocktail of growth factors that conveyed cells through a series of defined steps culminating in mitosis. A critical early phase, termed "competence," was defined in which cells treated with platelet-derived growth factor (PDGF) were competent to proceed through the cycle if they were supplied with additional factors* (Stiles et al., 1979). *The use of protein synthesis inhibitors, such as cycloheximide, revealed that, during acquisition of competence, there was a critical early period in which PDGF was required to stimulate expression of a set of genes, termed "competence genes" for progression through the cell cycle to occur* (Cochran et al., 1983). *Thus, this set of genes, later named immediate-early genes (see later), were induced rapidly by extracellular stimuli, even in the presence of protein synthesis inhibitors, and encoded proteins that were required, in combination with other signals, for the cellular growth response. This is the general concept that was borrowed from the field of growth regulation and applied to the study of signal transduction in neurons."* (Curran and Morgan, 1995)

Until know immediate early genes have been characterized and categorized based on their molecular function. Descriptive categories range from transcription factors, postsynaptic proteins, intracellular signaling molecules, secretory factor to membrane proteins (Okuno, 2011). The immediate early gene c-Fos was among the first ones to be discovered (Curran and Teich, 1982). After experiments showed that

its expression could be induced by external stimulation of neurons (Greenberg and Ziff, 1984), IEGs have classically been linked to neuronal activity (Bullitt, 1990; Garner et al., 2012; Knapska and Kaczmarek, 2004; Liu et al., 2012; Minatohara et al., 2015; Ramirez et al., 2013). Two more well studied examples of IEGs are Arc/Arg3.1 (Link et al., 1995; Lyford et al., 1995) (which is referred to as Arc throughout the text) and EGR1 or Zif268/NGFI-A/Krox-24/TIS8/ZENK (Lau and Nathans, 1987; Milbrandt, 1987) (which is referred to as EGR1 throughout the text, see (Knapska and Kaczmarek, 2004) for disambiguation). Many studies have provided evidence that c-Fos, Arc and EGR1 are important for learning and plastic changes at the synapse associated with learning, such as long term potentiation and long term depression (Bramham et al., 2010; Curran and Morgan, 1995; Veyrac et al., 2014).

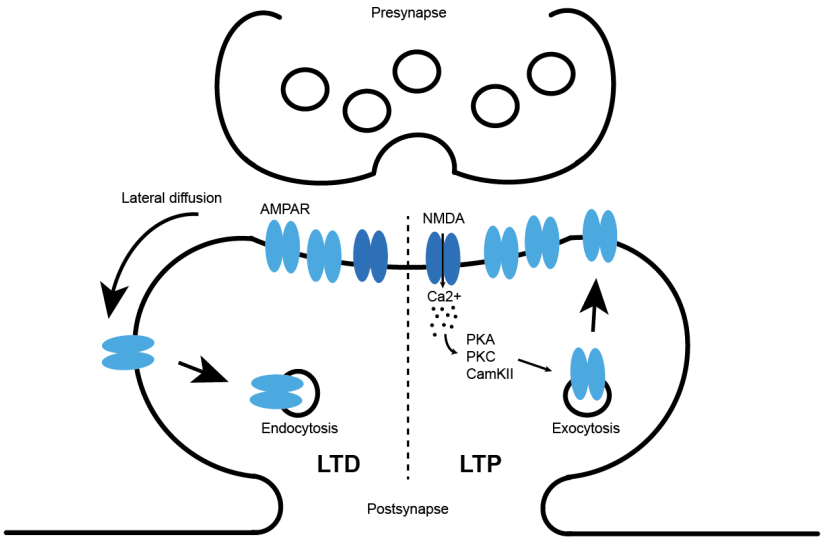

Figure 4: Immediate early genes impact neuronal plasticity at the synapse.

Both long term potentiation (LTP) and long term depression (LTD) are part of plastic changes at neuronal synapses that alter the response to incoming signals. Immediate early genes can be induced by incoming signals and play a critical role in regulating LTP and LTD. Modified from: (Vitureira and Goda, 2013)

In visual cortex the expression of c-Fos, Arc and EGR1 can be induced by over-night dark adaption followed by visual stimulation (Gao et al., 2010; Zangenehpour and Chaudhuri, 2002), however the expression of EGR1 is less effected by dark rearing (Yamada et al., 1999) and can even be increased by prolonged dark rearing (Mower and Kaplan, 2002) in visual cortex. Evidence that Arc is crucial for plasticity induced by feed-forward visual input is provided by several studies (Gao et al., 2010; Jenks et al., 2017; McCurry et al., 2010; Wang et al., 2006), however such implications are less clear for EGR1 (Mataga et al., 2001). From

the perspective of predictive coding visual cortex needs two types of functional input, motor-related and visual input, to form a comparison between predicted visual flow and actual sensory input (Attinger et al., 2017; Keller et al., 2012; Saleem et al., 2013). Given that such a comparison is learned and likely requires genes that impact learning, like immediate early genes, it's an easy step to speculate, together with the differential expression of Arc and EGR1 upon the lack of visual input, about a role of these immediate early genes during plastic changes that help to specify functional input to neurons within a predictive coding framework.

Aim of this thesis

As outlined on the previous pages this thesis builds upon the hypothesis that our brains not only detect features of the outside world, but also acquire knowledge about the world with experience and use this information to predict the consequences of movement. As such expectations are learned and require plastic changes of how signals are processed in visual cortex, immediate early genes are potential candidates that might mediate such changes within neurons. As a consequence such changes might influence sensory processing of outside stimuli itself.

Chapter 1 of this thesis aims to gain insight into the role of immediate early genes during visuomotor-learning in visual cortex and provides evidence that some IEGs are correlated with the functional type of input a neuron receives.

Chapter 2 of this thesis tries to gather more evidence that the expression of immediate early genes is correlated with plastic changes for specific functional input in another brain area, namely the hippocampal area CA1.

Chapter 3 of this thesis looks at how learning about external stimuli of the environment changes the quality of signals about these outside stimuli within visual cortex and thus impact sensory processing over time.

Chapter 1: Functional correlates of immediate early gene expression in mouse visual cortex

This chapter is based on a non-published manuscript, a revised version will be submitted to a peer-reviewed journal in the future. The text and figures of this chapter correspond largely to the manuscript, with minor adaptions to formatting and numbering to conform to the style of this thesis.

David Mahringer[1, 2], Pawel Zmarz[1, 2], Hiroyuki Okuno[4], Haruhiko Bito[5] & Georg B. Keller[1, 2 ,6]

[1] *Friedrich Miescher Institute for Biomedical Research, Basel, Switzerland*
[2] *Faculty of Natural Sciences, University of Basel, Basel, Switzerland*
[4] *Medical Innovation Center, Kyoto University Graduate School of Medicine, Kyoto, Japan*
[5] *Department of Neurochemistry, University of Tokyo Graduate School of Medicine, Tokyo, Japan*
[6] *Correspondence to: georg.keller@fmi.ch*

The expression of immediate-early genes (IEGs) in visual cortex is necessary for certain forms of neuronal plasticity and plays a critical role in visual development. How IEG expression correlates with neural activity and how it changes with visuomotor learning is still unclear. Using transgenic mice expressing GFP under control of different IEG promoters, we chronically recorded both neural activity using a red calcium indicator and IEG expression levels in primary visual cortex (V1) during visuomotor learning. We quantify correlations between neural activity and expression of three different IEGs c-Fos, EGR1 and Arc and find that expression of all three IEGs correlates positively with neural activity. However, we find that the different IEGs are regulated differentially during visuomotor learning, and that IEG expression profile correlates with functional response type of the neuron. Neurons that exhibit strong motor-related activity express higher levels of EGR1, while neurons that exhibit visually driven activity express higher levels of Arc. These findings suggest that different IEG expression levels might correlate with plastic changes in the functional type of input a neuron in V1 layer 2/3 receives.

Introduction

A specific subset of genes, whose expression can be induced by stimulation in neurons, referred to as immediate early genes (IEGs), are often used as a marker for neuronal activity *in vivo* (Okuno, 2011). Among the most widely used IEGs are c-Fos (Curran and Teich, 1982), EGR1 or Zif268/NGFI-A/Krox-24/TIS8/ZENK (Lau and Nathans, 1987; Milbrandt, 1987) (which we will refer to as EGR1 throughout the

text, see (Knapska and Kaczmarek, 2004) for disambiguation) and Arc/Arg3.1 (Link et al., 1995; Lyford et al., 1995) (which we will refer to as Arc throughout the text). Since the discovery that c-Fos expression can be induced by external stimulation in neurons (Greenberg and Ziff, 1984), these IEGs have been linked to neuronal activity (Bullitt, 1990; Garner et al., 2012; Knapska and Kaczmarek, 2004; Liu et al., 2012; Minatohara et al., 2015; Ramirez et al., 2013). In addition it was shown that they play a critical role in synaptic and neuronal plasticity during learning (Alberini, 2009; Duclot and Kabbaj, 2017; Gandolfi et al., 2017; Shepherd and Bear, 2011; Veyrac et al., 2014). However, it is less clear how these IEGs contribute to neuronal plasticity during visuomotor-learning. This form of learning requires two types of inputs, feed-forward visual and top-down motor-related input. This allows for functional classification of neurons, based on their response type during visuomotor-learning (Attinger et al., 2017). Evidence that Arc is important for plasticity induced by feed-forward visual input in visual cortex comes from several studies (Gao et al., 2010; Jenks et al., 2017; McCurry et al., 2010; Wang et al., 2006), still such implications are unclear for EGR1 (Mataga et al., 2001). For that reason, we speculated that Arc and EGR1 might correlate with different functional input during visuomotor-learning in visual cortex. This leads to a couple of testable hypothesis. As Arc is linked to plasticity for visual input and has been described as an inverse synaptic tag, that downregulates excitatory synapse number (Flavell et al., 2006; Okuno et al., 2012), its expression should correlate with functional types of neurons that are not driven by motor-related input and prefer visual input. In contrast and with respect to the finding that EGR1 does not affect plasticity for visual input, its expression should correlate with neurons that are driven by motor-related input. Consequently such differential preferred functional type of input should bias EGR1 neurons towards mismatch responses, that signal a deviation of expected visual flow from actual visual input (Attinger et al., 2017; Keller et al., 2012). To estimate IEG expression levels *in vivo*, we used three different mouse lines that express a GFP under an IEG promotor either as a fusion protein with the IEG in the case of c-Fos (Barth et al., 2004) and Arc (Okuno et al., 2012), or as simply as a reporter in the case of EGR1 (Xie et al., 2014).

Results

We first set out to quantify the correlation between neural activity and IEG expression levels in visual cortex in adult mice in response to a change in visual input. To do this, we used three groups of mice (4 Arc-GFP mice, 4 c-Fos-GFP mice, and 4 EGR1-GFP mice) and injected an AAV2/1-Ef1a-jRGECO1a viral vector into primary visual cortex to express the red calcium indicator jRGECO1a (Dana et al., 2016) in layer 2/3 excitatory neurons. Using an AAV2/1 with an Ef1a promoter will result in expression mainly in excitatory neurons (Attinger et al., 2017). 12 - 41 days after the virus injection, we dark-adapted mice for 24 hours and subsequently head-fixed them under a two-photon microscope on a spherical treadmill still in darkness. We then exposed them to visual input for 15 minutes after which the mice were returned to complete darkness again for the remainder of the experiment. We measured neural activity and IEG levels every 15 minutes starting immediately preceding the re-exposure to visual input until 6 hours after re-exposure visual input (**Fig. 1.1a**). We alternated between imaging neural activity for 4 minutes and measuring IEG expression levels in intervals of 15 minutes (see Experimental Procedures). This allowed us to measure both IEG expression levels and neural activity in the same neurons in layer 2/3 of visual cortex (**Fig. 1.1b, e, h**). We then computed the correlation between mean neural activity and IEG expression levels as a function of time between neural activity measurement and IEG expression measurement (**Fig. 1.1c, f, i**). Correlation peaked at a time lag of approximately +3 hours (3h 30min ± 30min, mean ± s.e.m) between neural activity measurement and IEG measurement for Arc and c-Fos and plateaued in a window from -2 hours to +3 hours almost flat for EGR1. To quantify peak correlation between neural activity and IEG expression we plotted IEG expression level measured at +3.5 hours against neural activity measured at time 0 for all neurons recorded (Arc: 1383 neurons, c-Fos: 1070 neurons, EGR1: 1319 neurons; **Fig. 1d, g, j**). Although correlations between IEG expression and neural activity were positive, IEG expression was a surprisingly poor predictor of mean neural activity. Correlation between neural activity and IEG expression was highest for c-Fos (corr. coeff. = 0.3904 ± 0.0658 (mean ± s.e.m), c-Fos vs. Arc: $p = 2.6897 \times 10^{-4}$, c-Fos vs.EGR1: $p = 5.8406 \times 10^{-9}$, Student's t-test), intermediate for Arc (corr. coeff. = 0.2621 ± 0.0547 (mean ± s.e.m.), Arc vs. EGR1: p = 0.0188, Student's t-test) and lowest for EGR1 (corr. coeff. = 0.2069 ± 0.0320 (mean ± s.e.m) (**Fig. 1c, f, i**).

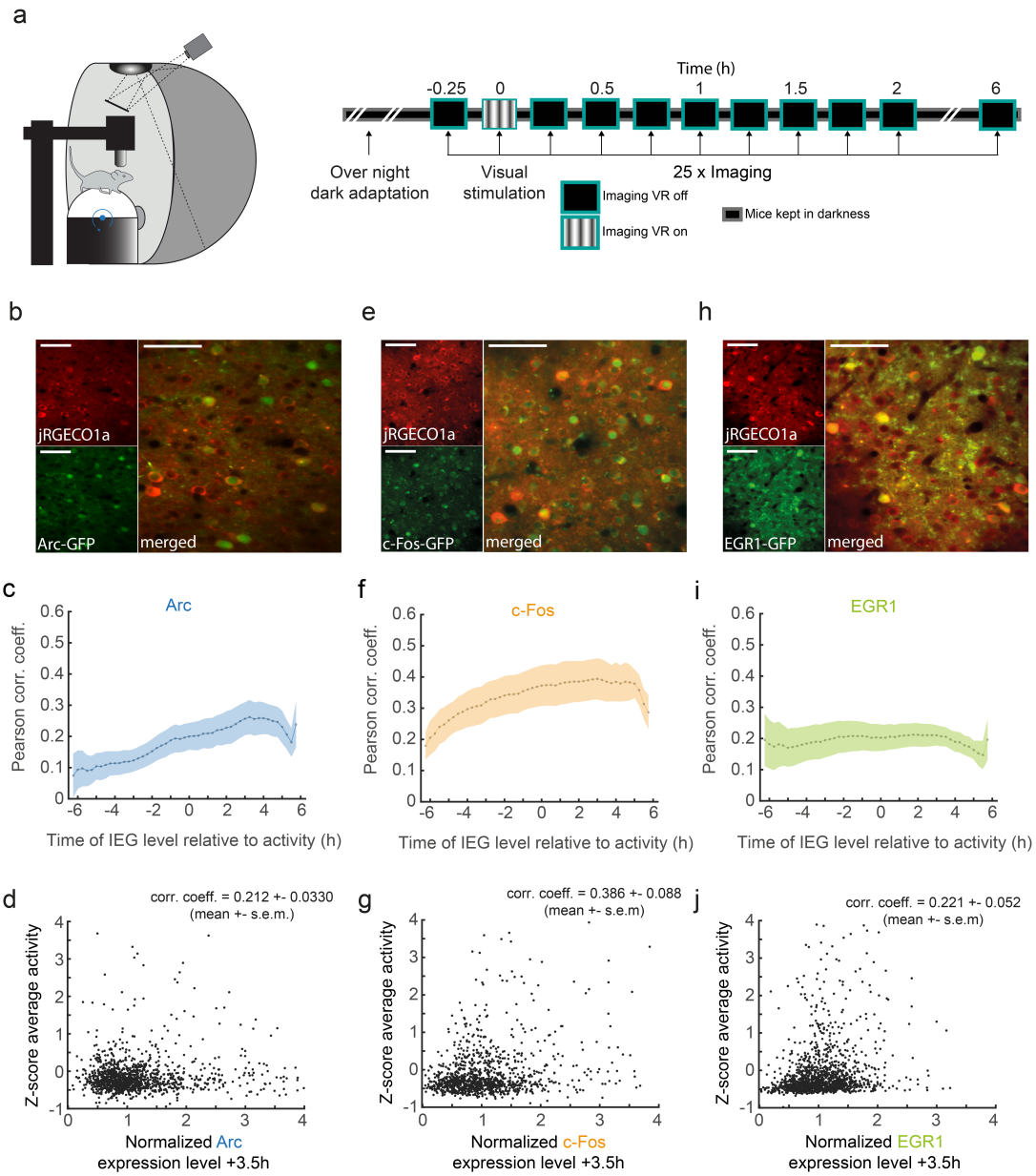

Figure 1.1: Simultaneous imaging of activity and immediate early gene expression in visual cortex.

(**a**), Left: Schematic of the virtual reality setup used for imaging experiments. Right: Schematic of the experimental time line. jRGECO1a was injected 12 - 29 days prior to experiments. Mice were dark adapted for 24 hours. Neural activity and IEG expression levels were recorded immediately before and after visual exposure in intervals of 15 minutes.

(**b**), Example images of jRGECO1a (red, top), Arc (green, bottom left) expression and the combined image (bottom right).

(**c**), Correlation of average activity and IEG expression level across the entire experiment, relative to the activity measurements. Blue line indicates average correlation, blue shadings indicates standard error of the mean (s.e.m) (n = 4).

(**d**), Scatter plot for Arc expression and average neuronal activity for each cell (n = 1382, 72 data-points not shown) 3.5 hours after stimulation.

(**e**), Same as in (B), but for c-Fos

(**f - g**), Same as in (C - D), but for c-Fos (n = 1070, 23 data-points not shown, n = 4).

(**h**), Same as in (B), but for EGR1

(**i - j**), Same as in (C - D), but for EGR1 (n = 1319, 17 data-points not shown, n = 4).

Differential expression of IEGs during sensorimotor learning

Neural activity in mouse visual cortex is driven both by visual input and motor related signals (Keller et al., 2012; Saleem et al., 2013), in such a way that individual excitatory neurons in layer 2/3 of visual cortex are differentially driven by these two types of inputs (Attinger et al., 2017). It is possible that the expression of a particular IEG is not equally driven by all neural activity, but that it depends on the source of the drive. Indeed, consistent with our results, c-Fos and Arc expression can be increased in mouse visual cortex by dark adapting the animal and exposing it to visual input (Gao et al., 2010; Zangenehpour and Chaudhuri, 2002), whereas EGR1 expression is less affected by dark rearing (Yamada et al., 1999) and can even be increased by prolonged exposure to darkness (Mower and Kaplan, 2002). To address the questions of whether expression of the IEG correlates with the functional response of individual neurons, we quantified IEG expression levels and neural activity during a mouse's first exposure to visual input in life and subsequent visuomotor learning. We dark reared three groups of mice from birth in complete darkness until P42 (7 Arc-GFP mice, 5 c-Fos-GFP mice, and 4 EGR1-GFP mice). At P28 - 30 mice received a cranial window implantation and an injection of AAV2/1-Ef1a-jRGECO1a viral vector into primary visual cortex to express the red calcium indicator jRGECO1a (Dana et al., 2016). Starting at P40, we imaged neuronal activity and IEG expression levels every 12h for a total of 6 days, while mice were head-fixed and free to run on a spherical treadmill surrounded by a toroidal screen. For the first four imaging sessions, mice were kept on the setup in complete darkness (condition 1). At the beginning of the 5th imaging session mice were exposed to light for the first time in their life, and for imaging sessions 5 to 8 mice were exposed to different visumotor conditions and visual stimuli, but remained in complete darkness in the time between the imaging sessions (condition 2). Following imaging session 8, mice were housed in a normal 12h light / 12 h dark cycle and the imaging paradigm remained unchanged for imaging session 9 through 12 (condition 3). In condition 1 imaging experiments consisted of 8 minute recordings of neural activity as mice were free to run on the spherical treadmill with an IEG expression level measurement before and after the activity recording session. In conditions 2 and 3, neural activity measurements consisted of 7 segments of 8 minutes each. We started with a dark segment, followed by a closed-loop segment. In the closed loop segment, the movement of the mouse in a linear virtual corridor was coupled to the locomotion of the mouse on the spherical treadmill, including short perturbations of the coupling between locomotion and visual flow we refer to as mismatch events (Attinger et al., 2017). The following two segments were open-loop and consisted of a playback of the visual flow the animal generated in the closed-loop session. Animals were free to run during these open-loop segments. Subsequently, mice were

exposed to a second dark segment, followed by a visual stimulation segment. During the visual stimulation segment mice experienced one of 8 drifting full field gratings of different orientations presented in random order (stationary 2s, drifting 3 s,). Finally, mice were exposed to a third dark session. Before and after every neural activity imaging segment we measured IEG expression levels (**Fig. 1.2a**). Experimental sessions lasted on average a total of 83 min ± 1min (mean ± s.e.m) (**Supplementary Fig. S1.1**).

We first quantified average expression of Arc, c-Fos and EGR1 over the course of all three conditions (**Fig. 1.2b**). Surprisingly, we found that the expression of all three IEGs was stable during the first 2 conditions but increased for Arc and decreased for EGR1 in condition 3 (change in normalized expression level from condition 2 to 3, Arc: 2.0775 ± 0.7784 (mean ± s.e.m.) - p = 0.0371, EGR1: -0.5758 ± 0.1669 (mean ± s.e.m.) – p = 0.0409, Student's t-test). Average c-Fos expression did not change systematically over the course of all three conditions (change in normalized expression level from condition 2 to 3, c-Fos: 0.0054 ± 0.1343 – p= 0.9698, Student's t test). To quantify the stability of the expression pattern of the IEG across neurons we correlated the IEG expression for all neurons across the 12 different imaging sessions (**Fig. 1.2c - e**). Arc expression pattern changed upon first exposure to visual input and exposure to a 12/12h light/dark cycle (**Fig. 1.2c**). In addition, we observed an increase in correlation for the change in Arc expression in condition 2, when mice were exposed to light on the setup, but still housed in complete darkness outside of imaging times. (**Fig. 1.2f**). c-Fos expression pattern stayed stable across the duration of the experiment (**Fig. 1.2d**), the change in c-Fos expression was only correlated at low levels across days (**Fig. 1.2g**). EGR1 expression pattern was stable during condition 1 and 2, but changed with the onset of condition 3 (**Fig. 1.2e**). Similar to c-Fos, the change in EGR1 expression was only weakly correlated across days (**Fig. 1.2h**). Seeing these differential changes in expression pattern for Arc, c-Fos and EGR1 during visuomotor-learning, we wanted to investigate if neuronal activity patterns undergo a change during visuomotor-learning as well.

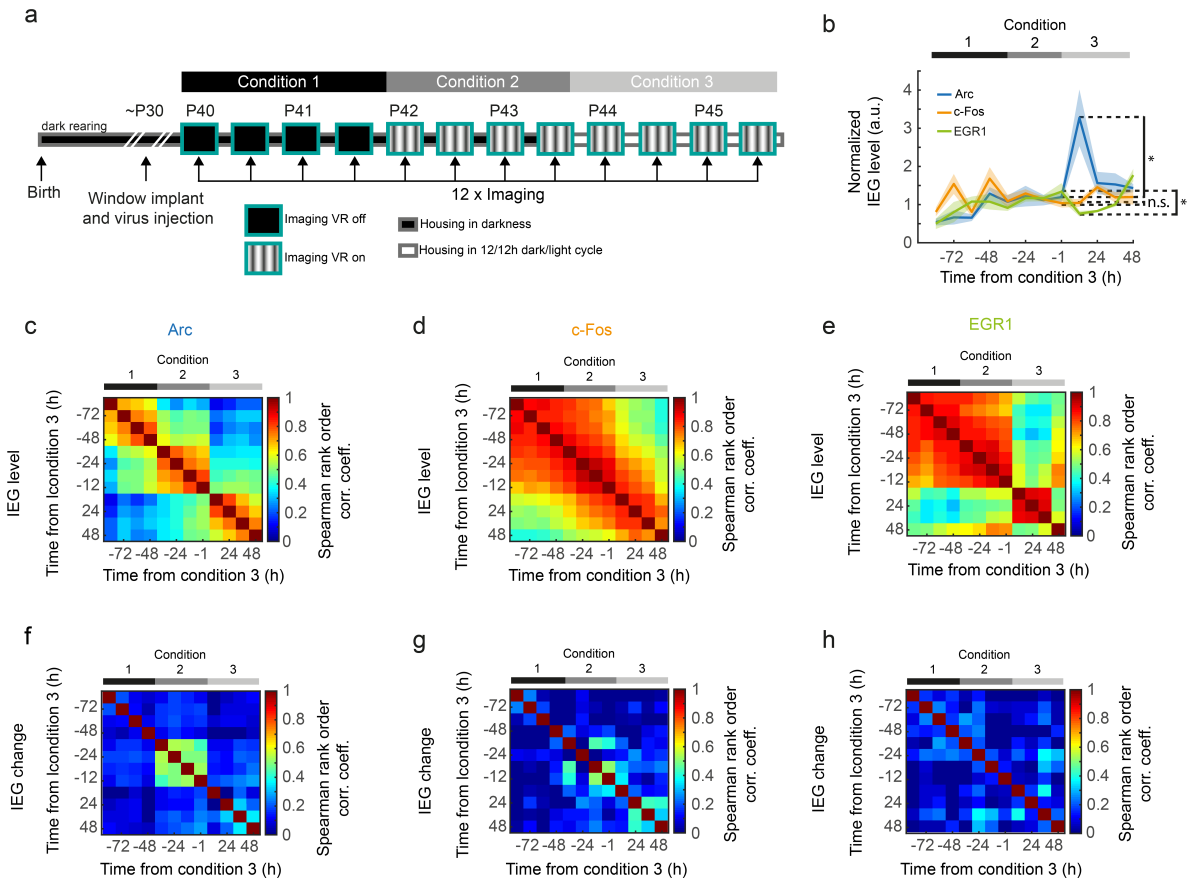

Figure 1.2: IEG expression dynamics during visuomotor learning.

(**a**), Left: Imaging setup of the virtual reality setup used for imaging experiments. Right: Schematic of the experimental time line. jRGECO1a was injected 10 – 12 days prior to the experiments. Mice were born and reared in complete darkness and we imaged calcium activity and IEG expression levels every 12h over the course of 6 days both before and after first visual exposure. On the first two days (condition 1) activity in V1 was recorded in complete darkness while mice were head-fixed and free to run on a spherical treadmill. On the third day of imaging we exposed them to visual feedback (first light exposure) in a virtual reality tunnel in which visual flow was coupled to the locomotion of the mouse. Outside of the imaging sessions mice were still housed in complete darkness (condition 2). Starting on day 5 mice were then subjected to a 12/12h light/dark cycle (condition 3).

(**b**), Expression level of Arc (blue, n = 1969 or 7 mice), c-Fos (orange, n = 1885 or 5 mice) and EGR1 (black, n = 1213 or 4 mice) during visuomotor-learning. Lines indicate average expression levels, shading s.e.m (change in normalized expression level from condition 2 to 3, Arc: 2.0775 ± 0.7784 (mean ± s.e.m.) - p = 0.0371, EGR1: -0.5758 ± 0.1669 (mean ± s.e.m.) – p = 0.0409, c-Fos: 0.0054 ± 0.1343 – p= 0.9698, Student's t test)

(**c**), Correlation pattern for Arc expression level during visuomotor-learning (condition 1 - 3).

(**d**), Correlation pattern for Arc expression change during visuomotor-learning (condition 1 - 3).

(**e - f**), Same as in (C) and (D), but for c-Fos.

(**g - h**), Same as in (C) and (D), but for EGR1.

Motor-related activity pattern changes upon visual exposure

Neuronal activity in visual cortex is known to be present before first exposure to visual input (Shen and Colonnese, 2016) and increases upon the onset of running behavior before first light exposure (**Supplementary Fig. S1.2**). It is likely that this input is used during visuomotor-learning and thus undergoes a learning related change at the time when running-related and visual signals can first be integrated together. Consistent with this assumption, we observed a gradual change in the activity pattern for motor-related input to V1 upon visuomotor-learning. In addition, we observed a decrease in the similarity of average activity patterns within each imaging session from condition 1 to 2 and 3 (**Fig. 1.3a, b**). In line with this, we find that the similarity in average activity patterns within a ± 12h window is higher in condition 1 and 2 compared to condition 3, suggestion a higher dynamic of motor-related input with visuomotor-learning (**Fig. 1.3c**). Neuronal activity pattern during closed-loop, open-loop and moving grating sessions did not change dramatically after the onset of visuomotor-learning (**Fig. 1.3d - f**). Still the overall similarity for activity pattern during visuomotor-learning was lowest for motor-related input compared to all other segments (**Fig. 1.3g**). We were intrigued to see both changes in expression pattern of IEGs and neuronal activity pattern during visuomotor-learning and wondered if the expression of an IEG can be related to the functional type of input a neuron receives in visual cortex during visuomotor-learning.

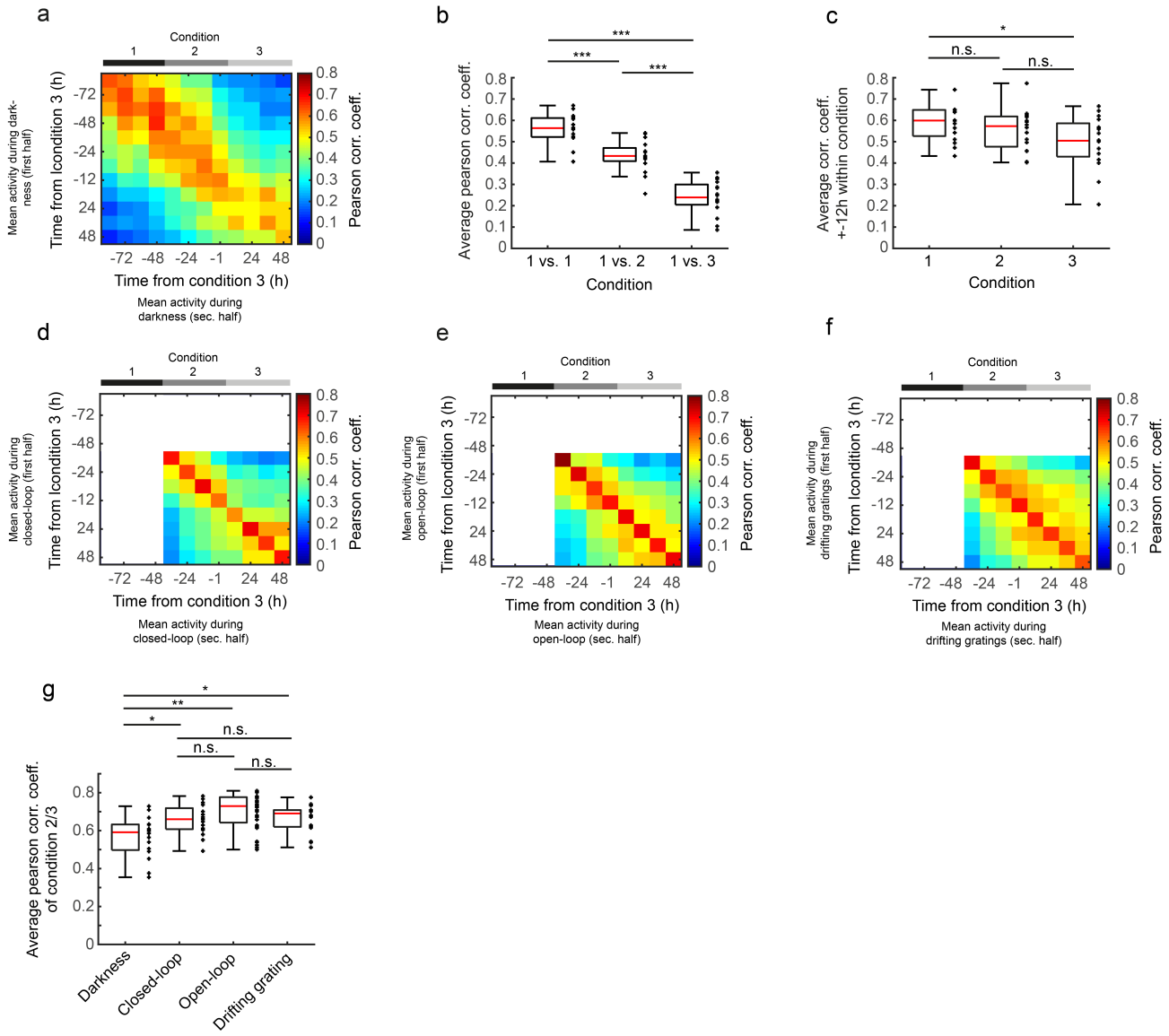

Figure 1.3: Motor-related and visual activity dynamics during visuomotor-learning

(**a**), Correlation pattern for average activity of either first or second of half during darkness across all experimental conditions (n = 5067 or 16 mice).

(**b**), Correlation of average activity in darkness in condition 1 with all other conditions. Crosses indicate individual mice (n = 16, Wilcoxon ranksum test, all significance values below 0.001).

(**c**), Correlation of average activity in darkness with average activity in darkness ± 12 hours during condition 1, 2 and 3. Crosses indicate individual mice (n = 16, Wilcoxon ranksum test, condition 1 vs. 2: p = 0.1935, condition 1 vs. 3: p = 0.0302, condition 2 vs. 3: p = 0.2503).

(**d**), Correlation pattern for average activity during closed-loop across all experimental conditions (n = 5067 or 16 mice).

(**e**), Correlation pattern for average activity during open-loop across all experimental conditions (n = 5067 or 16 mice).

(**f**), Correlation pattern for average activity during drifting gratings across all experimental conditions (n = 5067 or 16 mice).

(**g**), Average correlation coefficients for darkness, open-loop, closed-loop and drifting gratings segments in condition 2 and 3. Crosses indicate individual mice (n = 16, Wilcoxon ranksum test, darkness vs. closed-loop: p = 0.0151, darkness vs. open-loop: p = 0.00097, darkness vs. drifting gratings: p = 0.0122, closed-loop vs. open-loop: p = 0.0935, closed-loop vs. drifting gratings: p = 0.787, open-loop vs. drifting gratings: p = 1).

Functional cell type specific expression of immediate early genes

As neurons in visual cortex both receive motor-related input and visual input (Keller et al., 2012; Saleem et al., 2013) and these inputs can be used to generate different functional types of responses (Attinger et al., 2017), we set out to characterize neurons based on these responses and their immediate early gene expression. We selected the 10 percent of the top most expression Arc, c-Fos and EGR1 cells at the beginning of condition 3, as we both observed strong changes in average expression and expression pattern at this point in time during visuomotor-learning. When quantifying motor-related and visual responses in condition 3 for these neurons and plotted against each other, we found striking differences in their scattering pattern. Neurons with high Arc expression showed higher than population average responses to visual input, whereas their response to motor-related input is lower (**Fig. 1.4a**). Neurons with high c-Fos expression did not show significantly different responses compared to population average (**Fig. 1.4b).** In contrast, neurons with high EGR1 expression showed higher responses to motor-related input and similar population average responses to visual input (**Fig. 1.4c**). In line with the conclusion that such functional responses develop during visuomotor-learning (Attinger et al., 2017), we see a development for this specificity to functional input both for motor-related input (**Fig. 1.4d**) and visual input (**Fig. 1.4e**). To validate our findings we computed the correlation of both activity during darkness with running and activity during open-loop segments with visual flow. Similar to the scattering pattern observed in **Fig. 4a - c** we observe that neurons with high Arc expression cluster in the lower right quadrant, meaning they preferentially receive excitatory visual input and inhibitory motor-related input, whereas neurons with high EGR1 expression cluster along the positive y-axis, meaning they preferentially receive excitatory motor-related input (**Fig. 1.4f**). This preferential input characterized by correlation of activity with running or visual flow develops throughout visuomotor-learning, as visualized by the centroids of the scatters for high IEG cells (**Fig. 1.4g**). In condition 3 these preferential inputs are significantly different from each other for cells with high IEG expression (**Fig. 1.4h**). Such functional inputs to neurons in visual cortex can be used to compute signals that indicate deviations of expected input from actual sensory input (Attinger et al., 2017; Keller et al., 2012; Saleem et al., 2013; Zmarz and Keller, 2016). Since closed-loop segments included brief halts of visual flow, we consequently were able to record mismatch signals and relate them to neurons with high IEG expression. Histograms for quantified mismatch responses show that the fraction of neurons with high Arc expression is increased in bins for negative mismatch responses (**Fig. 1.4i, Supplementary Fig. 1.3**). Neurons with high c-Fos expression showed little to no bias (**Fig. 1.4j, Supplementary Fig. 1.3**), whereas neurons with high EGR1 expression are biased towards bins with

positive mismatch signals (**Fig. 1.4k, Supplementary Figure 1.3**). This bias together with the selectivity for the preferred functional type of input suggests that neurons with high Arc expression become visual input responsive neurons and neurons with high EGR1 expression motor-related input responsive neurons during visuomotor-learning.

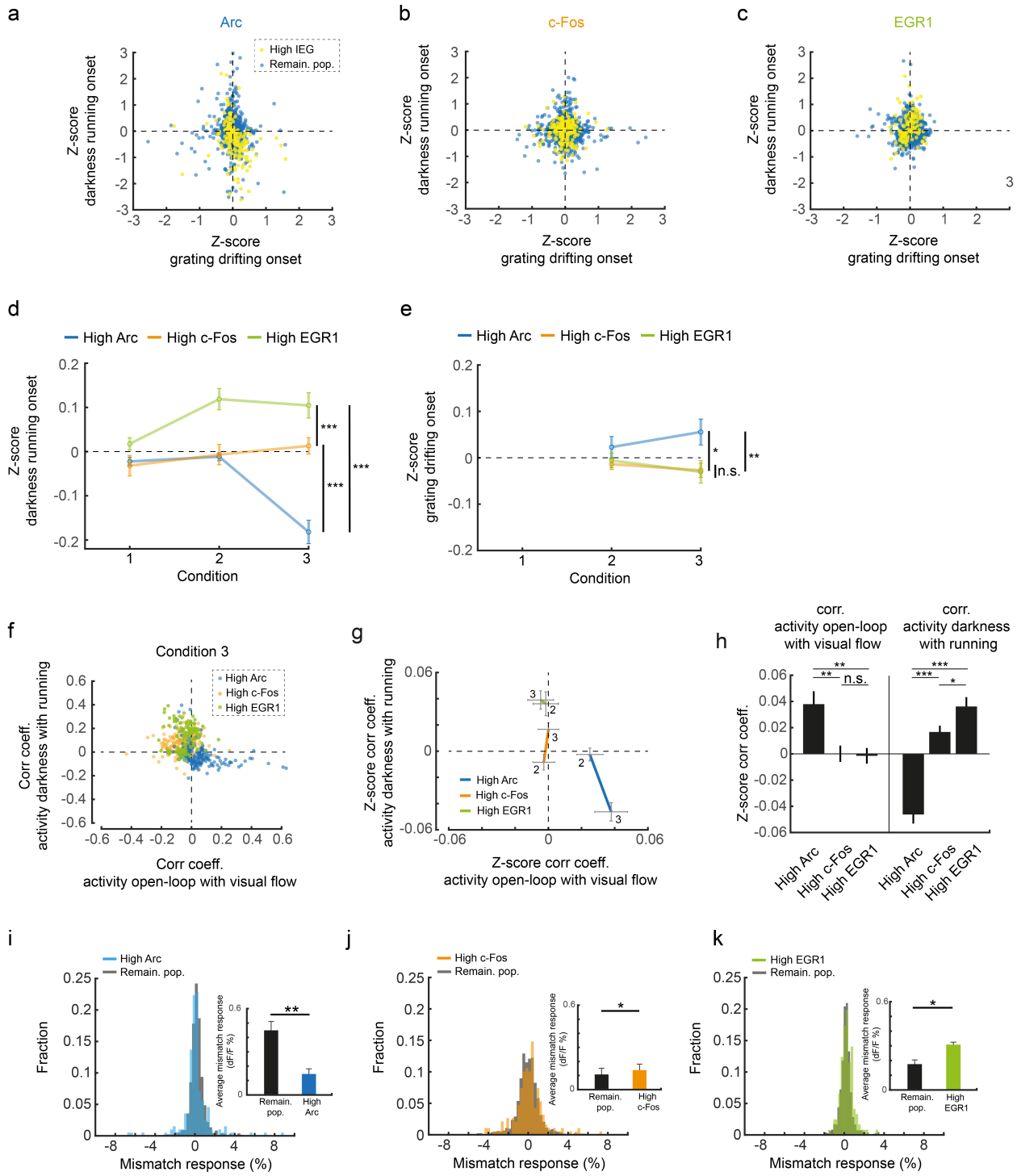

Figure 1.4: Functional cell type specific expression of IEGs in V1

(**a**), Scatter plot of high Arc cells (yellow, n= 197) and the remaining population of cells (n = 1772) for the quantification of running in darkness and drifting grating onsets in condition 3.

(**b**), Same as in (A), but for high c-Fos (cells yellow, n = 189) and the remaining population of cells (n = 1696).

(**c**), Same as in (A), but for high EGR1 cells (n = 121) and the remaining population of cells (n = 1092).

(**d**), Quantification of running onset events during darkness for high IEG cells across all experimental conditions. Lines indicate mean, errorbars s.e.m (blue: Arc, orange: c-Fos, gray: EGR1, same cells as in (A - C), Student's t-test, Arc vs. c-Fos - $p < 0.001$, Arc vs. EGR1 - $p < 0.001$, c-Fos vs. EGR1 - $p = 0.0057$).

(**e**), Quantification of drifting grating onset events for high IEG cells across all experimental conditions. Lines indicate mean, errorbars s.e.m (blue: Arc, orange: c-Fos, gray: EGR1, same cells as in (A - C), Student's t-test, Arc vs. c-Fos - $p = 0.0112$, Arc vs. EGR1 - $p = 0.0348$, c-Fos vs. EGR1 - $p = 0.8987$).

(**f**), Scatter of correlation coefficients for correlation of activity traces with traces of either running during darkness or visual flow during open-loop segments for high IEG cells (same cells as in A - C) in condition 3.

(**g**), Centroids of scatter in (F) for condition 2 and 3. Errorbars indicate s.e.m.

(**h**), Quantification of centroids in (G) for all datapoints. Errorbars indicate s.e.m (Student's t-test, left: Arc vs. c-Fos - $p = 0.0015$, Arc vs. EGR1 - $p = 0.005$, c-Fos vs. EGR1 - $p = 0.8732$; right: Arc vs. c-Fos - $p < 0.001$, Arc vs. EGR1 – $p < 0.001$, c-Fos vs. EGR1 - $p = 0.0411$);

(**i**), Histogram for the quantification of mismatch responses for high Arc cells (blue, n = 197) and the remaining population of cells (black, n = 1772). Figure inset: Quantification of mean response amplitude of the distributions. Errorbars indicate s.e.m (Student's t-test, $p = 0.0054$).

(**j**), Same as in (I), but for c-Fos. Errorbars indicate s.e.m (Student's t-test, $p = 0.0184$).

(**k**), Same as in (I), but for EGR1. Errorbars indicate s.e.m (Student's t-test, $p = 0.0149$).

Discussion

In this study, we found that the two immediate early genes Arc and EGR1 are expressed in neurons that receive functionally different inputs in primary visual cortex. The development of functional different responses in neurons with either high Arc or EGR1 expression, together with the bias towards positive or negative visuomotor-mismatch signals, suggests that these IEGs shape the integration of top-down and bottom-up inputs during visuomotor-learning. These findings are line with results which show that these immediate early genes are important for synaptic plasticity (Alberini, 2009; Bozon et al., 2003; Chowdhury et al., 2006; Messaoudi et al., 2007; Shepherd et al., 2006; Tzingounis and Nicoll, 2006; Waung et al., 2008). Our results cannot be explained by an underestimation of the correlation between neuronal activity and immediate early gene expression, correlation coefficients are similar and not significantly different between +90min after stimulation and at peak time (Arc: $p = 0.1009$, c-Fos $p = 0.6887$, EGR1: $p = 0.7229$, Student's t-test) (**Fig. 1.1c, f, i**). jRGECO1a is less sensitive to subthreshold activity compared to other red calcium indicators (Dana et al., 2016; Inoue et al., 2014), still we find many of the most active neurons to have low immediate early gene expression (**Fig. 1.1d, g, j**). In addition histological experiments proof that the expression of GFP overlaps with the expression of either Arc, c-Fos or EGR1 in the used mouse lines (Barth et al., 2004; Okuno et al., 2012; Xie et al., 2014; Yassin et al., 2010). Recent evidence from studies looking at the immediate early genes NARP (Tsui et al., 1996) and Npas4 (Spiegel et al., 2014), suggest that the expression a subset of IEGs correlates with functional types of neurons. NARP is exclusively expressed in parvalbumin positive, inhibitory neurons and impacts plasticity periods by regulating excitatory synapses onto these cells (Chang et al., 2010; Gu et al., 2013). Npas4 restricts the number of synapses of mossy-fiber input specifically onto CA3 pyramidal cells during learning (Weng et al., 2018). In this study, we identified Arc and EGR1 to be expressed in neurons that preferentially either receive visual or motor-related input during visuomotor-learning in visual cortex. These findings are consistent with the notion that IEGs play a key role in neuronal plasticity and learning.

Acknowledgements. We thank the whole Keller lab for helpful discussions and comments on earlier versions of this manuscript. We thank Daniela Gerosa-Erni for production of the AAV vectors, and Bo Wang for help with the construction of the microscope and virtual reality setup, and the members of the Keller lab for support. This work was supported by the Swiss National Science Foundation, the Novartis Research Foundation, the Human Frontier Science Program.

Author contributions. D.M. and P.Z. performed the experiments, D.M. analyzed the data. H.O. and H.B. made the mEGFP-Arc mouse. D.M. and G.K., wrote the manuscript, G.K. supervised the project.

Supplementary Figures

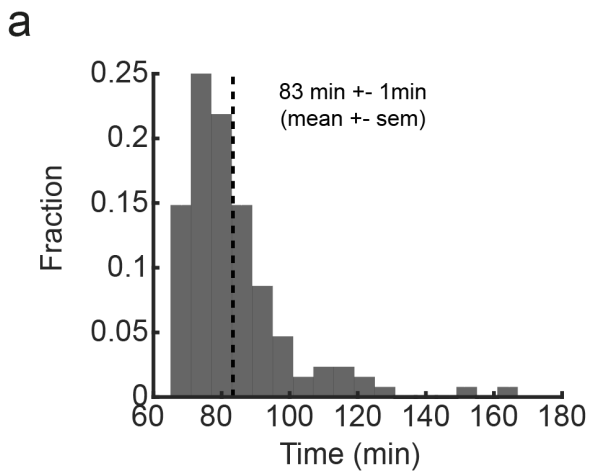

Supplementary Figure S1.1: Durations of imaging session

(**a**), Histogram for durations of imaging times of all experimental time-points. On average one session lasted for approximately 83 min.

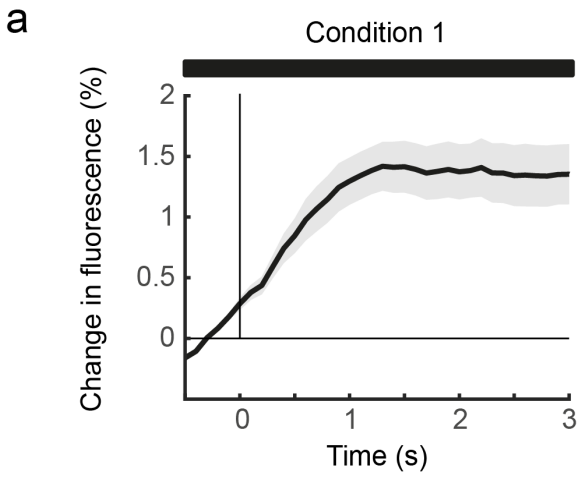

Supplementary Figure S1.2: Running – related activity before first visual exposure

(**a**), Average change in fluorescence upon the onset of running behavior (time 0s) in condition 1 before mice have experienced visual exposure (mean ± s.e.m), shading indicates s.e.m (n = 5067 or 16 mice).

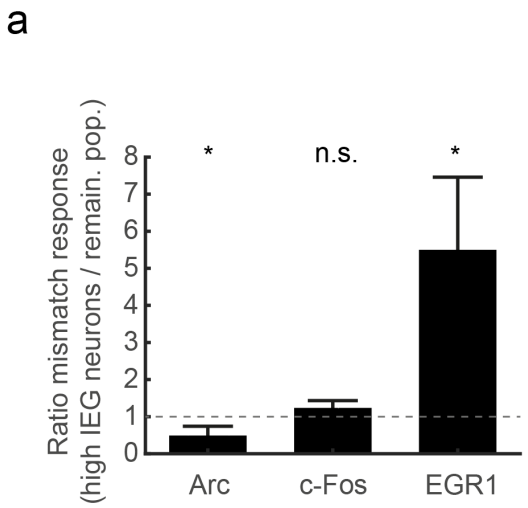

Supplementary Figure S1.3: Differential mismatch responses in high IEG neurons

(**a**), Ratio of mismatch responses of high IEG neurons and the remaining population (significance to mean of 1 - Arc: p = 0.0461, c-Fos: 0.2273, EGR1: 0.0234, Student's t-test)

Experimental procedures

Animals and surgery. All animal procedures were approved by and carried out in accordance with guidelines of the Veterinary Department of the Canton Basel-Stadt, Switzerland. We used imaging data from a total of 11 mEGFP-Arc mice (Okuno et al., 2012), 9 c-Fos-GFP- mice (Barth et al., 2004) and 8 EGr1-GFP mice (Xie et al., 2014), aged 40 days at the start of the visuomotor-learning imaging series (Figure 2 - 4) or aged 100-104 (Arc), 279-291 (c-Fos) and 120-124 (EGR1) days (Figure 1). No statistical methods were used to predetermine sample sizes, but our sample sizes are similar to those generally employed in the field. Mice were group housed in a dark cabinet and in a vivarium (light/dark cycle: 12/12 h). Viral injections and window implantation were performed as previously described. Briefly, at P30 mice were anesthetized in darkness using a mix of fentanyl (0.05 mg/kg), medetomidine (0.5 mg/kg) and midazolam (5 mg/kg), additionally their eyes were covered with a thick, black fabric during all surgical procedures. A 3-5 mm craniotomy was made above V1 (2.5mm lateral of lambda (Paxinos, 2013)) and AAV2/1-Ef1a-NES-jRGECO1a-WPRE ((Dana et al., 2016); titer $7.2x10^{10}$ – 6.8×10^{12} TU/ml) was injected into region V1. The craniotomy was sealed with a 3-5 mm cover slip. A titanium head bar was attached to the skull and stabilized with dental cement.

Imaging, virtual reality and experimental design. Imaging commenced 10 – 12 (visuomotor-learning experiments, **Fig. 1.2** – **1.4**) or 12 – 29 (**Fig. 1.1**) days following injection and was done using a custom-built two-photon microscope. Illumination source was an Insight DS laser (Spectra Physics) tuned to a wavelength of either 950nm, 990nm or 1030nm. Imaging was performed using an 8-kHz resonance scanner (Cambridge Technology) resulting in frame rates of 40 Hz at a resolution of 400 × 750 pixels. In addition, we used a piezo-actuator (Physik Instrumente) to move the objective (Nikon 16×, 0.8 NA) in steps of 15 µm between frames to acquire images at four different depths, thus reducing the effective frame rate to 10 Hz. The behavioral imaging setup was as previously described (Leinweber et al., 2014). Briefly, for V1 experiments mice were head fixed in complete darkness after a brief Isoflurane anesthesia and the setup was light-shielded before every imaging session. Mice were free to run on an air-supported polystyrene ball, the motion of which was restricted to the forward and backward directions by a pin. The ball's rotation was coupled to linear displacement in the virtual environment that was projected onto a toroidal screen surrounding the mouse. The screen covered a visual field of approximately 240 degrees

horizontally and 100 degrees vertically. All displayed elements of the tunnel or sinusoidal gratings were calibrated to be isoluminant.

Experimental design. For visuomotor-learning experiments (**Fig. 1.2- 1.4**) all mice were born and reared in complete darkness, housed in complete darkness until P44 and then transferred to a vivarium with a 12/12h light/dark cycle. Experimental sessions started on P40 and were approximately 2 h long. They occurred twice per day, spaced 12 h apart. On experimental day 1 and 2 recordings were done in complete darkness, afterwards mice were exposed to the virtual environment and sinusoidal drifting grating stimuli. In early phases of the experiment mice were encouraged to run by applying occasional mild air puffs to the neck. For experiments shown in **Fig. 1.1** all mice were dark adapted for 24h 17min ± 10 min (mean ± s.e.m) before head-fixation under the microscope in darkness. Activity and immediate early gene expression were recorded every 15 minutes for 6 hours. Except for the time of visual stimulation with sinusoidal gratings moving in 8 different directions, mice were kept in complete darkness under the microscope for the entire duration of the experiment.

Statistics. Parametric (Student's t-test) and non-parametric tests (Wilcoxon rank sum test) were performed for analyses.

Data analysis. Imaging data were full-frame registered using a custom-written software (Leinweber et al., 2014). Neurons were selected manually based on their mean fluorescence or maximum projection. This biased our selection towards active neurons. Fluorescence traces were calculated as the mean pixel value in each region of interest per frame, and were then median-normalized to calculate ΔF/F. ΔF/F traces were filtered as previously described (Mukamel et al., 2009). GFP intensities were calculated as the mean pixel value in each region of interest (ROI) for mean fluorescence projections. Normalization was performed with the following formula: ROIs(x) – ROIs(min) / ROIs(median) –ROIs(min), where "x" denotes the mean pixel values if an individual ROI, "min" the minimum ROI value, "median" the median ROI value, both computed across all experimental time-points. No blinding of experimental conditions was performed in any of the analyses.

For all plots of stimulus-triggered fluorescence changes fluorescence traces were mean-subtracted in a window 5 to 1 frames (−500 ms to −100 ms) preceding the stimulus onset (**Fig. 1.4a, b, c, d, e, i, j, k** and **Supplementary Fig. S1.2**). Quantification of changes in fluorescence in **Fig. 1.4** were calculated based on

a time window 5 to 30 frames (+0.5 seconds to +3 seconds) after the stimulus onset (**Fig. 1.4a, b, c, d, e**). A quantification window of +0.2 seconds to +2 seconds was used for the response in **Fig. 1.4i, j, k** due to different response dynamics. Top 10% high IEG neurons were selected based on a population vector for each dataset (**Fig. 1.4a, b, c, d, e, f, g, h, i, j, k**).

Code availability. All imaging and image processing code can be found online at https://sourceforge.net/projects/iris-scanning/ (IRIS, imaging software package) and https://sourceforge.net/p/iris-scanning/calliope/HEAD/tree (Calliope, image processing software package). Code used for all data analysis is available from the corresponding author upon reasonable request.

Data availability. The data that support the findings of this study are available from the corresponding author upon reasonable request.

Competing Financial Interests Statement. The authors declare no competing financial interests.

Chapter 2: Immediate early gene expression of Arc and c-Fos marks hippocampal CA1 neurons that are plastic in a two-alternative forced choice paradigm

This chapter is based on a non-published manuscript, a revised version will be submitted to a peer-reviewed journal in the future. The text and figures of this chapter correspond largely to the manuscript, with minor adaptions to formatting and numbering to conform to the style of this thesis.

David Mahringer[1, 2, *], Anders V. Petersen[3, *], Hiroyuki Okuno[4], Haruhiko Bito[5], Jean-François Perrier[3] & Georg B. Keller[1, 2, 6]

[1] *Friedrich Miescher Institute for Biomedical Research, Basel, Switzerland*

[2] *Faculty of Natural Sciences, University of Basel, Basel, Switzerland*

[3] *Department of Neuroscience and Pharmacology, University of Copenhagen, Copenhagen, Denmark*

[4]*Medical Innovation Center, Kyoto University Graduate School of Medicine, Kyoto, Japan*

[5]*Deptartment of Neurochemistry, University of Tokyo Graduate School of Medicine, Tokyo, Japan*

[6] *Correspondence to: georg.keller@fmi.ch*

** These authors contributed equally to this work.*

Immediate early genes (IEG) are markers of synaptic and learning related plasticity. IEGs are commonly used for identifying brain regions active during a particular behavior. So far IEG detection has been performed at single points in time and did not provide any information about dynamics of gene expression. Here we monitored the variations of IEG expression in real time in pyramidal cells from the CA1 hippocampal region in transgenic mice expressing either Arc-GFP or c-Fos-GFP fusion proteins. By measuring the activity of the same neurons with red shifted calcium indicators during the learning of a tone discrimination task, we found that neuronal activity was weakly, positively correlated with IEG expression. Surprisingly we observed that the fraction of neurons expressing highest levels of IEGs before learning were the ones that showed the highest degree of plasticity by becoming selectively responsive to task relevant tone cues.

Introduction

Learning is associated with persistent changes in the central nervous system. These changes can manifest as a strengthening or weakening of synaptic weights (Hebb, 1949) as they occur during long-term potentiation (LTP) and long-term depression (LTD) (Bi and Poo, 1998; Bliss et al., 1973), or the appearance or elimination of synapses (Engert and Bonhoeffer, 1999; Maletic-Savatic et al., 1999). The molecular and gene expression changes underlying this neural plasticity are not fully understood but have been shown to involve increases in the expression of set of genes, referred to as immediate early genes (IEGs) (Okuno, 2011). Plasticity is thought to be triggered by specific changes in Ca^{2+} that activate calcium-dependent kinase cascades, which then lead to the activation of transcription factors such as the Ca2+/cAMP-response element binding protein (CREB) (Mermelstein et al., 2000) or c-Fos (Worley et al., 1993) and other IEGs like Arc (activity-regulated cytoskeletal associated protein, or Arg 3.1) (Vazdarjanova et al., 2006). c-Fos and Arc are considered as markers of synaptic plasticity and memory-related plasticity, and have been used to identify brain regions which are activated by sensory stimuli (Kawashima et al., 2014). Indeed, both the induction of LTP and exposure of an animal to spatial tasks are followed by an increase in the level of mRNA of c-Fos (Cole et al., 1989; Dragunow and Faull, 1989; Guzowski et al., 2001; Ranieri et al., 2012; Vann et al., 2000) and Arc (Link et al., 1995; Lyford et al., 1995). Both c-Fos and Arc are involved in learning related plasticity. Knocking out c-Fos in all neurons results in impaired LTP magnitude in the hippocampus and in deficits in hippocampus-dependent spatial and associative learning tasks (Fleischmann et al., 2003). Moreover, the selective inhibition of CA1 neurons that express c-Fos upon fear conditioning suppresses the expression of the fear memory (Tanaka et al., 2014). Oppositely, the re-activation of the neurons that expressed c-Fos in the dentate gyrus during the initial fear-context exposure leads to freezing-behavior in another context that was not associated with the aversive stimuli (Liu et al., 2012). Inhibition of neurons that express Arc in the dentate gyrus or in CA3 during contextual fear conditioning also leads to an impairment of the fear memory (Denny et al., 2014) and knocking down or knocking out Arc impairs LTP (Guzowski et al., 2000; Plath et al., 2006). With the development of an Arc-GFP mouse, used for this study, it was discovered that Arc targets silent synapses that previously received strong activation. Here, Arc mediates AMPA receptor endocytosis and thereby synaptic downscaling (Okuno et al., 2012). In the same way, the development of the c-Fos-GFP mouse, also used in this study, allowed for targeted electrophysiological characterization based on protein expression levels (Barth et al., 2004).

Most measurements of IEG have been performed at a single time point after learning or exposure. Hence, it is still unclear how IEG levels are dynamically regulated by neural activity during learning. Here, we describe, the expression dynamics of c-Fos and Arc in CA1 pyramidal neurons during learning of a tone discrimination task. We show that neurons with the highest expression of IEGs are the ones that become selectively responsive to task relevant tone cues.

Results

To measure learning related changes of neural activity and IEG expression we trained mice in a two-alternative, forced choice tone discrimination task. We used transgenic mice that expressed either a c-Fos-GFP (Barth et al., 2004) or an Arc-GFP (Okuno et al., 2012) fusion protein. Mice were head-fixed in a cylinder with two lick spouts presented in front of them. Visual stimuli that indicated the start of a trial were presented on a toroidal screen in front of the animal. Next to the animal, a speaker would present one of two tones, which indicated which lick spout the animal should select for a water reward (**Fig. 2.1a**). Failure in selecting a lick spout or selecting the wrong lick spout would result in a mild air puff as well as an increased inter-trial interval delay. Mice were familiarized to the setup and the experimenter by two-training days to associate licking with receiving rewards from both lick spouts (see Experimental Procedures). For the following seven days, each animal went through a one hour training session. Each trial in a training session consisted of an initial visual stimulus indicating the trial onset. After 2 seconds, one of two tones (6 kHz or 11 kHz) was presented for the next following 4 seconds. After a two second grace period (Connor et al., 2010) during which licking had no consequence, the first lick elicited either a reward or an mild air puff to the neck (**Fig. 2.1b**). To facilitate learning, mice received a reward on the corresponding lick spout independent of which spout they licked on a random 10% of the trials. Mice learned to perform this task over the course of the seven training sessions (**Fig. 2.1c**). For later analysis we used days 2 and 3 as early time points and days 6 and 7 as late time points during learning.

Throughout the training sessions we chronically recorded neural activity in the same CA1 pyramidal neurons using the genetically encoded calcium indicator jRGECO1a (expressed using an AAV2/1-Ef1a-jRGECO1a) (Dana et al., 2016), and IEG expression levels. To allow for two photon imaging of calcium activity and IEG expression levels in CA1, the cortex above the left or right hippocampus was aspirated and a chronic window was implanted after viral injection of the calcium indicator vector, as previously

described (Fiser et al., 2016) (**Fig. 2.1d**). Calcium activity was measured throughout training, while IEG levels were measured every 8 min during 30 second breaks in the training paradigm. This allowed us to simultaneously quantify calcium dynamics and IEG expression level changes in the same CA1 pyramidal cells throughout learning (**Fig. 2.1e**).

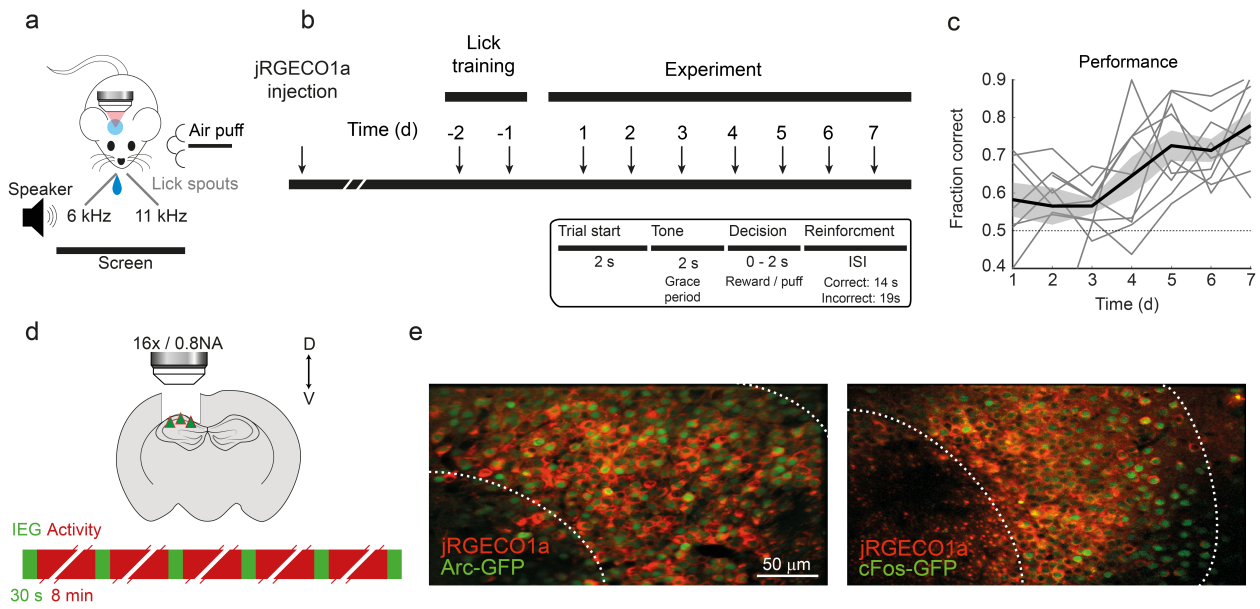

Figure 2.1. Imaging calcium activity and Arc or c-Fos expression during learning of a two alternatives forced choice paradigm.

(**a**), Schematic of the experimental setup.

(**b**), Schematic of the experimental timeline and the task description.

(**c**), Learning curves for the two alternatives forced choice tone discrimination task), for individual animals (gray lines) and mean performance (black lines) with gray shading depicting SEM across animals (n = 9).

(**d**), Top: Schematic of CA1 imaging strategy. Bottom: Structure of imaging strategy during training sessions.

(**e**), Left: Example two-photon image of CA1 neurons co-expressing the genetically encoded calcium indicator jRGECO1a and the fusion protein Arc-GFP. Right: Example two-photon image of CA1 neurons co-expressing the genetically encoded calcium indicator jRGECO1a and the fusion protein c-Fos-GFP.

IEG Expression in CA1 during learning

To investigate how dynamic IEG expression in CA1 is during tone discrimination learning we quantified average IEG levels throughout learning in 1271 neurons from Arc-GFP animals (n = 4) and 1819 neurons from c-Fos-GFP animals (n = 5). We observed CA1 responses to all parts of the task (**Fig. 2.2a**). For individual ROIs, raw fluorescence intensities were extracted from the averaged IEG recording. The expression level was then normalized by setting the minimum expression level to 0 and the median to 1, to facilitate a comparison across all datasets (see Experimental Procedures). On average, c-Fos expression levels were stable, while Arc expression levels decreased over the course of learning (**Fig. 2.2b**). IEG expression dynamics were not reflected in mean calcium activity, which was stable from the second day onwards (**Fig. 2.2b**). Expression levels did not follow a normal or log-normal distribution (one-sample Kolmogorov-Smirnov test, $p > 0.05$, n = 9 animals) over pyramidal neurons and shifted as a whole (Arc) or remained stable (c-Fos) with learning (**Fig. 2.2c**). Stability of IEG expression levels remained high throughout learning (**Fig. 2.2d**). Consistent with this, the stability of change of IEG expression within a training session was below chance (Wilcoxon signed-rank test, $p > 0.05$) (**Fig. 2.2e**). Over the course of each training session (54 ± 5 min, mean ± SD) (**Fig. 2.2f**), Arc and c-Fos expression remained relatively stable (**Fig. 2.2g**). This suggests that CA1 neurons maintained relative IEG expression levels, while it is dynamic which population of cells that gets up- or downregulated during acquisition of the task.

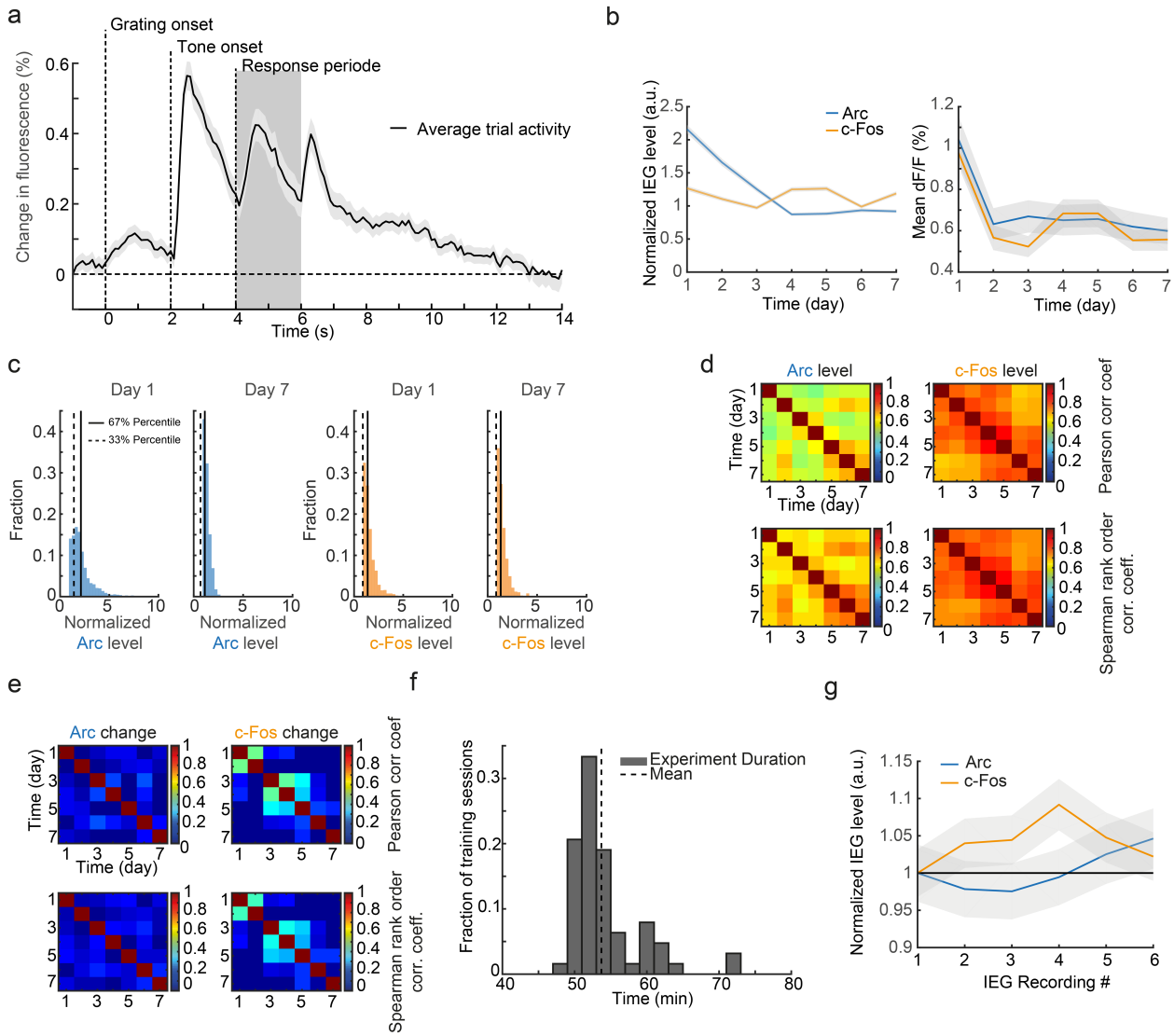

Figure 2.2. IEG Expression characterization in CA1 in vivo during learning.

(**a**), Average trial activity across all animals on session 7. Mean trial activity (solid black line) across trials, with onsets for grating, tone and passive air-puff (dashed lines) and response period (dark gray area). Gray shading indicates SEM across cells (n = 3090).

(**b),** Overall IEG expression is stable or decreases during learning. Normalized IEG expression of Arc (solid line) and c-Fos (dashed line) across days. Grey shading represents SEM across animals.

(**c**), IEG expression distribution is skewed. Left: Distribution of Arc expression on day 1 and 7 showing low Arc cells below the 33rd percentile (dashed line) and high Arc cells above the 67th percentile (solid line) (n = 4 animals, 1271 cells). Right: Distribution of c-Fos expression on day 1 and 7 showing low c-Fos cells below the 33rd percentile (dashed line) and high c-Fos cells above the 67th percentile (solid line) (n = 5 animals, 1819 cells).

(**d**), Correlation of IEG expression across days. Top: Parametric Pearson correlation of Arc expression across days (left) and in c-Fos expression across days (right). Bottom: Non-parametric Kendall's tau correlation of Arc expression across days (left) and in c-Fos expression across days (right).

(**e**), No correlation in IEG expression change across days. Top: Parametric Pearson correlation of Arc expression across days (left) and of c-Fos expression across days (right). Bottom: Non-parametric Kendall's tau correlation of Arc expression across days (left) and of c-Fos expression across days (right).

(**f**), Histogram of training session duration across animals (n = 9).

(**g**), Change in IEG expression over the course of 45 min within a training session of Arc (blue line, n = 4 animals) and c-Fos (red line, n = 5 animals).

Mean IEG expression level correlates only weakly with activity

To quantify how IEG expression levels depend on calcium activity, we correlated IEG expression levels with mean and maximum activity during the training sessions. We found that mean activity was positively correlated with IEG expression levels (**Fig. 2.3a)**, but was a very poor predictor of changes in IEG expression during the training session (**Fig. 2.3b**). The correlation of maximum activity and IEG expression levels was slightly higher than that with mean activity (**Fig. 2.3c**), however maximum activity did not correlate strongly with change in IEG expression levels (**Fig. 2.3d**). Our estimation of change in Arc and c-Fos protein levels might be affected by a post-transcriptional maturation phase for GFP before fluorescence peaks (Tsien, 1998). This might bias our estimation of IEG expression change by introducing a delay from translation peak to fluorescence peak. Another bias could come from changed degradation speeds induced by the IEG-protein fusion with GFP, although this does not seem to be the case at least for c-Fos-GFP (Barth et al., 2004). Correlation of IEG and calcium activity remained stable even when correlating activity and IEG expression on different days (**Fig. 2.3e, f**). There was no change in correlation between maximal activity and Arc or c-Fos expression from early to late sessions (Wilcoxon rank-sum test, $p > 0.05$) (**Fig. 2.3e, f**).

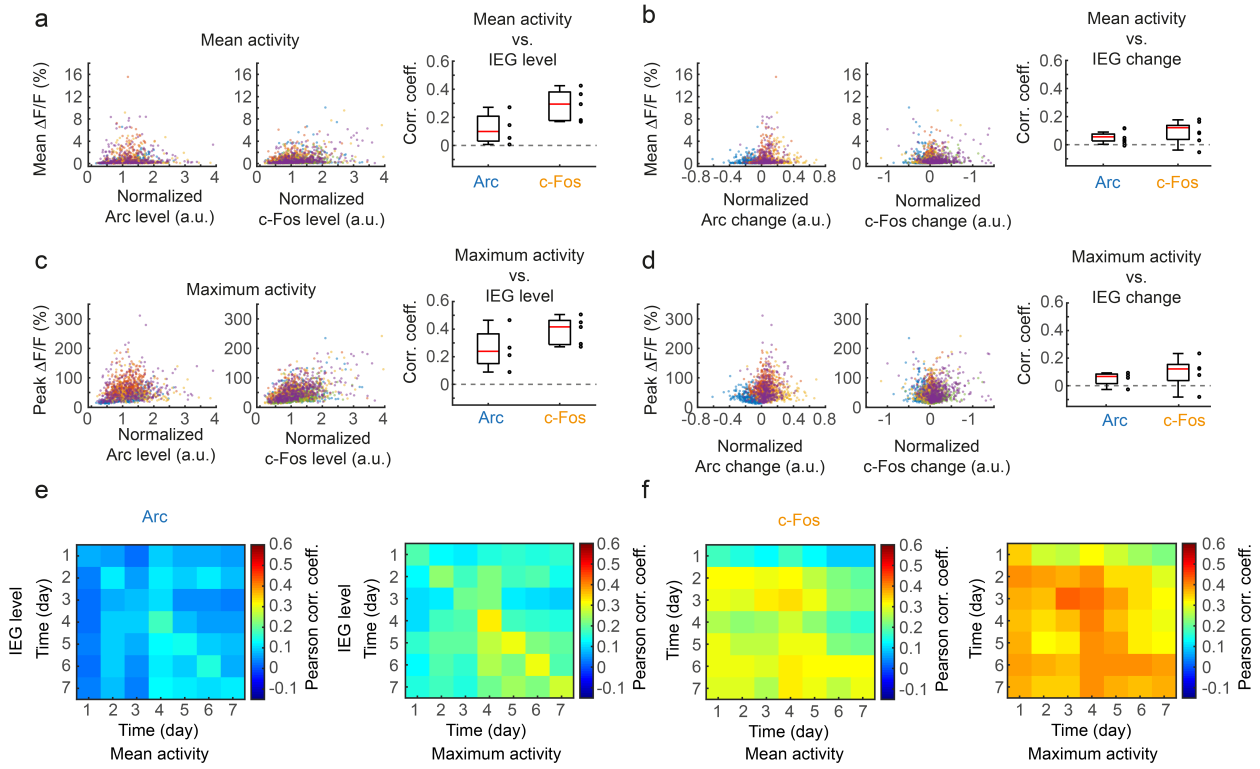

Figure 2.3. Characterization of correlation of IEG expression and activity.

(**a**), Scatter plot of IEG expression level versus mean or maximum activity for Arc (left, all data points shown) and c-Fos (right, 6 data points not shown) for all cells averaged across all days. Mean correlation coefficient of the correlation of IEG level with mean activity. Error bar: mean ± sem across animals and days (4 animals for Arc, 5 animals for c-Fos). Colors show individual animals.

(**b**), Scatter plot of IEG expression change versus mean or maximum activity for Arc (left, all data points shown) and c-Fos (right, 2 data points not shown) for all cells averaged across all days. Mean correlation coefficient of the correlation of IEG change with mean activity. Error bar: mean ± sem across animals and days (4 animals for Arc, 5 animals for c-Fos). Colors show individual animals.

(**c**), Similar to A, but with maximal activity.

(**d**), Similar to B, but with maximal activity.

(**e-f**), Correlation of mean Arc (E) / c-Fos (F) level with mean (left) or maximum (right) activity for all days.

Increased tone representation and response during learning is predictive of performance and correlates with IEG expression.

To probe how the task is represented in CA1, we investigated the neural responses to different stimuli during learning. A visual grating cue used to signal the start of each trial induced the activation of only a small fraction of cells (2.55% ± 0.29, mean ± sem, n = 9 animals). The number of responding cells did not change during the learning task (**Fig. 2.4a;** early vs. late, $p > 0.05$, Wilcoxon ranked-sum test, n = 9 animals).

Rewards and air-puffs associated with correct and wrong behaviors were represented by higher fractions of CA1 neurons that responded with a high degree of specificity to their stimulus (**Fig. 2.4a - b**). During learning, the proportion of cells responding to these stimuli did not change (**Fig.** 2.**4a**; early vs. late, $p > 0.05$, Wilcoxon ranked-sum test, n = 9 animals). By contrast, at the beginning of the learning task, tones, informative about the choice to be made, evoked an activity in a marginal fraction of cells (5.7% ± 1.08, mean ± sem, n = 9 animals) (**Fig. 2.4a**). With learning the proportion of tone responsive cells increased dramatically (**Fig. 2.4a**; Early vs. late, $p < 0.001$, Wilcoxon ranked-sum test, n = 9 animals). Moreover, the activity of the population in response to the tone increased with learning, in contrast to the reward and air puff which stayed similar over time. (**Fig. 2.4b**).

Which neurons are responsive for this increase in activity to the tone stimulus? At the beginning of the learning procedure, tones evoked small responses in cells expressing high levels of c-Fos and Arc (top 10% IEG expressing cells, see Experimental Procedures) (**Fig. 2.4c**). However, at the end of the learning, high IEG expressing cells increased their response to tones specifically (**Fig. 2.4c**). In agreement, the tone response increased in correlation with the level of expression of Arc and c-Fos during learning (**Fig. 2.4d**). In support of the specificity of tone responsive cells, we found that the increase in tone response was negatively correlated with changes in puff and reward responses (**Fig. 2.4e**). Moreover, the cells that became highly tone responsive, were primarily the cells that responded to tones already before learning and to a smaller degree to puff or reward at the beginning of the procedure (**Fig. 2.4f**). This suggests that tone responsive cells develop from a separate population characterized by levels of Arc and c-Fos expression.

Next we tested the meaningfulness of the tone response by testing if it was sufficient for predicting the animal performance. After splitting tone responses between correct (reward), incorrect (active puff), and not associated with behaviors (passive puff), we found that the response was stronger for correct trials (**Fig. 2.4g**; Correct vs. Incorrect trials on late sessions, $p < 0.001$, Wilcoxon ranked-sum test, n = 1349 cells).

In contrast the responses of the tone non-responsive cells were similar before the puff or the reward (**Fig. 2.4g**). This suggests that the difference is specific for the tone cells. In addition, we observed a difference in lick behavior for correct vs. incorrect trials (**Fig. 2.4h**). Finally, we tried to predict the behavior of the mice, based on the activity of tone cells. After training a random forest classifier on an equal number of correct and incorrect trials, the population activity before the onset of the reward or air-puff became sufficient for predicting the outcome of the mouse response (Student's t-test, $p = 0.0146$) (**Fig. 2.4i**). In comparison, the activity of the same cells recorded before the tone onset did not lead to classification accuracy above chance (Student's t-test, $p = 0.1713$) (**Fig. 2.4i**).

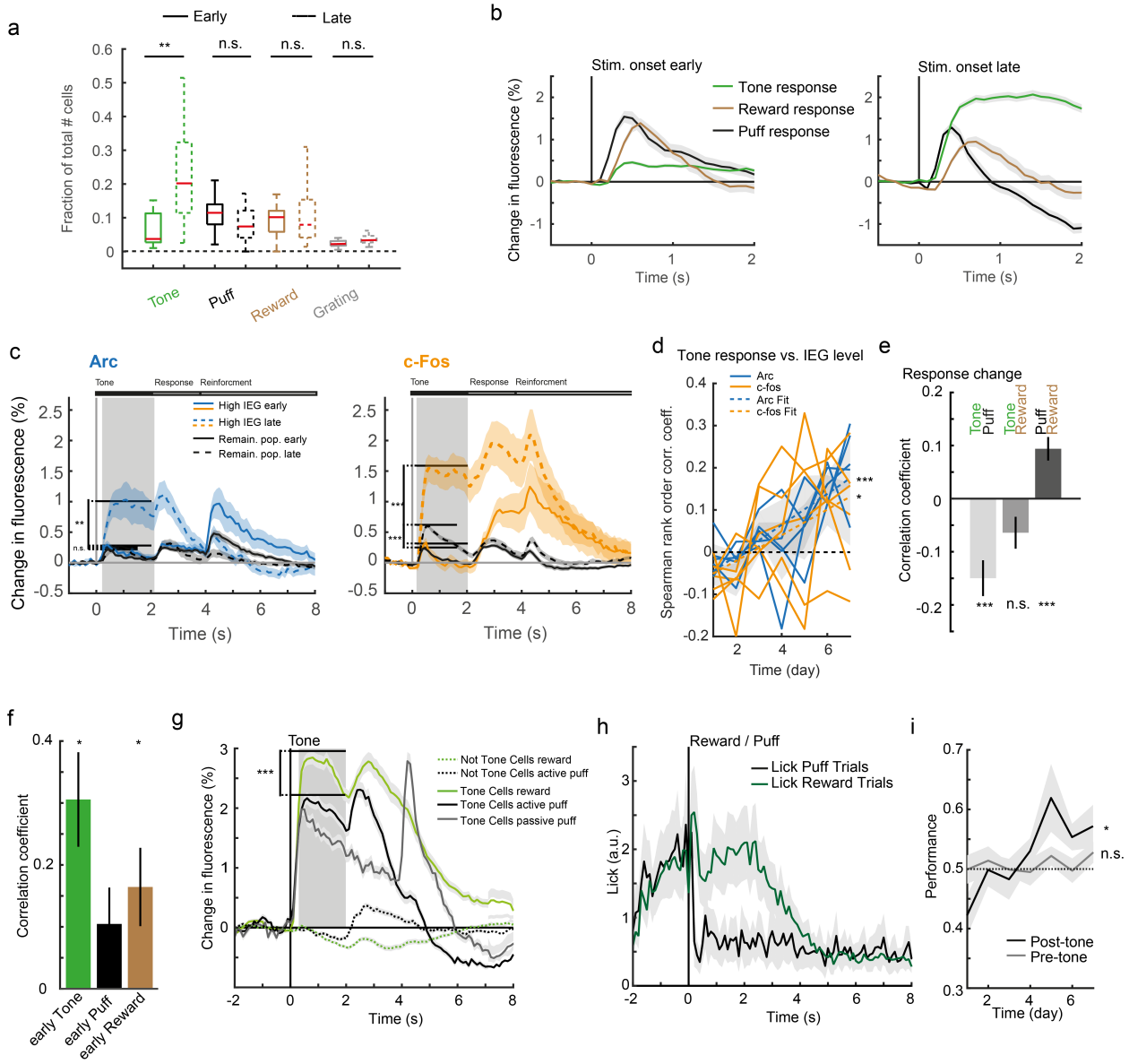

Figure 2.4. Cells that express IEG increase their response to the tone concurrent with the animal learning the task.

(**a**), Fraction of cells being significantly stimulus responsive at early and late training sessions. Boxplots of early (solid line) and late (dashed line) fraction of tone cells (green), puff cells (black), reward cells (gold) and (n = 9 animals) (Wilcoxon rank sum test, early vs late: tone - p = 0.000058, puff – p = 0.0713, reward – p = 0.9748).

(**b**), Development of population responses at the onset of 3 different stimuli (tone - green, air-puff - black, reward - gold) Note the specific increase to the tone stimulus (n = 9 animals).

(**c**), Left: Tone response at early (solid line) and late (dashed line) training sessions for high Arc cells (blue) and the remaining population (black). Right: Tone response at early (solid line) and late (dashed line) training sessions for c-Fos cells (orange), and the remaining population (black). Grey shading indicates SEM across cells (Arc: n = 4 animals, c-Fos: n = 5 animals) (left: high Arc

early vs late - $p = 0.0032$, remaining population - $p = 0.2127$; right: high c-Fos early vs late – $p < 0.0005$, remaining population – $p < 0.0005$).

(**d**), Spearman correlation between change in tone response amplitude and IEG expression level. Correlation of ΔTone~Arc (blue) and ΔTone~c-Fos (orange) and the corresponding linear fits (dashed lines). Gray shading depicts SEM across animals (Arc: n =4 animals, Arc linear model fit $p = 0.000108$, c-Fos: n = 5 animals, c-Fos linear model fit $p = 0.0097$).

(**e**), Tone cells become more selective to the tone cue. Correlation of ΔTone~ΔPuff (Light gray), ΔTone~ΔReward (intermediate gray) and ΔPuff~ΔReward (Dark gray). Error bars: Mean ± SEM across animals (n = 9 animals, ΔTone~ΔPuff $p = 0.00015$, ΔTone~ΔReward $p = 0.0542$, ΔPuff~ΔReward $p = 0.000096$, Wilcoxon signed-rank test).

(**f**), Pearson correlation between late tone response vs. early tone (green), puff (black) or reward response (gold). Error bars: Mean ± SEM across animals (n = 9 animals, early tone vs. late tone reponse $p = 0.0195$, early puff vs. late tone response $p = 0.2031$, early reward vs. late tone response $p = 0.0391$, Wilcoxon signed-rank test).

(**g**), Increased tone response on reward trials. Left: Onset responses for air puff (black) and reward (green) in response to licking at early (solid line) and late (dashed line) training sessions. Gray shading depicts SEM across all cells (n = 3090 cells).

(**h**), Lick behavior on correct and incorrect trials. Lick responses at puff trials (black) and reward trials (green) at early (dashed line) and late (dashed line) training sessions. Gray shading depicts SEM across all animals (n = 9 animals).

(**i**), Classification of reward or air-puff trial. Average of 20 training and classification repetitions. Left: Random forest classifier trained on the population onset activity during the last second before puff or reward (black line) or 1 second before tone onset (gray line) in order to predict upcoming correct (reward) or incorrect (air-puff) trials. Gray shading indicates SEM across animals (n = 9 animals).

Discussion

There is a general agreement that expression of IEGs is reflected in neuronal activity (Guzowski et al., 2005; Kawashima et al., 2014). In this study, we found that the CA1 neurons that get tuned to relevant cues are the ones that display highest levels of Arc and c-Fos expression during learning. Our results suggest that Arc and c-Fos label cells that are capable of undergoing plastic changes during learning, which receive specific sensory input. In addition, we found that neuronal activity is best correlated with IEG expression levels but not with IEG expression changes (**Fig. 2.3a - d**).

Different reports have shown an increase in c-Fos and Arc expression in CA1 in response to massive non-physiological stimulations such as global ischemia (Jorgensen et al., 1989), seizures (Le Gal La Salle, 1988) or kindling (Dragunow and Robertson, 1987). More natural behaviors such as odor discrimination, running, spatial exploration or spatial learning also induce increases in c-Fos or Arc transcription in CA1 (Guzowski et al., 2001; Hess et al., 1995a, 1995b; Kelly and Deadwyler, 2002; Soya et al., 2007). However, in all of these *in vivo* studies, several parameters were involved and it was not possible to demonstrate a link of causality between neuronal activity and IEG level changes. Other studies reported that LTP induced in CA1 failed to induce any change in IEGs (Dragunow and Faull, 1989; French et al., 2001). Furthermore, in a study where evoked synaptic activity was monitored in single CA1 pyramidal cells, a non-consistent correlation pattern was found between synaptic activity and c-Fos expression (Mackler et al., 1992). Altogether these studies suggest that Arc and c-Fos in CA1 are regulated by more parameters than just average neuronal activity. In agreement, we found that average neuronal activity was only weakly positively correlated with c-Fos and Arc expression (**Fig. 2.3c, d**). One could argue that we underestimated the correlations between neuronal activity and changes in IEGs due a delayed maturation of the GFP (Tsien, 1998) or possible increase in degradation dynamics caused by the GFP fusion. However, the measurements we made of individual cells show that we could detect variations in GFP during individual sessions (**Fig. 2.3b, d**). This demonstrates that Arc and c-Fos expression was dynamically regulated within the duration of our measurements (54 ± 5 min., mean ± s.e.m). In support, it was found that Arc mRNA translocates to the cytoplasm within 30 minutes (Guzowski et al., 1999).

During the learning task, plastic changes occurred for neurons that displayed high levels of c-Fos and Arc. These cells originally responded to tone, reward and puff and gradually became more selective for tones (**Fig. 2.4**). This suggests that synapses activated during tones were reinforced and that synapses related to puff or reward were suppressed. Are IEGs involved in this reorganization? It was shown that Arc can

reduce the strength of excitatory synapses. Indeed, Arc mRNAs are transported into dendrites and their translation reduces the amplitude of synaptic currents mediated by AMPA receptors (Rial Verde et al., 2006; Shepherd et al., 2006). Arc could, at least in part, explain the enhancement of tone specificity in a similar way as it increases the specificity of visual responses in cortical neurons (Wang et al., 2006). The role of c-Fos in synaptic plasticity remains to be determined.

The two alternatives forced choice task used in this study is based on tone discrimination. In accordance with our results, CA1 neurons have been shown to display auditory responses in tone discrimination tasks (Itskov et al., 2012; Sakurai, 2002, 1994), where they can encode tone identity (Itskov et al., 2012). The hippocampus is not only active in discrimination tasks, but it is directly involved in the performance. Lesions to the hippocampus impairs discrimination of both olfactory (Eichenbaum et al., 1989), visual (Woodruff and Isaacson, 1972) and mixed auditory and visual (Rudy and Sutherland, 1989) stimuli. Moreover, we can use the neural activity before reward or air-puff delivery to predict correct and incorrect trials. Our results therefore suggest that the cue response development of high IEG expressing neurons in CA1 is directly linked to the performance of the discrimination task.

Acknowledgements. We thank all member of the Keller and Perrier lab for helpful discussions and comments on earlier versions of this manuscript. We thank Daniela Gerosa-Erni for production of the AAV vectors and the members of the Keller lab for technical support. This work was supported by the Swiss National Science Foundation, the Novartis Research Foundation, the Human Frontier Science Program.

Author contributions. D.M. and A.V.P conceived and performed the experiments and analyzed the data. H.O. and H.B. made the Arc mouse. D.M., A.V.P., J.P. and G.K., wrote the manuscript, and J.P. and G.K. supervised the project.

Competing Financial Interests Statement. The authors declare no competing financial interests.

Experimental procedures

Animals and surgery. All animal procedures were approved by and carried out in accordance with guidelines of the Veterinary Department of the Canton Basel-Stadt, Switzerland. We used imaging data from a total of 4 mEGFP-Arc mice (Okuno et al., 2012) and 5 c-Fos-GFP- mice (Barth et al., 2004), aged 60 to 80 days at the start of the imaging series. All animals were group-housed in a vivarium (light/dark cycle: 12/12 h). No statistical methods were used to predetermine sample sizes, but our sample sizes are similar to those generally employed in the field. Mice were water-restricted for the duration of the experiment but received water rewards during experiments. Weight of all mice remained above 80% of starting weight. Viral injections and window implantation were performed as previously described. Briefly, mice were anesthetized using a mix of fentanyl (0.05 mg/kg), medetomidine (0.5 mg/kg) and midazolam (5 mg/kg) for all surgical procedures. For hippocampus imaging experiments, a 3 mm craniotomy was made above either left or right dorsal hippocampus and posterior parts of cortex were aspirated, and AAV2/1-Ef1a-NES-jRGECO1a-WPRE (ref. 35; titer 1.2×10^{11} TU/ml) was injected into region CA1. The craniotomy was sealed with a 3 mm cover slip. A titanium head bar was attached to the skull and stabilized with dental cement. Imaging commenced approx. 28 days following injection and was done using a custom-built two-photon microscope. Illumination source was an Insight DS laser (Spectra Physics) tuned to a wavelength of either 990nm or 1030nm. Imaging was performed using an 8-kHz resonance scanner (Cambridge Technology) resulting in frame rates of 40 Hz at a resolution of 400 × 750 pixels. In addition, we used a piezo-actuator (Physik Instrumente) to move the objective (Nikon 16×, 0.8 NA) in steps of 15 µm between frames to acquire images at four different depths, thus reducing the effective frame rate to 10 Hz.

Training and experimental design. Animals were handled with tubes similar to the ones used during experiments in their home-cages five days prior to experiment start by the experimenter. Two days prior the start of the experiment animals were head-fixed on the setup and randomly rewarded every 20 seconds through one of the two lick spouts to ensure familiarization. Experimental sessions were 10 minutes long, and each behavioral condition consisted of five such sessions, one per day, spaced on average 24 hours apart. During experimental sessions animals on average experience 20 trials or 100 trials per day, in which their performance and activity was recorded. Each trial lasted in total for either 20 or 25 seconds with a varying inter-trial interval, depending on the animal's performance (correct vs incorrect or passive). Each trial started with the presentation of an orientated grating, after 2 seconds one of the tones

in random order would appear and after another 2 seconds the licking behavior of the animal was scored. If correct, animals received a reward through the chosen lick spout, otherwise a mild air-puff. The trial ended after a total of 6 seconds, after which passive animals also received an air-puff. Animals were rewarded randomly on 10% of the trials regardless of their behavior to promote licking behavior.

Statistics. Nonparametric tests (Wilcoxon rank-sum test or Wilcoxon signed-rank test) or parametric tests (Student's t-test) were performed for analyses.

Data analysis. Imaging data were full-frame registered using a custom-written software (Leinweber et al., 2014). Neurons were selected manually based on their mean fluorescence or maximum projection. This biased our selection towards active neurons. Fluorescence traces were calculated as the mean pixel value in each region of interest per frame, and were then median-normalized to calculate ΔF/F. ΔF/F traces were filtered as previously described (Mukamel et al., 2009). GFP intensities were calculated as the mean pixel value in each region of interest (ROI) for mean fluorescence projections. Normalization was performed with the following formula: ROIs(x) – ROIs(min) / ROIs(median) –ROIs(min), where "x" denotes the mean pixel values if an individual ROI, "min" the minimum ROI value, "median" the median ROI value, both computed across all experimental time-points. High IEG cells were selected based on a population vector. No blinding of experimental condition was performed in any of the analyses.

For all plots of stimulus-triggered fluorescence changes fluorescence traces were mean-subtracted in a window 10 to 1 frames (−1000 ms to −100 ms) preceding the stimulus onset unless noted otherwise. Neurons were classified as stimulus-responsive if their mean $\Delta F/F$ in a 5-frame (500 ms, +400ms to +900ms) window after stimulus onset was significantly larger than the mean $\Delta F/F$ in a 5-frame (500 ms, -700ms to -200ms) window before stimulus onset (one-sided paired t-test, with significance level < 0.01).

Classification of correct vs. incorrect trials using neuronal activity was done using Matlab's TreeBagger algorithm. A separate classifier was trained on each training session for each animal. 50 classification trees were used for each classifier. The input to the classifier was the mean $\Delta F/F$ calcium response of each neuron for each puff or reward presentation within a 10-frame window before reward/air-puff or tone onset. The training was repeated 20 times to decrease variance from randomness in the TreeBagger algorithm. Performance of the classifier was evaluated as the mean accuracy of predicting both correct and incorrect trials.

Code availability. All imaging and image processing code can be found online at https://sourceforge.net/projects/iris-scanning/ (IRIS, imaging software package) and https://sourceforge.net/p/iris-scanning/calliope/HEAD/tree (Calliope, image processing software package). Code used for all data analysis is available from the corresponding author upon reasonable request.

Data availability. The data that support the findings of this study are available from the corresponding author upon reasonable request.

Chapter 3: Experience-dependent spatial expectations in mouse visual cortex

This chapter is based on a paper that has been published in Nature Neuroscience (Fiser et al., 2016). The text and figures of this chapter correspond largely to the submitted manuscript, with minor adaptions to formatting and numbering to conform to the style of this thesis.

Aris Fiser[1,2,4], David Mahringer[1,2,4], Hassana K. Oyibo[1,2,4], Anders V. Petersen[3], Marcus Leinweber[1] & Georg B. Keller[1,2]

[1]*Friedrich Miescher Institute for Biomedical Research, Basel, Switzerland*

[2]*Faculty of Natural Sciences, University of Basel, Basel, Switzerland*

[3]*Department of Neuroscience and Pharmacology, Faculty of Health and Medical Sciences, University of Copenhagen, Denmark*

[4]*These authors contributed equally.*

Correspondence to: georg.keller@fmi.ch

In generative models of brain function, internal representations are used to generate predictions of sensory input, yet little is known about how internal models influence sensory processing. Here we show that, with experience in a virtual environment, the activity of neurons in layer 2/3 of mouse primary visual cortex (V1) becomes increasingly informative of spatial location. We found that a subset of V1 neurons exhibited responses that were predictive of the upcoming visual stimulus in a spatially dependent manner, and that the omission of an expected stimulus drove strong responses in V1. Stimulus predictive responses also emerged in V1-projecting anterior cingulate cortex (ACC) axons, suggesting that ACC serves as a source of predictions of visual input to V1. These findings are consistent with the hypothesis that visual cortex forms an internal representation of the visual scene based on spatial location, and compares this representation with feed-forward visual input.

Introduction

Evidence for the existence of internal representations of the environment in the brain has come, most prominently, from the discovery of spatial maps in the hippocampus and entorhinal cortex (Hafting et al., 2005; O'Keefe and Dostrovsky, 1971). Visual cues exert a strong influence on the structure and arrangement of such maps (Hafting et al., 2005; O'Keefe and Conway, 1978). Little is known, however, about how internal models of the environment influence sensory processing. Indirect evidence for an influence of internal representations on visual processing comes from the findings that hippocampal replay during sleep is accompanied by replay in visual cortex (Ji and Wilson, 2007), and from the appearance of theta oscillations in the LFP in visual cortices during locomotion in mice (Niell and Stryker, 2010) and during short-term memory tasks in monkeys (Lee et al., 2005). We speculated that if a direct influence of spatial maps on visual processing develops with experience, it could manifest as a prediction of visual stimulus based on spatial location. The underlying conceptual model is that spatial representations of the environment activate the corresponding visual representations of stimuli encountered in specific locations. This would likely be mediated by top-down projections to V1 from areas involved in spatial memory, like the anterior cingulate cortex (ACC) (Frankland et al., 2004; Maviel et al., 2004; Teixeira et al., 2006; Weible et al., 2012). This leads to a number of testable predictions. First, visual representations of the environment should change systematically with increasing experience in a given environment. Second, we should find non-sensory stimulus-predictive responses that are tied to a conjunction of spatial location and the visual stimulus previously encountered at this location. Third, if the stimulus encountered at a given location is different from the one previously encountered at the same location this should lead to detectable mismatch signals.

Results

To probe for the existence of experience-dependent spatial expectations in mouse primary visual cortex, we repeatedly let mice explore a virtual tunnel over the course of several days. Throughout exploration, we chronically recorded the activity of the same 1630 neurons in V1 layer 2/3 of 9 adult C57BL/6 mice, using two-photon imaging of the genetically encoded calcium indicator GCaMP6f (Chen et al., 2013) (AAV2/1-Ef1a-GCaMP6f-WPRE). For all imaging experiments, mice were head-fixed and free to run on a

spherical treadmill (Dombeck et al., 2007; Holscher et al., 2005). Rotation of the spherical treadmill was restricted to forward and backward directions and controlled movement in a virtual tunnel that was projected onto a toroidal screen surrounding the mouse (**Fig. 3.1a**). Upon reaching the end of the tunnel, mice received a water reward and their position was reset to the beginning of the tunnel. The walls of the virtual tunnel were lined with four different landmark stimuli and five uniform gray areas, marking locations at which one of two orthogonal sinusoidal gratings (henceforth referred to as ***A*** and ***B***) were presented when the mouse reached the corresponding gray area (**Fig. 3.1b, Supplementary Video 1**). This was done to ensure precise control of when the mouse would first see the grating. During the first two sessions the sequence of the five grating stimuli was identical (***A-B-A-B-A***) on every traversal (condition 1). In subsequent sessions the identity of the last grating stimulus changed to a ***B*** on randomly selected traversals (90% ***A*** and 10% ***B*** in condition 2; 100% ***B*** in condition 3; and 10% ***A*** and 90% ***B*** in condition 4). In the fifth condition we omitted the grating in position 5 altogether on 10% of randomly selected traversals. Each condition comprised two recording sessions that lasted between 1 and 2 hours and occurred daily (spaced by 24 ± 4 hours, with the exception of condition 5 which immediately followed condition 4). We imaged from the same neurons chronically throughout the duration of the experiment. Animals traversed the tunnel an average of 109 times per session (**Supplementary Fig. 3.1a**). Each traversal lasted between 10 and 120 seconds (**Supplementary Fig. 3.1b**). In addition, we measured responses of the same neurons during anesthesia to passive presentations of the tunnel presented at a constant visual flow speed both before the first condition (pre-experience anesthesia) and after the last condition (post-experience anesthesia). In total we recorded the activity of 1147 L2/3 neurons in V1 of 6 animals exposed to conditions 1 through 5 (**Fig. 3.1b**), of which 899 neurons were responsive to at least one visual element of the tunnel (tunnel responsive; 78.4%, see Methods). We also recorded from 483 neurons in conditions 1 and 2 in an additional 3 animals, of which 436 neurons were classified as tunnel responsive (90.2%; in total 1335 of 1630 or 81.9% of neurons were tunnel responsive).

To compare dynamics of spatial signals in V1 to potential changes in the spatial map in hippocampus, we chronically recorded the activity of the same 1736 neurons in hippocampal region CA1 in 5 animals exposed to conditions 1 through 5 (**Supplementary Fig. 3.2a; Supplementary Video 2;** see Methods). Changes in spatial signals in V1 could be the result of changes in the spatial representation in hippocampus, or changes in the way V1 is activated by the spatial representation. In either case, these changes should be reflected in top-down inputs to V1. One of the candidate structures for such top-down inputs to V1 is the anterior cingulate cortex (ACC). ACC is known to project to V1 (Miller and Vogt, 1984; Vogt and Miller, 1983; Zhang et al., 2014), and has been shown to be involved in long-term memory

storage (Frankland et al., 2004; Maviel et al., 2004; Teixeira et al., 2006; Weible et al., 2012). To test if spatial information could be relayed to V1 via ACC, we recorded the activity of ACC axons in layer 1 of V1 in condition 1 (3513 axons, 5 sites) and in condition 4 (8599 axons, 10 sites) in 5 animals (see Methods). Note that, unlike for the V1 and CA1 experiments, we were unable to chronically record from the same ACC axons on different days. The combination of the high density of ACC axons in layer 1 of V1 and the low baseline fluorescence made it impossible for us to ensure that we were recording from the same axons on different days. However, there likely was a large overlap between the axons recorded on different days as imaging regions (5 of 10) were realigned based on blood vessel patterns (**Supplementary Fig. 3.2b, Supplementary Video 3**). We imaged activity on the first and the sixth (2 sites, 1 animal) or seventh (8 sites, 4 animals) day in the tunnel. As the total experience in the tunnel between the two imaging time points was comparable to the difference between condition 1 and condition 4 in the V1 and CA1 data we will use the same nomenclature for the ACC data.

V1 activity becomes descriptive of spatial location

To probe for a spatial component in V1 activity, we investigated whether location in the environment modulates neuronal responses to identical visual stimuli. We found that peak calcium fluorescence amplitudes of grating-responsive neurons were different for the presentation of the same grating in different positions in the tunnel (**Fig. 3.1c,d**). In order to quantify the spatial heterogeneity of neuronal responses in the population, we trained a classifier (Matlab Treebagger, see Methods) to predict which grating location the mouse was traversing in each trial for each behavioral condition using the average population activity within a 667 ms (10 frames) window following each grating onset. Based on V1 activity, the classifier was able to predict not only the identity of the grating the mouse was seeing but also where in the tunnel the mouse was seeing the grating (**Fig. 3.1e**). Classification performance, measured as the mean of the diagonal of the confusion matrix for each condition (see Methods), significantly increased between conditions 1 and 4 (condition 1: 53.3 % ± 7.7 %; condition 4: 81.7 % ± 4.6 %, mean ± s.e.m.; $p = 0.029$, Wilcoxon Rank Sum test). The classifier also performed considerably better in post-experience, compared to pre-experience anesthesia (**Fig. 1e; Supplementary Fig. 3a**; Ane. Pre: 31.3 ± 6.2%; Ane. Post: 67.2 ± 7.2%; $p = 0.031$, Wilcoxon Rank Sum test). To ensure that the difference in responses to the same stimulus in different locations was not due to running speed tuning (Keller et al., 2012; Niell and Stryker, 2010), we trained a classifier to predict the animal's location based on running speed. The classifier did

not perform better than chance (**Supplementary Fig. 3.3b**). Training a classifier on slow traversals and testing it on fast traversals, and vice versa, yielded classification accuracy that remained well above chance in both cases (**Supplementary Fig. 3.3c**), suggesting that speed tuning is not a major contributor of predictive power in the classification. To test if calcium dynamics influence the change in classification performance, we deconvolved raw calcium traces using an exponential kernel with a time constant of 0.5 s (Chen et al., 2013; Yaksi and Friedrich, 2006) (**Supplementary Fig. 3.3d**; see Methods) and trained the classifier on the deconvolved traces. Average accuracy was slightly decreased when the classifier was trained on deconvolved traces, but the increase between condition 1 and 4 was unchanged (**Supplementary Fig. 3e**).

In addition to a spatial component in V1 activity, an increase in stimulus selectivity could also influence the discriminability of stimuli in the environment. We quantified the selectivity of all neurons to the two grating stimuli ***A*** and ***B*** using a selectivity index (SI) as $(R_A-R_B)/(R_A+R_B)$, where R_A is the average response to ***A*** in positions 1 and 3, and R_B is the average response to ***B*** in positions 2 and 4; SI was set to 0 for neurons without a significant response to either ***A*** or ***B*** (**Supplementary Fig. 4a**; see Methods). We found that, with experience, neurons in V1 that are grating-selective become more selective with time (**Supplementary Fig. 3.4b,c**), an effect that cannot be explained by their mean activity (**Supplementary Fig. 3.4e**). Furthermore, the stability of these selective neurons increased with experience, an effect not explained by stability in motor behavior (**Supplementary Fig. 3.4f**).

Activity in CA1 exhibited place-like responses that reflected the pattern of visual stimuli along the tunnel. Neurons either responded to landmark stimuli or gratings, and locations with similar visual stimuli elicited similar neural responses (**Fig. 3.1f,g; Supplementary Fig. 3.5a**), with no clear anatomical clustering of neurons that responded to gratings or landmarks in CA1 (**Supplementary Fig. 3.5b,c**). Consistent with previous reports (Ziv et al., 2013), we found that activity patterns were only partially stable over different conditions or days. For 14.8 % of neurons, the location of peak activity in the tunnel was stable over the five behavioral conditions (**Supplementary Fig. 3.6a,c**; within 5% of tunnel length; see Methods). By comparison, in V1, 32% of neurons exhibited a stable location of peak activity (**Supplementary Fig. 3.6b,c**). The instability of CA1 activity may have been augmented by the unilateral removal of cortical tissue necessary to image CA1 pyramidal neurons. Previous work, however, has argued that place field responses measured by imaging using similar methods are not different from those measured with electrophysiological techniques (Dombeck et al., 2010). Classification of grating identity based on grating onset responses using CA1 data was only slightly above chance (**Fig. 1h**). This was likely due to the absence

of clear grating onset responses (**Fig. 3.1g**); using mean activity instead of grating onset responses, classification performance in condition 1 was not different from that based on V1 data (**Fig. 3.1h**; condition 1: 53.9 ± 4.4%; condition 4: 32.3 ± 4.8%, mean ± s.e.m.; $p = 0.043$, Wilcoxon Rank Sum test). Interestingly however, classification performance decreased with experience, indicating that CA1 activity becomes less informative of spatial location. Furthermore, neurons that were stimulus-selective on average showed decreasing selectivity with experience and maintained high trial-to-trial response variability (**Supplementary Fig. 3.4d-f**). This is opposite to the trend we observed in V1 activity where decoding performance increased with experience. The experience-dependent effects found in V1 therefore cannot be explained by a concurrent change of a spatial map in CA1.

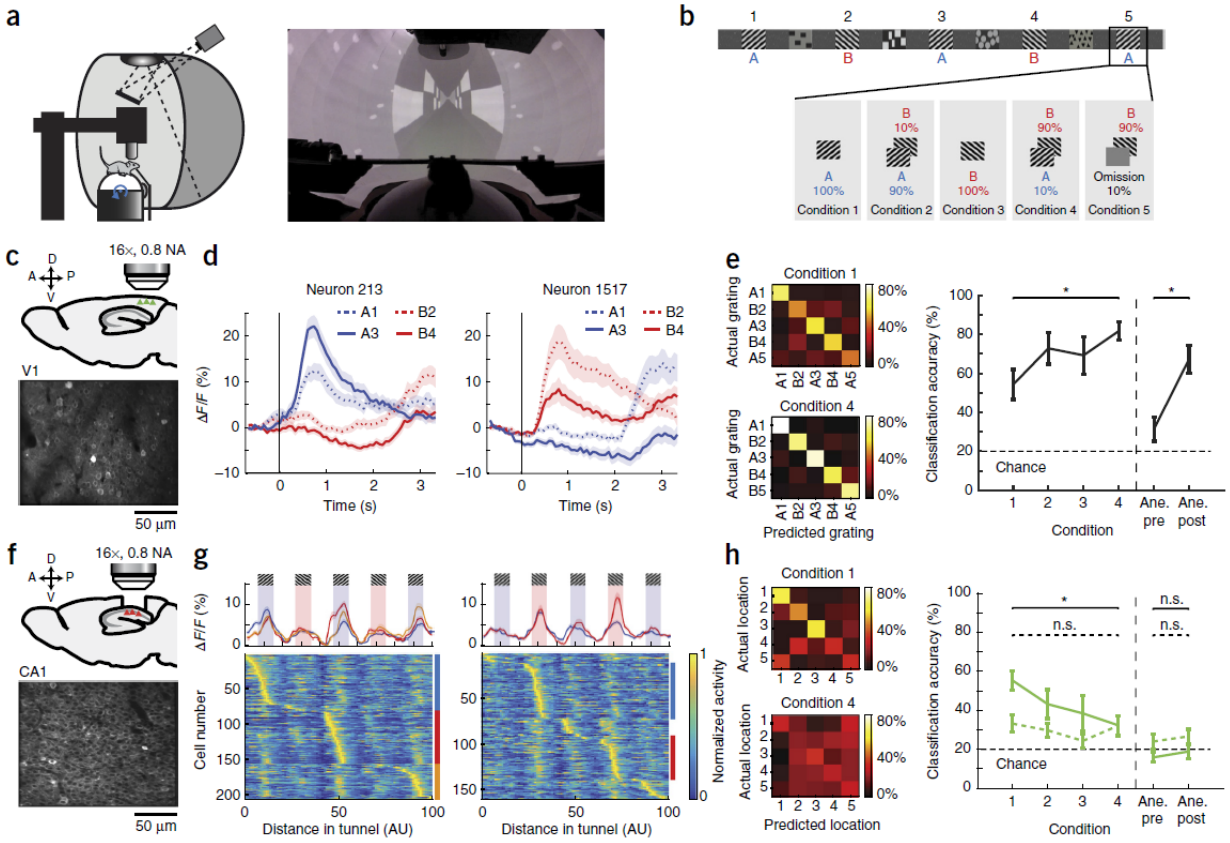

Figure 3.1: Identical visual stimuli in different spatial locations can elicit different responses in V1 and similar responses in CA1.

(**a**), Schematic of the experimental setup.

(**b**), Schematic representation of the texture lining both walls of the tunnel. Gratings ***A*** and ***B*** in positions 1-5 were only shown once the animal reached the corresponding position in the tunnel (**Supplementary Video 1**). In between the grating positions were four permanent landmark stimuli. The probability of encountering an ***A*** or ***B*** in position 5 changed with conditions as shown.

(**c**), Top: schematic of V1 imaging strategy. Bottom: example two-photon image of V1 L2/3 neurons.

(**d**), Average responses of an example ***A***-selective neuron (left) and an example ***B***-selective neuron (right) to ***A***1, ***B***2, ***A***3 and ***B***4. Note that the responses to the preferred stimulus depend on where in the tunnel the stimulus in encountered (position 1 (2) versus position 3 (4)). Shading indicates s.e.m. across grating presentations (left: 178 presentations; right: 218 presentations).

(**e**), Classification accuracy of grating location and identity based on neural activity increases with experience. Left: Confusion matrices of the distributions of classified grating location (x-axis) based on grating onset responses, as a function of actual grating location (y-axis). Right: Mean classification accuracy for all conditions, measured as the mean of the diagonal of the confusion matrix for each condition. Note, for these plots V1 data recorded in conditions 1-2 (from 9 animals) and data recorded in conditions 1-4 (from 6 animals) were combined. Mean ± s.e.m. across animals. Ane-pre: pre-experience anesthesia; Ane-post:

post-experience anesthesia. *: p = 0.029 (conditions 1 and 4); p = 0.031 (pre- and post-experience anesthesia), Wilcoxon Rank Sum test.

(**f**), Top: Schematic of CA1 imaging strategy. Bottom: Example two-photon image of CA1 pyramidal neurons.

(**g**), Heatmaps showing normalized fluorescence traces of CA1 neurons in condition 1, selective to ***A*** (left) and ***B*** (right), sorted by peak position. Traces on top are the mean activity of neurons shown below, highlighted by the blue, red and green vertical bars respectively.

(**h**), Left: As in **e**, but based on mean response, not grating onset response. Right: as in **e**, for mean response (solid line) and for grating onset response (dashed line). Ane-pre: pre-experience anesthesia; Ane-post: post-experience anesthesia. Mean ± s.e.m. across animals (n = 5). *: p = 0.043, n.s.: p = 0.931 (conditions 1 and 4); n.s.: p = 0.524, p = 0.463 (pre- and post-experience anesthesia), Wilcoxon Rank Sum test.

V1 develops predictive responses to upcoming visual stimuli

A potential role for the spatial modulation of V1 activity is to enhance the discriminability of similar stimuli in different contexts. In this scenario, a spatial input would trigger predictions of expected visual input at a given spatial position. Indeed, we found a group of neurons (5.6% or 50 of 899 tunnel-responsive neurons) that, with increasing experience in the tunnel, started firing prior to the appearance of the upcoming grating in an ***A***- or ***B***-selective manner (**Fig. 3.2a,b**). As responses both preceded the stimulus and signaled the identity of the upcoming stimulus, we will refer to these signals as stimulus-predictive. The response in predictive neurons developed with experience and was absent in the first condition (**Fig. 3.2b**) and during anesthesia (**Supplementary Fig. 3.7a**). In contrast, responses in neurons classified as visual and selective to either ***A*** or ***B*** (4.9% or 44 of 899 tunnel-responsive neurons) were present already in the first condition and exhibited a much smaller increase with experience (**Fig. 3.2c**). Predictive and visual neurons were equally selective for ***A*** or ***B*** (**Supplementary Fig. 3.7b**; predictive neurons: mean SI = 0.79 ± 0.04; visual neurons: 0.82 ± 0.03). Using a classifier trained on the activity of predictive neurons preceding the appearance of the stimulus we could predict the identity of the upcoming visual stimulus (**Fig. 3.2d;** accuracy = 81.4 ± 5.1%, mean ± s.e.m.). Once present, predictive responses are stable over conditions. The correlation of the mean responses of predictive neurons between conditions 3 and 4 was almost as high as for visual neurons (predictive neurons: $r = 0.81$, $p = 1.1*10^{-27}$; visual neurons: $r = 0.95$, $p = 5.4*10^{-47}$). Moreover, only one neuron classified as predictive in condition 3 was classified as visual in condition 4.

In conditions 2 and 4 we presented a different grating on 10% of randomly selected traversals in the final location (**Fig. 3.1b**). On these traversals, with an unexpected grating in the final location, stimulus-predictive neurons fired as if the predicted grating would appear, but visual neurons fired in response to the actual grating shown (**Fig. 3.2e,f**). Predictive responses to an unexpected ***A*** (***A***5) were also apparent when plotting the average response of the 20% (n = 229) neurons that responded strongest to an expected ***B*** (**Supplementary Fig. 3.7c**). Given that stimulus-predictive neurons were as selective for the upcoming stimulus (***A*** or ***B***) on average as visual neurons, it is unlikely that predictive responses are responses to the preceding stimulus. To confirm this, we aligned responses of stimulus-predictive neurons to either the preceding landmark stimulus or the upcoming grating for fast and slow traversals separately. Alignment of the responses for fast and slow traversals should be best for the stimulus (previous or upcoming) that actually drives the responses. We found that responses were best aligned with the upcoming stimulus

(**Fig. 3.2g**), and thus are best explained by distance, and not time, from the last stimulus. This implies that predictive activity relies on spatial location to signal the upcoming visual stimulus.

Stimulus-predictive signals could reflect the frequency of having encountered a certain stimulus in a specific location. Thus predictive signals should be higher when the same stimulus is always encountered as opposed to when in a specific location different stimuli were encountered during experience. Therefore, the predictive response to ***B***5 should be lower than the predictive response to mean ***B***, as the stimulus presented in position 5 varied with session (**Fig. 3.1b**), whereas in position 2 and 4 the animal always encountered a ***B***. This was indeed the case: in condition 4, ***B***-selective predictive neurons were significantly less active prior to grating ***B***5 (90% ***B***) than on average to gratings ***B***2 and ***B***4 (100% ***B***) (**Fig. 3.2h**, mean ***B***: ΔF/F = 9.1% ± 2%; ***B***5: ΔF/F = 4.4% ± 1.3%; p = 0.00015, Wilcoxon Signed-Rank test). Conversely, one could argue that ***A***-predictive neurons should be more active prior to ***B***5 as the animal encounters an ***A*** in this location on 10% of the traversals. A rare encounter, however, did not lead to a measureable increase in predictive activity in V1 (**Fig. 2h**, mean ***B***: ΔF/F = 2.3%; ± 2% ***B***5: ΔF/F = 3.1% ± 2.9%; p = 0.7, Wilcoxon Signed-Rank test).

In predictive coding models, the primary visual cortex communicates the error between predicted and actual visual stimuli to downstream visual areas (Bastos et al., 2012; Rao and Ballard, 1999). If predictive activity scales with the frequency of having encountered a visual stimulus in a particular location, then the strength of the visual response to the stimulus may signal the surprise of seeing it. This would be reflected in lower visually-driven activity on trials when prediction of a grating was high. We observed that on traversals with high predictive activity preceding each grating, visually evoked activity to the grating was lower (ΔF/F = 8.0% ± 0.5%, mean ± s.e.m.) than on traversals with low predictive activity (ΔF/F = 11.2% ± 0.5%, mean ± s.e.m.; **Fig. 3.2i; Supplementary Fig. 3.7d**). In sum, this suggests that stronger visual responses report the discrepancy between predicted and actual visual input, and that activity in stimulus-predictive neurons may lead to a reduction of visual responses.

If activity in stimulus-predictive neurons indeed signals the identity of the upcoming stimulus, one would expect a difference in the visual response when an unpredicted stimulus is encountered. We found that the responses of ***A***-selective visual neurons to the unexpected ***A*** at position 5 were stronger when ***B***-predictive neurons fired strongly in anticipation to the grating presentation (**Fig. 3.2j**). Traversals were split into two groups by median amplitude of the response of predictive neurons (average visual responses on high traversals with high predictive activity: 21.4% ± 3.1% ΔF/F; and on traversals with low predictive activity 12.5% ± 2.2% ΔF/F; mean ± s.e.m.; p = 0.02, Wilcoxon Rank Sum test). Altogether, these findings

indicate that the strength of predictive responses preceding a stimulus strongly affect the visual responses to it, suggesting a dynamic interplay between stimulus prediction and stimulus response.

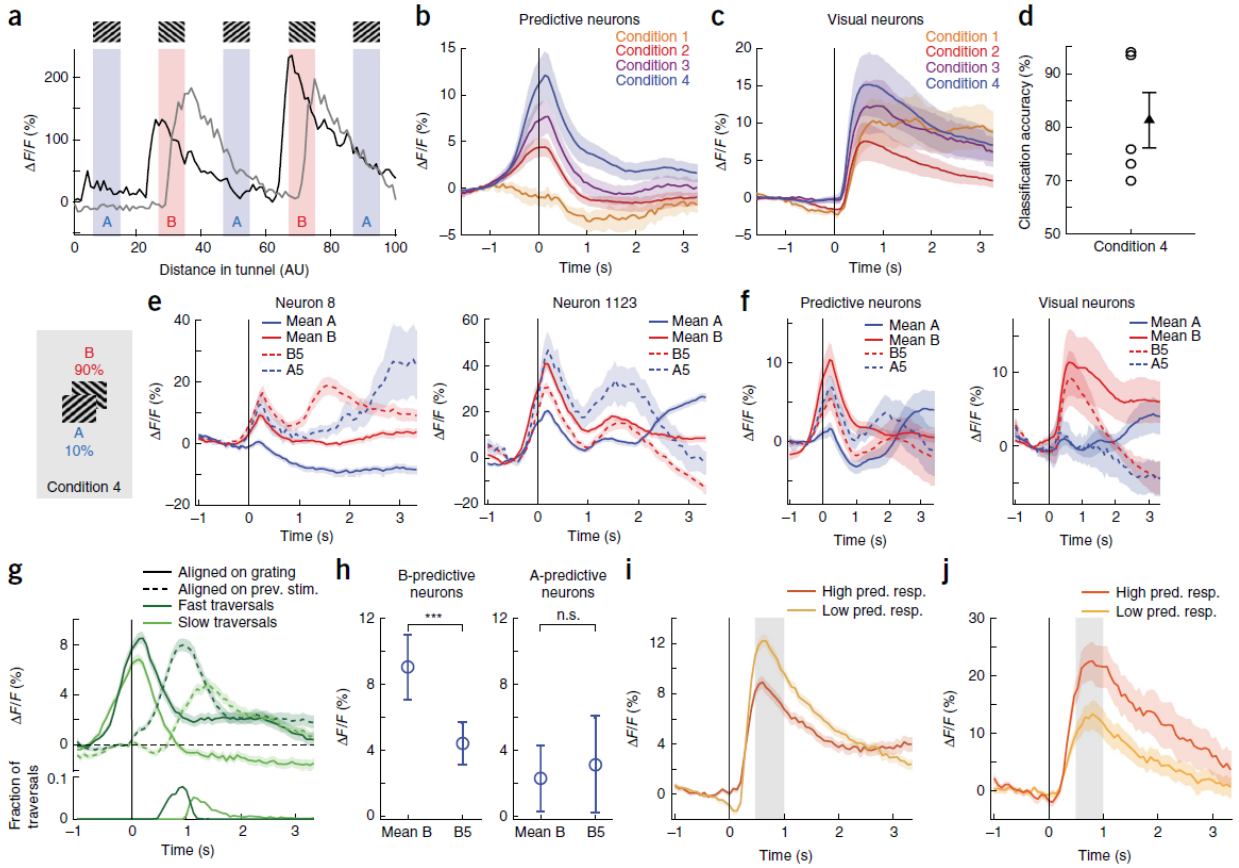

Figure 3.2: V1 neurons develop predictive responses to approaching visual stimuli with experience.

(**a**), The activity of two ***B***-selective neurons during a single traversal of the tunnel. Note that one neuron (black line) fires in anticipation of each ***B*** presentation, whereas the other fires causally with a delay after the presentation.

(**b, c**), The average response of predictive (**b**, 50 neurons) and visual (**c**, 44 neurons) stimulus-selective neurons to their preferred grating orientation in conditions 1-4. In these and all following panels shading along curves indicates s.e.m.

(**d**), Classification accuracy of a classifier trained on the activity of predictive neurons (n = 50) to decode grating identity (***A***3 vs ***B***4) prior to the stimulus (-333ms to 0ms) in condition 4. Circles: individual sites (5 sites); Triangle: Mean; Error bars: s.e.m. Data in **d-i** are from condition 4.

(**e**), Average responses of two example ***B***-selective neurons to mean ***A***1 & ***A***3 (blue line), mean ***B***2 & ***B***4 (red line), unexpected ***A***5 (blue dashed), and the expected ***B***5 (red dashed).

(**f**), Average responses of predictive (n = 50) and visual (n = 44) neurons to mean ***A***1 & ***A***3, mean ***B***2 & ***B***4, expected ***B***5 and unexpected ***A***5.

(**g**), Upper panel: Responses of predictive neurons (n = 50) aligned to either previous landmark stimulus (dashed lines) or upcoming grating stimulus (solid lines) for fast (dark green) and slow traversals (light green). Note that responses for slow and fast traversals align best with upcoming grating onset. Lower panel: histogram of time between previous landmark stimulus and upcoming grating onset for fast (dark green) and slow (light green) traversals. Fast and slow traversals were classified by mean running speed in a window of 467 ms (7 frames) preceding onset of the grating stimulus.

(**h**)**,** Strength of predictive responses of ***B***-predictive neurons (n = 39, left) and ***A***-predictive neurons (n = 11, right) to ***B***2 & ***B***4 (mean ***B***) and ***B***5 in condition 4 where the animal always encountered ***B*** in position 2 and 4, but only with 90% probability in position 5. Mean ± s.e.m. across neurons. (***: p = 0.00015, n.s.: p = 0.7, Wilcoxon Signed-Rank test).

(**i**), Responses of visual neurons on traversals of high (orange) and low (yellow) activity in predictive neurons. Strong predictive activity before a grating (in the top 20%, 787 grating presentations) correlated with weak visually driven responses, and vice versa (in the bottom 20%, 787 grating presentations). Mean responses are calculated in the window indicated with gray shading.

(**j**), Average responses of visually selective neurons in response to the unexpected ***A***5 in traversals with weak (yellow; 51 ***A*****5** presentations) and strong (orange; 52 ***A*****5** presentations) activity in predictive ***B***-selective neurons. The higher the activity in predictive ***B***-selective neurons, the higher the mean visual responses to the unexpected ***A*** (mean responses are calculated in the window indicated with gray shading).

ACC conveys stimulus predictive signals to V1

As the source of predictive signals must be extra-retinal, one would expect that at least some of the top-down inputs to primary visual cortex exhibit signals that are stimulus-predictive, and that this predictive input develops with experience. To test this, we imaged from ACC axons in V1 (**Fig. 3.3a**). When classifying grating position based on the activity of ACC axons we found an increase in classification accuracy with experience, similar to the increase in V1 (**Fig. 3.3b**; condition 1: 31.7 ± 18.3%; condition 4: 88.6 ± 2.4%, mean ± s.e.m.; p = 0.03, Wilcoxon Rank Sum test). We then compared the activity of ACC axons that exhibit selective responses for either ***A*** or ***B*** in early and late conditions. Using the same criteria as for responses in V1 (**Fig. 3.2b,c**) we were able to classify axons as either predictive or visual in both early and late conditions (**Fig. 3.3c, d**). We found that in early conditions there were visual responses but no predictive responses and that in late conditions stimulus-predictive responses emerged (**Fig. 3.3d**). Note, even axons classified as visual exhibited activity that preceded the presentation of the stimulus in condition 4. The contribution of these predictive responses to the total population response to gratings was larger in ACC than in V1 (**Supplementary Fig. 3.7e**). As in V1 (**Fig. 3.2h**), the strength of predictive responses depended on the reliability of having encountered a certain stimulus in a specific location. Predictive responses to ***B***2 and ***B***4 (100% ***B***) were larger than the predictive responses to ***B***5 (90% ***B*** – 10% ***A***, in condition 4; Mean ***B*:** ΔF/F = 6.5 ± 0.6%; ***B***5: ΔF/F = 4.2% ± 0.8%; mean ± s.e.m.; p = 0.00028, Wilcoxon Signed-Rank test), and different from activity in V1, ***A***-predictive activity was higher prior to ***B***5 as compared to ***B***2 and ***B***4 (**Fig. 3.3e;** Mean ***B***: ΔF/F = 2.2% ± 0.3%; ***B***5: ΔF/F = 4.4% ± 0.5%; mean ± s.e.m.; p = 0.00015, Wilcoxon Signed-Rank test). Predictive inputs from ACC could signal spatial location (in spatial coordinates) or signal the predicted visual stimulus (in visual coordinates). To test if axons classified as visual in condition 4 were actually visually driven, we compared responses of expected and unexpected presentations of ***A*** or ***B*** (condition 4). Responses of axons that were ***B***-selective had visual responses to an expected ***B***5 comparable to the mean response to ***B***. Responses to the unexpected ***A*** still showed predictive activity, but diverged from ***B*** responses following stimulus onset (**Fig. 3.3f**). Conversely, axons selective for ***A*** exhibited predictive responses to an expected ***A***1 or ***A***3 and only small responses to the expected ***B***5, but showed clear visual responses to the unexpected ***A***5 (**Fig. 3.3g)**. Thus, predictive signals in V1 are likely conveyed by top-down signals carrying an expectation of the visual input based on spatial location.

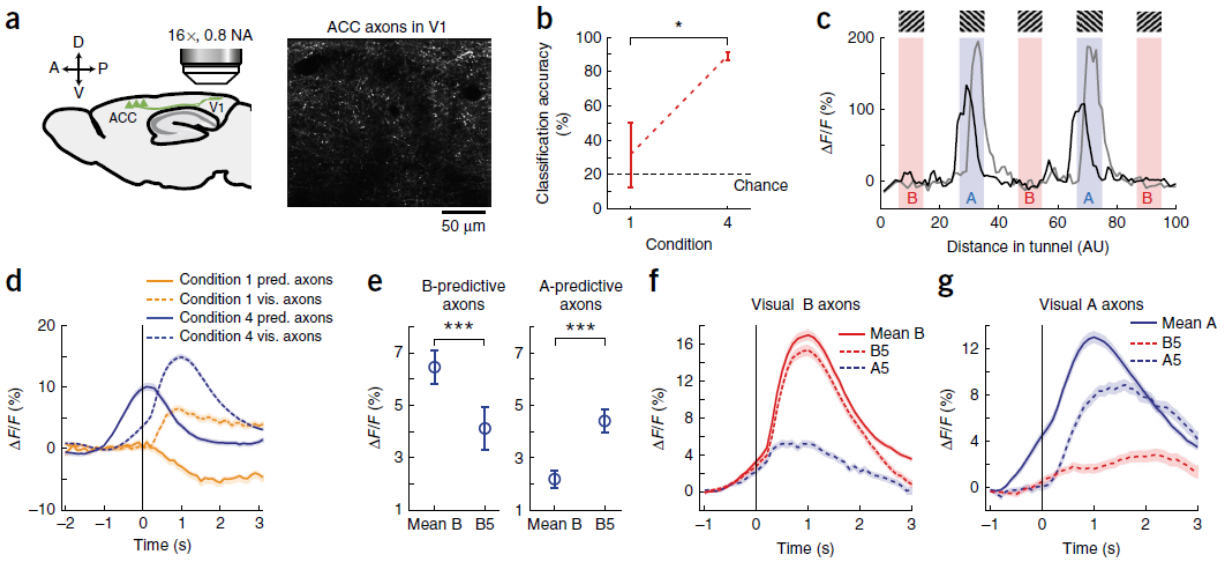

Figure 3.3: ACC projections to V1 carry visual stimulus predictions.

(**a**), Left: schematic of ACC axon imaging strategy. Right: Example two-photon image of ACC axons in V1.

(**b**), Classification accuracy for a classifier trained to decode grating location based on grating onset responses (as in **Fig. 1e, h**). The accuracy of the classifier increases with time. Mean ± s.e.m. across sites (condition 1: 3 sites; condition 4: 10 sites). *: p = 0.03, Wilcoxon Rank Sum test.

(**c**), Activity of two ***A***-selective axons during a single traversal of the tunnel. One axon (black line) fires in anticipation of each ***A***, whereas the other (gray line) peaks after each stimulus.

(**d**), As in V1, stimulus-predictive responses emerge with experience. Orange lines indicate mean activity of predictive (solid; n = 654) and visual (dashed; n = 1377) axons in condition 1, whereas blue lines indicate activity of the corresponding axons in condition 4 (736 predictive and 2559 visual axons). Shading indicates s.e.m. across axons.

(**e**), As in **Fig. 2h**, for V1-projecting ACC axons. Strength of predictive responses of ***B***-predictive axons (left) and ***A***-predictive axons (right) to ***B***2 & ***B***4 (mean ***B***) and ***B***5 in condition 4 where the animal always encountered ***B*** in position 2 and 4, but only with 90% probability in position 5. Mean ± s.e.m. across axons (312 A-predictive and 500 B-predictive axons). ***: p = 0.00015 (A-predictive), p = 0.00028 (B-predictive), Wilcoxon Signed-Rank test.

(**f**), Activity of visual ***B*** axons (n = 1175) to mean ***B*** (***B***2 & ***B***4) (solid red), expected ***B***5 (dashed red) and unexpected ***A***5 (dashed blue).

(**g**), As in **f,** but for visual ***A*** axons (n = 1384). Note the visually evoked response to the unexpected ***A***5. Shading in **f** and **g** indicates s.e.m.

Omitting an expected stimulus drives strong responses in V1

To probe if expectations can drive responses in V1 in the absence of a visual stimulus, we omitted the final stimulus altogether in 10% of randomly selected traversals (condition 5). In these omission traversals, no grating would appear as the mouse reached the gray area marking the location of the final grating presentation (**Supplementary Video 1**). The omission of the stimulus elicited a strong response in the V1 population (**Fig. 3.4a, Supplementary Fig. 3.8a, Supplementary Video 4**). Moreover, a subset of neurons selectively responded to the omission (**Fig. 3.4b;** 2.3% or 21 of 899 tunnel-responsive neurons). If this omission response indeed signals a deviation between predicted and actual visual input, one would expect the strength of the predictive response to correlate with the omission response. To test this, we split all traversals into two categories depending on how strong the average response of predictive ***A***- and ***B***-selective neurons was prior to the omission. The average omission response in trials with low predictive activity was significantly smaller than in trials with high predictive activity (**Fig. 3.4c**; omission-evoked activity on trials with high predictive activity: $\Delta F/F = 35.2\% \pm 8.5\%$; on trials with low predictive activity: $\Delta F/F = 16.6\% \pm 2.2\%$, mean ± s.e.m.; $p = 0.00018$, Wilcoxon Rank Sum test with bootstrapping, see Methods). The lack of local visual flow during the grating omissions raises the possibility that these responses are instances of sensorimotor mismatch (Keller et al., 2012). To test this, we compared the omission responses of the omission-selective neurons to their responses to the expected uniform gray stimulus that the animals encountered while running at the beginning and end of the tunnel. We found no response to the expected gray stimulus in omission selective neurons (**Supplementary Fig. 3.8b**). Thus, omission responses can best be explained by a deviation between expected and actual visual stimulus based on what the mouse had seen in this position on previous traversals. Furthermore, omission responses were absent in ACC axons (**Supplementary Fig. 3.8c**), suggesting that visual cortex compares visual stimulus predictions, relayed by top-down cortical input, to actual visual input.

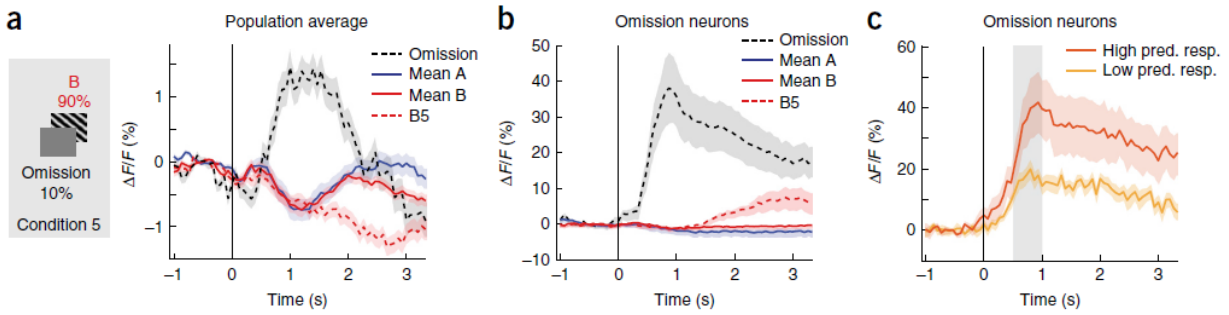

Figure 3.4: The omission of an expected grating strongly drives activity in V1.

(**a**), Average population response (1147 neurons) to the omission of grating B5 (black dashed line) in comparison to the average response to ***A*** (blue line), ***B*** (red line) and ***B***5 (red dashed line). Shading indicates s.e.m. across neurons.

(**b**), As in **a**, but for omission selective neurons (21 of 899 tunnel-responsive). Shading indicates s.e.m. across neurons.

(**c**), Average omission responses in omission selective neurons on traversals of high activity in predictive neurons (orange line; 13 traversals) and on traversals with low activity in predictive neurons (yellow line; 12 traversals). Gray shading indicates window over which mean activity was calculated. Shading indicates s.e.m. over traversals.

Discussion

In this study, we show that the activity of neurons in the primary visual cortex of the mouse is shaped by experience. The increase in selectivity and trial-to-trial stereotypy of stimulus-selective neurons suggests that the representation of an environment in visual cortex is dynamic and becomes increasingly stable with experience. The emergence of stimulus-predictive activity with experience and the presence of an error signal in response to an unexpected stimulus, the strength of which correlates with the strength of the predictive activity preceding it, indicate that processing in V1 in a familiar environment relies on predictions of visual stimuli. These findings build upon previous work on internal representations showing that motor-related signals are integrated with sensory signals in primary sensory cortices to generate sensorimotor-mismatch signals (Eliades and Wang, 2008; Keller et al., 2012; Keller and Hahnloser, 2009; Saleem et al., 2013).

Our results cannot be explained by timing dependent recall of activity or reward anticipation. Cue-triggered recall of activity, for example, has been shown to occur in visual cortex after repeated experience of rapid sequences of stimuli (Gavornik and Bear, 2014) and fast moving spots (Xu et al., 2012).

Sequence learning, however, is specific to the timing used for training; a change in timing of the stimuli of as little as 150 ms abolishes the effect (Gavornik and Bear, 2014). Predictive responses in our experiments persisted even though trial to trial differences in traversal times were on the order of tens of seconds (**Fig. 3.2g; Supplementary Fig. 3.1b**). Moreover, the cue-triggered recall was only observed when the animal was anesthetized, or the animal was awake but cortex was in a synchronized state (characteristic of quiet wakefulness), and the effect was absent when cortex was in a desynchronized state (characteristic of motor behavior) (Xu et al., 2012). Another effect that has been shown to drive activity in visual cortex is reward anticipation (Shuler and Bear, 2006). Neurons that code for a rewarded stimulus are selectively activated in anticipation of reward-predicting stimuli (Poort et al., 2015). However, as in our data predictive activity is stimulus selective and omission responses are independent of the reward delivered at the end of the tunnel, reward anticipation cannot explain the spatial modulation we describe here.

The decrease in spatial information in CA1 with experience we observe implies that the experience-dependent effects found in V1 do not merely reflect a concomitant change in the hippocampal formation. Rather, place-like responses in CA1, which are tied to visual elements of the virtual tunnel, could serve as a scaffold for spatially modulated and stimulus-predictive activity in higher cortical areas that is then relayed to V1 via top-down input. It is interesting to note that decoding of spatial location based on CA1 activity resulted in poorer accuracy than when decoding spatial location from V1 activity. This could be a direct consequence of the virtual environment and head fixation or due to the fact that to image CA1 we removed a part of visual cortex above CA1. Note, however, that one of the main factors contributing to poor decoding of spatial location from CA1 activity is the fact that CA1 neurons responded in multiple visually identical locations. It is unlikely that this is the result of damage to visual cortex. Lastly, although the head fixation and navigation in a virtual environment degrade the spatial representation in CA1 (Aghajan et al., 2014), this does not affect our ability to decode spatial information from V1 and ACC activity after experience.

Direct projections from cortical areas containing spatial representations of the environment, like the retrosplenial (Alexander and Nitz, 2015; Cho and Sharp, 2001) or the anterior cingulate cortex (Weible et al., 2009), exist in rodent V1 (Miller and Vogt, 1984; Vogt and Miller, 1983; Zhang et al., 2014). We have shown that one of these top-down projections carries a prediction of visual stimulus based on the mouse's location in the environment. Top-down mediated predictions could be compared against feed-forward sensory input to compute deviations between actual and predicted sensory input, and such deviations could be used to update expectations and guide learning. Our results are consistent with a predictive

coding framework, in which sensory input is compared to an internal model of the environment to detect deviations from expectations.

Acknowledgements. We thank T. Mrsic-Flogel, E. Feinberg and A. Lüthi for helpful discussion and comments on earlier versions of this manuscript. We thank D. Gerosa-Erni for production of the AAV vectors, and B. Wang for help with the construction of the microscope and virtual reality setup, and the members of the Keller lab for discussion and support. This work was supported by the Swiss National Science Foundation, the Novartis Research Foundation, the Human Frontier Science Program, and by a PhD fellowship from the Boehringer Ingelheim Fonds (A.F.).

Author Contributions. A.F., D.M., and H.K.O. performed the V1 experiments. D.M., A.F. and A.V.P. performed the CA1 experiments. M.L. performed the ACC experiments. A.F. analyzed the V1 data. A.F. and A.V.P. analyzed the CA1 data. A.F. and M.L. analyzed the ACC data. A.F., D.M., H.K.O. and G.B.K. wrote the manuscript.

Competing Financial Interests Statement. The authors declare no competing financial interests.

Supplementary Figures

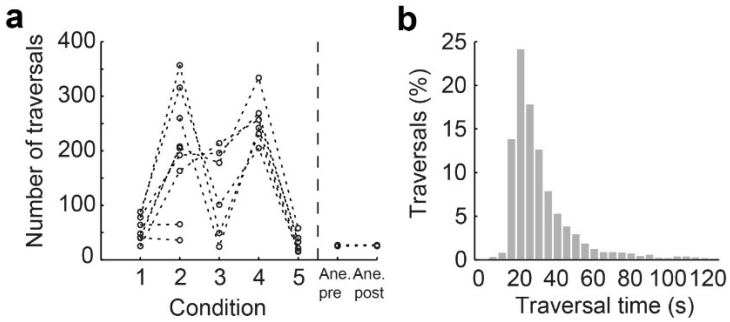

Supplementary Figure 3.1: Number and timing of virtual-corridor traversals.

(**a**), Number of traversals per condition for each animal. Note recording times were shorter for condition 3 and 5.

(**b**), Histogram of traversal times for all conditions.

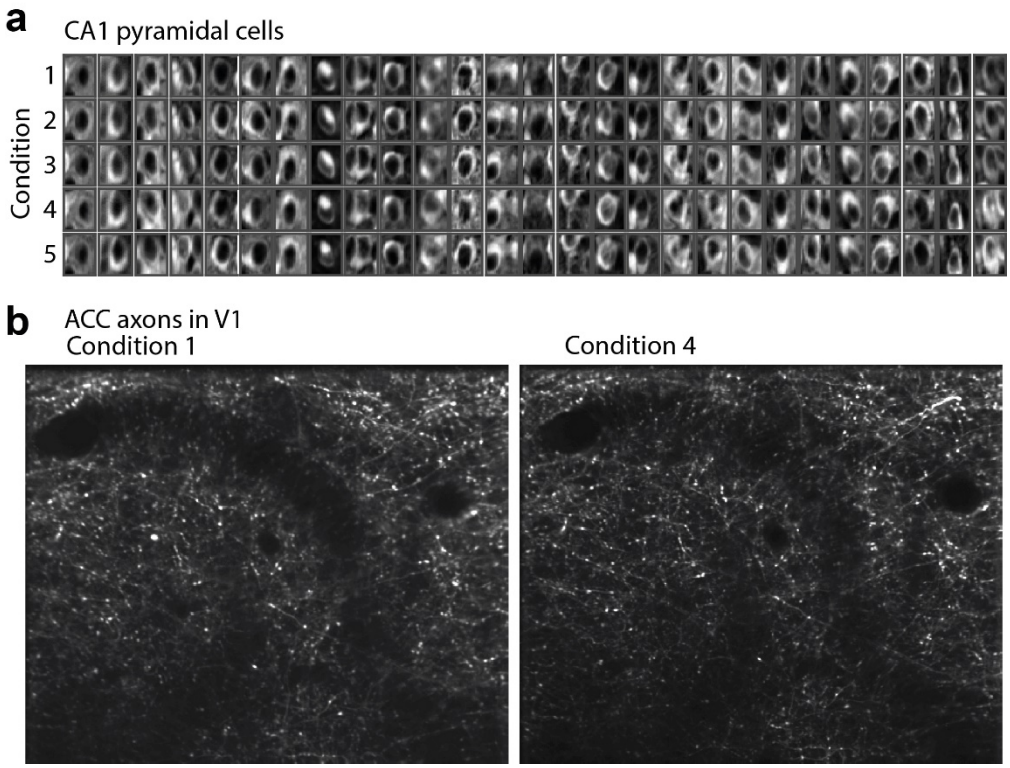

Supplementary Figure 3.2: Stability of imaging of CA1 pyramidal neurons and ACC axons in V1.

(**a**), Example CA1 neurons recorded in the 5 different conditions.

(**b**), Example imaging regions for the ACC axons in V1. Note that due to the high density of axons and the low baseline fluorescence, alignment of the imaging regions for the ACC experiments was performed on blood vessel patterns and not on the axons themselves.

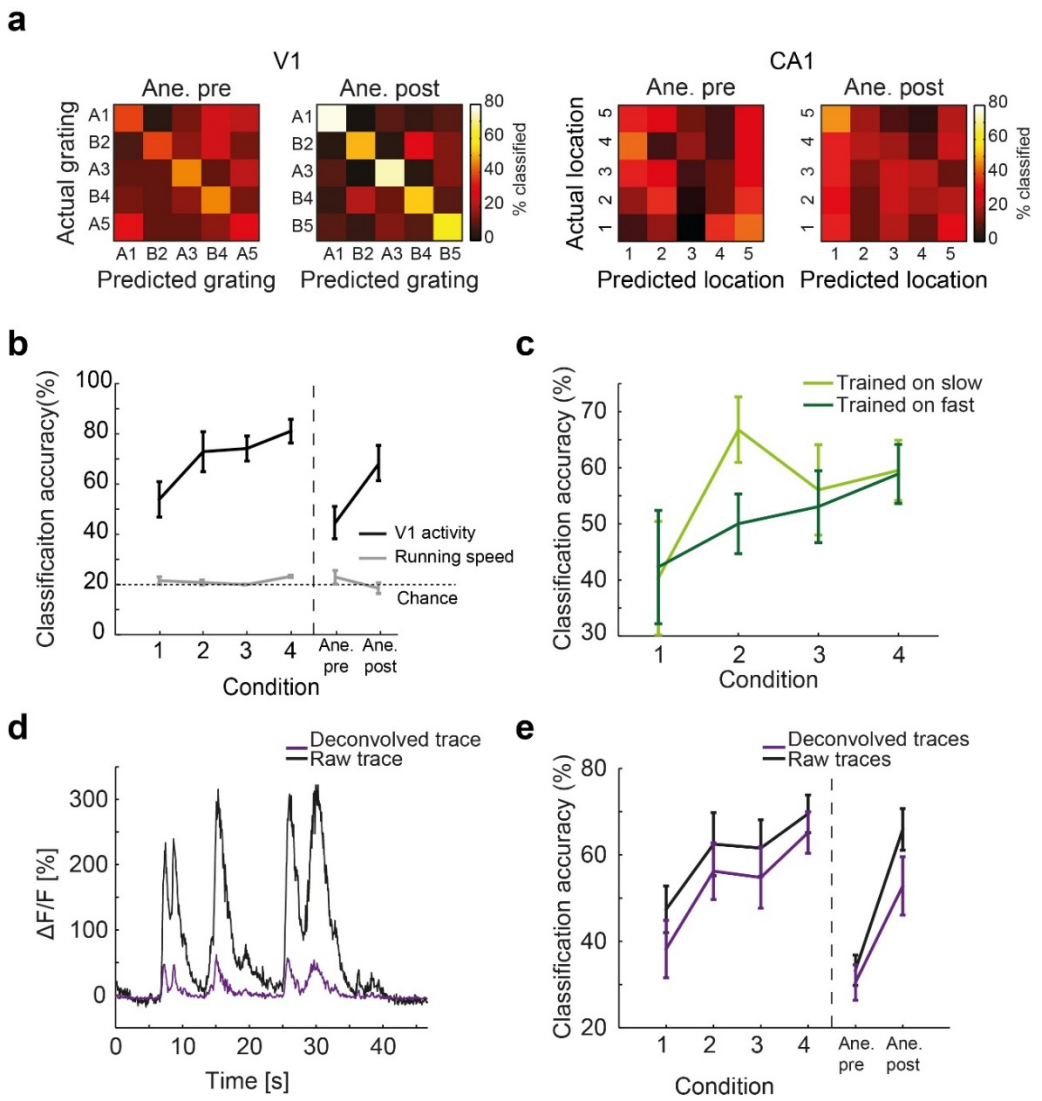

Supplementary Figure 3.3: The increase in classification accuracy of grating position in V1 cannot be explained by running speed or GCaMP dynamics.

(**a**), Confusion matrices as in **Fig. 1e,h** for pre- and post-anesthesia in V1 (left) and CA1 (right). In this and subsequent panels, Ane-pre: pre-experience anesthesia; Ane-post: post-experience anesthesia.

(**b**), Accuracy of the classifier predicting the animal's location in the tunnel based on either neural activity (black line) or running speed (gray line) for conditions 1 through 4. Chance level of 20% (dashed line) is given by the 5 possible grating locations in the tunnel. Error bars: s.e.m.

(**c**), Classifier accuracy when trained on neural activity during fast (slow) traversals and tested on slow (fast) traversals. Error bars: s.e.m.

(**d**), Example of a raw activity trace in time (black), and the same trace deconvolved using an exponential deconvolution kernel with a time constant of 0.5 s (magenta).

(**e**), Classifier performance using raw and deconvolved traces. The similar performance suggests that down-sweeps in calcium signals are not the main predictors of spatial location in population activity. Error bars: s.e.m.

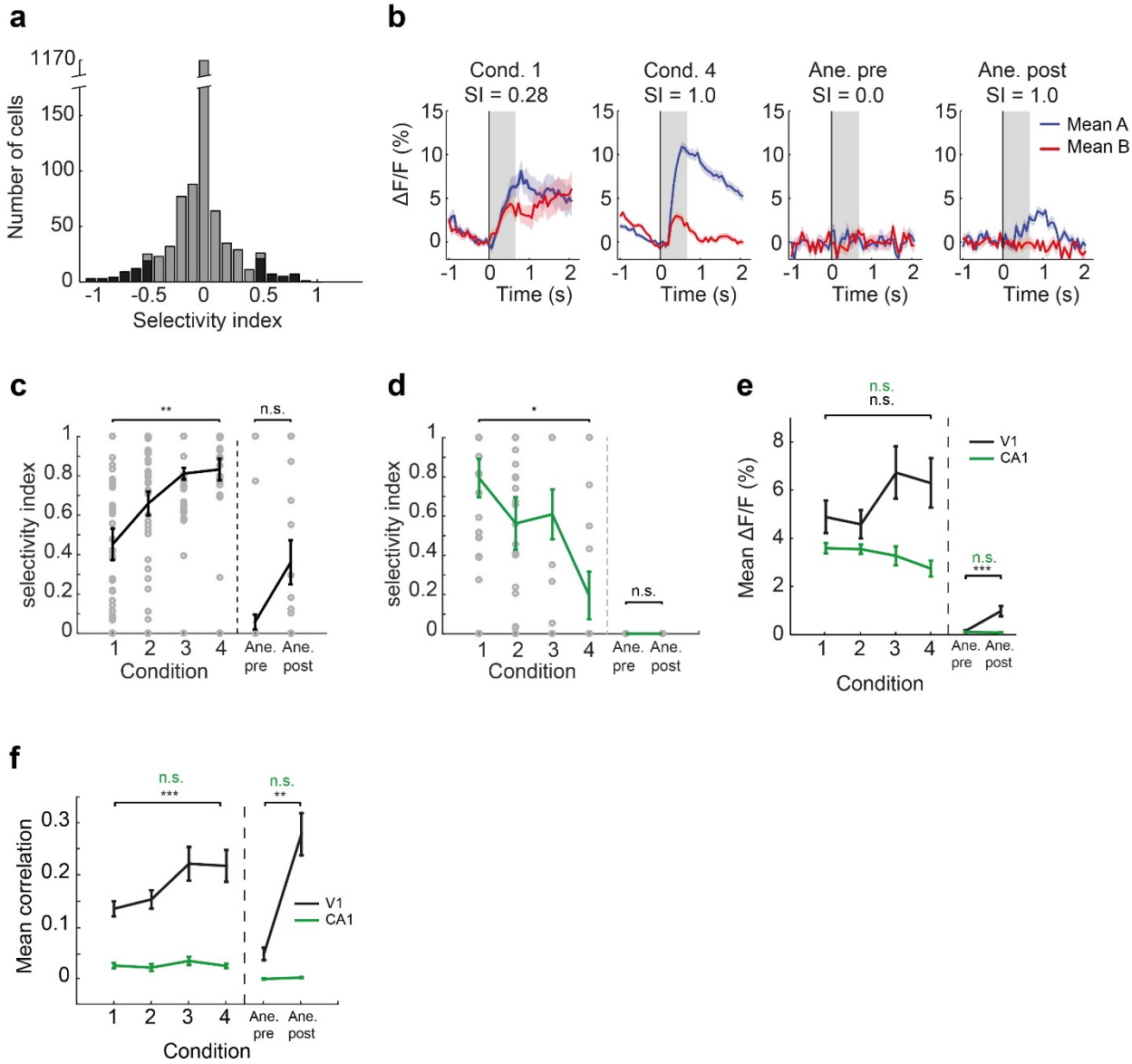

Supplementary Figure 3.4: Orientation-selective neurons in V1 (CA1) become more (less) selective with experience.

(**a**), Histogram of the selectivity index (SI) of all neurons averaged across conditions. Black bars: neurons with a SI ≥ 0.5 (≤ -0.5) were considered to be selective for ***A*** (***B***).

(**b**), Average responses of an example neuron to ***A*** (blue lines) and ***B*** (red lines) across presentations. Note the increase in selectivity between conditions 1 and 4, as well as between pre- and post-experience anesthesia. Gray shading indicates time window used to calculate SI. Blue and red shading indicate s.e.m.

(**c**), Average SI per condition for V1 as in **a**, showing the selectivity indices for each cell included (gray circles). Mean ± s.e.m. across animals. **: p = 0.0047, n.s.: p = 0.125, Wilcoxon Rank Sum test.

(**d**), As in **c**, but for CA1. *: p = 0.009; n.s.: p = 1, Wilcoxon Rank Sum test.

(**e**), Average activity of the same neurons (V1: black; CA1: green) shown in **c** per condition does not increase with time. Mean ± s.e.m. Conditions 1-4: V1: p = 0.093, CA1: p = 0.12 (conditions 1-4). Pre- and post-anesthesia: V1: p = 1.5e-5; CA1: p = 1, Wilcoxon Rank Sum test.

(**f**), Average trial-to-trial stereotypy of activity increased with experience. Shown is the mean correlation coefficient r of activity traces of neurons shown in **c** and **d** in different traversals with the same and across different conditions. Mean ± s.e.m. (Note, for this analysis traversals were subsampled to match stereotypy of running speed across conditions). Conditions 1-4: V1: p = 0.00085; CA1: p = 0.44. Pre- and post-anesthesia: V1: p = 2.5e-8; CA1: p = 1, Wilcoxon Rank Sum test.

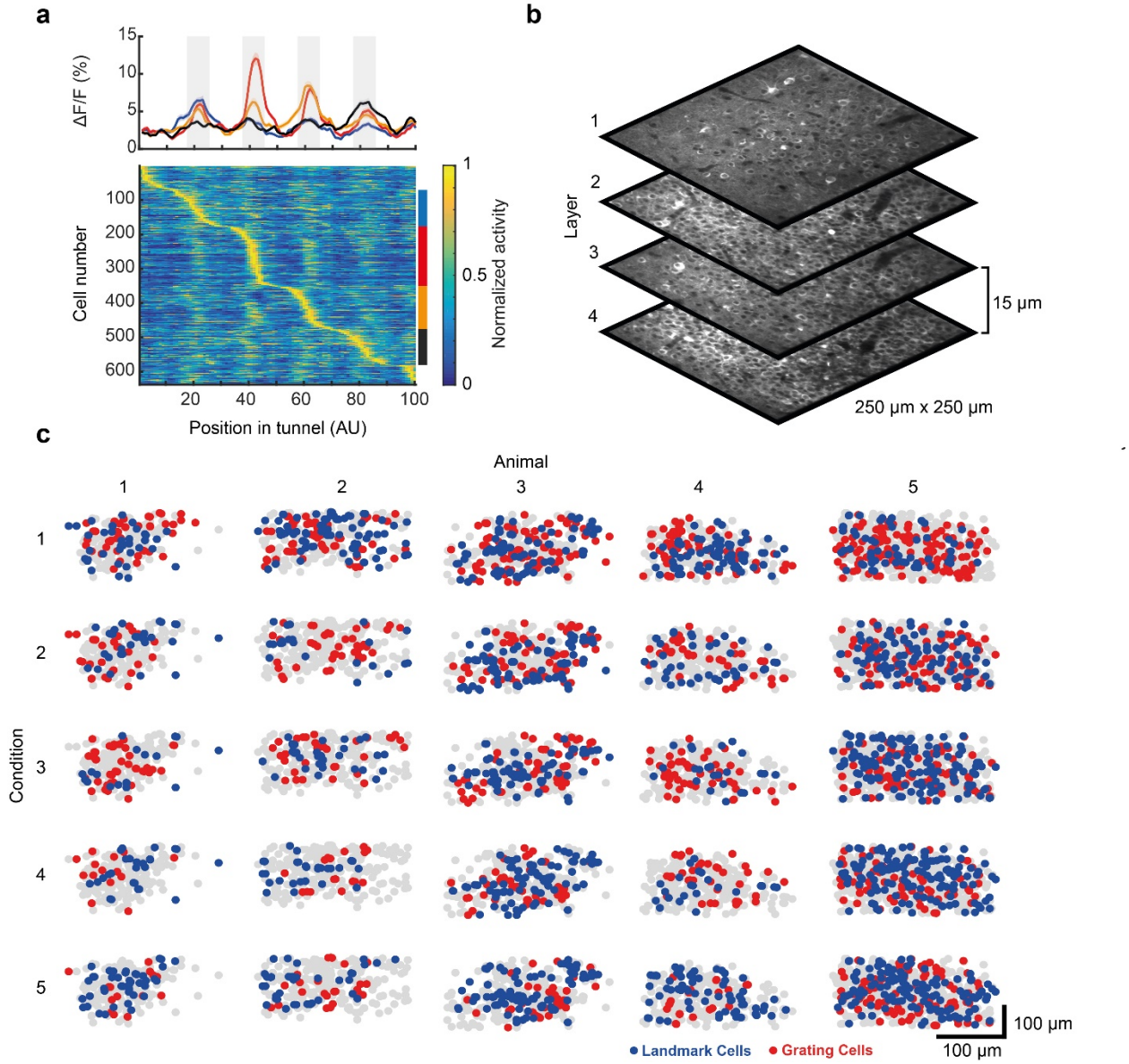

Supplementary Figure 3.5: Landmark responses in CA1 neurons.

(**a**), As in **Fig. 1g,** but for landmark responsive CA1 neurons. Note that neurons that respond to one landmark also exhibited responses to all other landmarks. Traces in the top panel are colored to indicate the neurons chosen from the matrix in the bottom panel.

(**b**), Schematic representation of the four-layer imaging in CA1. Field of view was approximately 250 µm by 250 µm and the spacing between the layers approximately 15 µm.

(**c**), Schematic representation of the position neurons in CA1 that responded to landmarks (blue), gratings (red), or were unresponsive (gray) for all five animals and conditions separately. Note, that there is no clear arrangement of neurons that respond to landmarks or gratings.

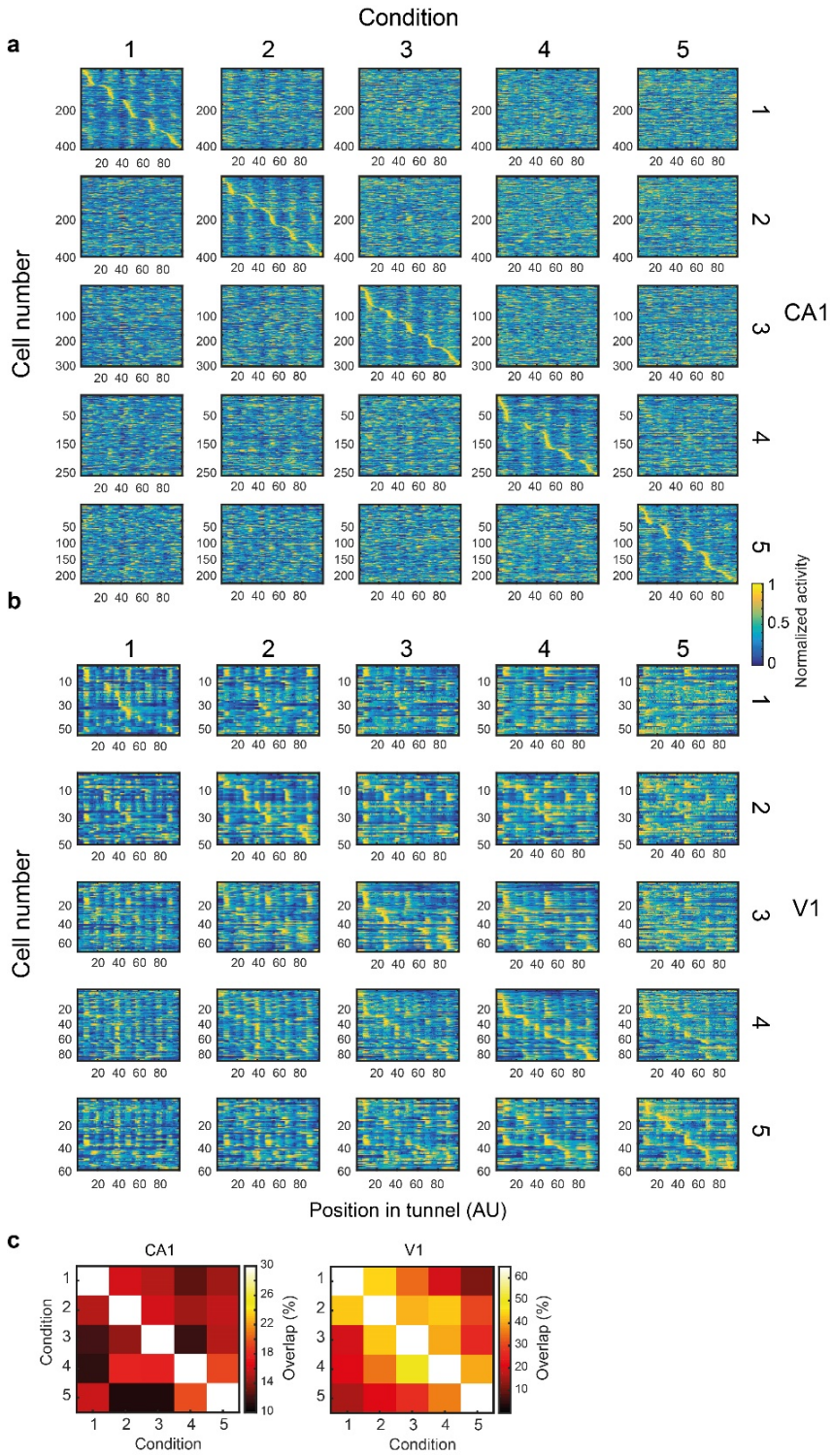

Supplementary Figure 3.6: Stability of grating responses between conditions is higher in V1 than in CA1.

(**a**), Normalized activity of grating selective CA1 neurons (SI ≥ 0.1) sorted by position of peak response in the tunnel. Selection of grating responsive neurons and sorting was done on condition 1 for the first row of plots. Data are shown for the same neurons using the same sorting for condition 2 through 5 in the remaining plots of the first row. Similarly for the remaining rows of plots.

(**b**), As in a, but for V1 data.

(**c**), Quantification of stability of responses in V1 and CA1. Shown is the fraction of neurons plotted in a and b that peak within 5% of tunnel length (or one texture length) between the conditions indicated.

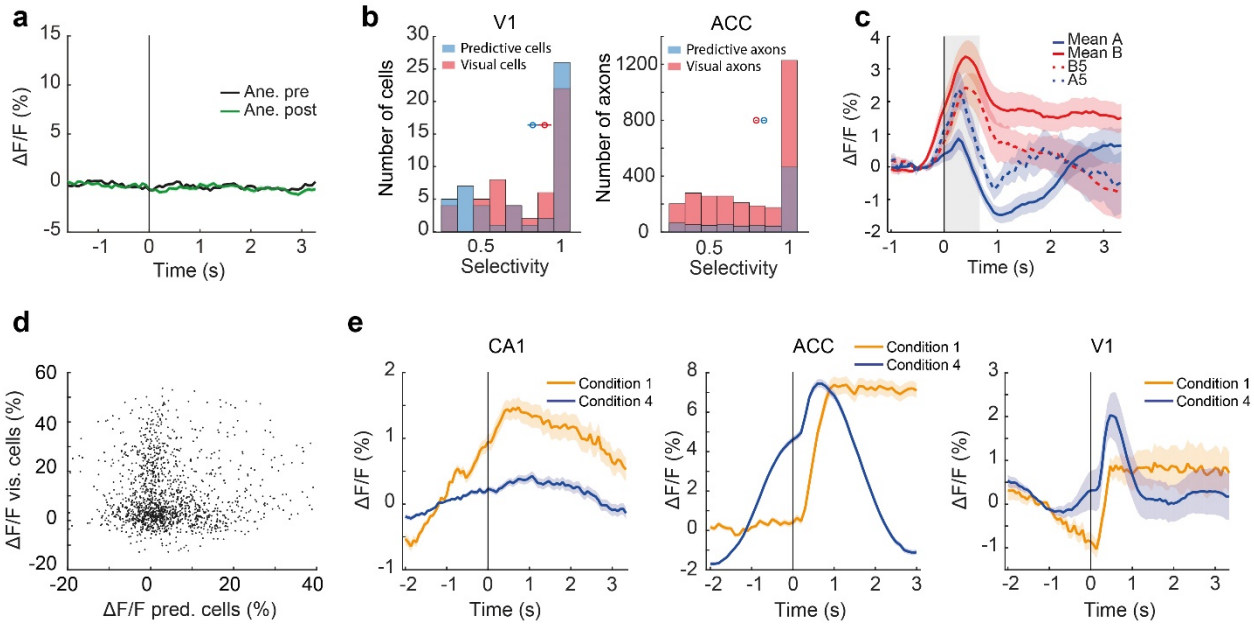

Supplementary Figure 3.7: Dynamics of predictive and visual responses in V1, CA1 and ACC.

(**a**), Mean grating response of predictive neurons shown in **Fig. 2b** during pre- and post-experience anesthesia conditions.

(**b**), Histogram of selectivity of predictive (blue) and visual (red) neurons in V1 (left) and ACC axons in V1 (right). Mean selectivity index (SI) was similar for all four populations (V1 predictive: SI = 0.79 ± 0.04, V1 visual 0.82 ± 0.03, ACC predictive: 0.84 ± 0.008, ACC visual: 0.79 ± 0.004). Colored circles indicate mean SI, horizontal bars indicate s.e.m.

(**c**), Mean grating-triggered responses of the 20% of neurons (n = 229) with the highest response to grating B4. Gray shading marks time window used to quantify responses. Colors and shading as in **Fig. 3e**.

(**d**), Mean activity of predictive neurons plotted against mean activity of visual neurons for each presentation of gratings ***A***3 and ***B***4 in condition 4.

(**e**), Grating responses in condition 1 (orange) and condition 4 (blue) for grating-selective neurons (SI>0.1) for CA1 neurons, ACC axons, and V1 neurons. Note, grating related responses in CA1 decrease with experience, and anticipatory responses emerge in ACC and V1 data.

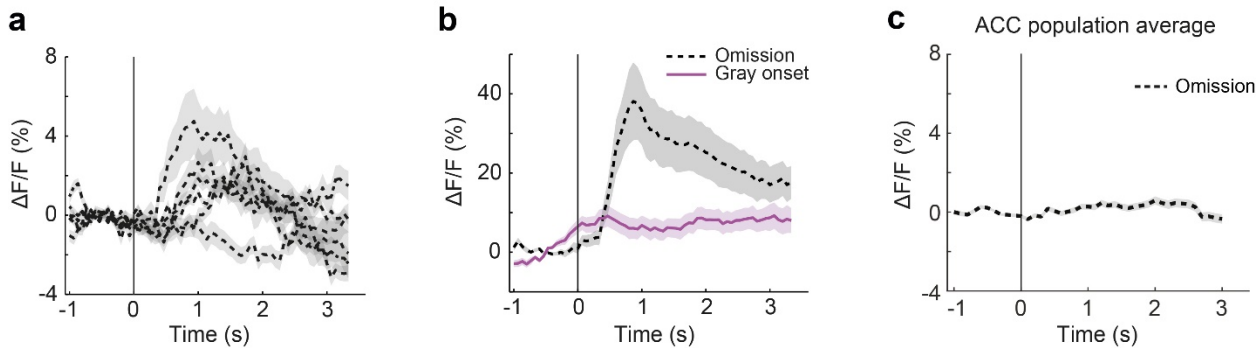

Supplementary Figure 3.8: Responses to grating omission are present in most animals and do not reflect sensorimotor mismatch.

(**a**), Population mean response to grating omission for each animal (dashed black lines, n=6). Shading indicates s.e.m.

(**b**), Responses of omission selective neurons to omission events and onsets of gray areas in the tunnel locations that are always encountered as gray. Shading indicates s.e.m.

(**c**), Average ACC axon population response (8599 axons) to the grating omission. Shading indicates s.e.m.

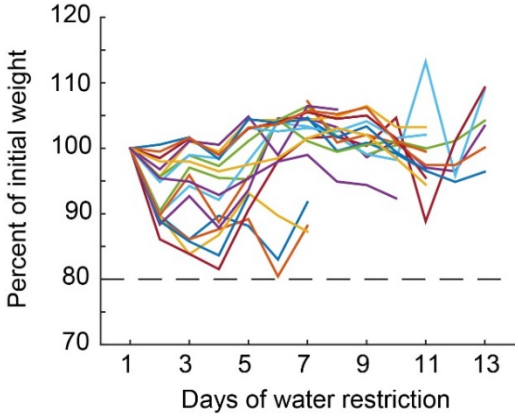

Supplementary Figure 3.9: Body weight trajectories.

Body weight in percent of starting weight for all animals used in V1 and CA1 experiments as a function of time since start of water restriction. Dashed line indicates the 80% threshold under which water restriction is halted.

Experimental procedures

Animals and imaging. All experiments were carried out in accordance with protocols approved by the Veterinary Office of the Canton of Basel, Switzerland. For the V1 experiments, we used imaging data from a total of 9 female C57BL/6 mice, aged 75 to 90 days at the start of the imaging series. For CA1 experiments, we used imaging data from a total of 6 female C57BL/6 mice, aged 60 to 80 days at the start of the imaging series, and for ACC experiments, a total of 5 female C57BL/6 mice, aged 71 days at the start of the imaging series. All animals were group-housed in a vivarium (light/dark cycle: 12/12 hours). The data of two V1 animals with visible z-axis motion were discarded. No statistical methods were used to pre-determine sample sizes, but our sample sizes are similar to those generally employed in the field. Mice were water restricted for the duration of the experiment, but allowed to drink water ad libitum for one hour per day in addition to receiving water rewards during experiments. Weight of all mice remained above 80% of starting weight (**Supplementary Fig. 3.9**). Viral injections and window implantation were performed as previously described (Leinweber et al., 2014). Briefly, mice were anesthetized using a mix of fentanyl (0.05 mg/kg), medetomidine (0.5 mg/kg) and midazolam (5 mg/kg) for all surgical procedures. For primary visual cortex imaging experiments, a craniotomy was made over visual cortex and AAV2/1-Ef1a-GCaMP6f-WPRE (titer 7.0 x 10^{10} or 5.0 x 10^{11} TU/ml) was injected, and the craniotomy was sealed with a 4 mm or 5 mm glass coverslip. For hippocampus imaging experiments, a 3 mm craniotomy was made above either left or right dorsal hippocampus and posterior parts of cortex were aspirated, and AAV2/1-Ef1a-NES-jRGECO1a-WPRE (Dana et al., 2016) (titer 1.2 x 10^{11} TU/ml) was injected into region CA1. The craniotomy was sealed with a 3 mm cover slip. For ACC axon imaging experiments, a craniotomy was made over visual cortex and sealed with a 4 mm glass coverslip. Additionally, a small craniotomy over ACC (0.3 mm lateral of bregma) was made and AAV2/1-Ef1a-GCaMP6f-WPRE (titer 1.0 x 10^{11} TU/ml) was injected before the region was sealed with cyanoacrylate. All viral vectors were injected at a volume of ~150 nl per site. A titanium head bar was attached to the skull and stabilized with dental cement. Imaging commenced 10 to 14 days (primary visual cortex), 23 days (hippocampus) or 30 days (ACC) following injection, and was done using a custom built two-photon microscope (Leinweber et al., 2014). Illumination source was an Insight DS laser (Spectra Physics) tuned to a wavelength of 910 nm. We used a 12 kHz resonance scanner (Cambridge Technology) for line scanning, which enabled frame rates of 60 Hz at 400 x 750 pixels resolution. Imaging of ACC axons was performed using an 8 kHz resonance scanner (Cambridge Technology) resulting in frame rates of 40 Hz at 400 x 750 pixels resolution. In addition, we used a piezo actuator (Physik Instrumente) to move the objective (Nikon 16x, 0.8 NA) in steps of 15 µm

between frames to acquire images at 4 different depths, thus reducing the effective frame rate to 15 Hz for the V1 and CA1 experiments, and 10 Hz for ACC experiments. Note, the use of different setups for axonal and cell body imaging were the result of lab logistics.

Virtual reality and behavior. The behavioral imaging setup was as previously described (Leinweber et al., 2014). Briefly, head-fixed mice were free to run on an air-supported polystyrene ball, the motion of which was restricted to the forward and backward directions by a pin (**Fig. 3.1a**). The ball's rotation was coupled to linear displacement in the virtual environment that was projected onto a toroidal screen surrounding the mouse. The screen covered a visual field of approximately 240 degrees horizontally and 100 degrees vertically. All elements of the tunnel including the gratings were calibrated to be isoluminant. Gratings were presented on a uniform gray area once the mouse entered the gray area. A reward zone was located at the end of the tunnel. Reaching the reward zone triggered a 5 s timeout during which the mouse could lick for a water reward provided by a spout located in front of the mouse. After the timeout, the mouse was teleported to the beginning of the tunnel to start the next trial. In early traversals animals were encouraged to run by applying occasional mild air puffs to the neck.

Experimental design. Experimental sessions were one to two hours long, and each behavioral condition consisted of two such sessions, one per day, spaced on average 24 hours apart. Behavioral conditions occurred on subsequent days, with the exception of condition 5 (grating omission), which took place immediately following condition 4. For anesthetized recordings, mice were lightly anesthetized using a mix of fentanyl (0.025 mg/kg), medetomidine (0.25 mg/kg) and midazolam (2.5 mg/kg) at half surgical dose, and head fixed on the setup and passively viewed the tunnel which was presented at a constant visual flow speed. The pre-experience anesthesia condition took place one day before condition 1, and post-experience anesthesia took place either immediately after condition 5 or the following day.

Statistics. Non-parametric tests were performed for all analyses (Wilcoxon Rank-Sum test, Wilcoxon Signed-Rank test). Paired tests were used where appropriate. No assumptions were made about data distributions in any of the analyses. Further details can be found in the Supplementary Methods Checklist, available online.

Data analysis. Imaging data were full-frame registered using a custom-written software (Leinweber et al., 2014). Neurons were selected manually based on their mean fluorescence or maximum projection. This biased our selection towards active neurons. Regions of interest in the axonal data were automatically selected by a combination of independent component analysis and image segmentation as previously described (Mukamel et al., 2009). Fluorescence traces were calculated as the mean pixel value in each region of interest per frame, and were then median-normalized to calculate ΔF/F. ΔF/F traces were filtered as previously described (Dombeck et al., 2007). No blinding of experimental condition was performed in any of the analyses.

Figure 3.1. For all plots of stimulus triggered fluorescence changes (**Figs. 3.1d, 3.2b-j, 3.3d-g, 3.4a-c, Supplementary Figs. 3.4b,3.7a,c,e and 3.8a-c**) fluorescence traces were mean-subtracted in a window 10 to 5 frames (-667 ms to -333 ms for V1 and CA1; -700ms to -300ms for ACC) preceding the stimulus onset unless noted otherwise. Neurons were classified as tunnel-responsive if their mean ΔF/F in a 10-frame (667 ms) window post-stimulus onset was at least 1.5% on average for any condition, for any grating or landmark stimulus in the tunnel.

Classification of grating position using neuronal activity was done using Matlab's TreeBagger algorithm. A separate classifier was trained on each condition for each animal. 500 classification trees were used for each classifier. The input to the classifier was the mean ΔF/F of each neuron for each grating presentation in each traversal within a 10-frame window post-grating onset. Traversals were randomly interleaved, and then activity was averaged over three of the randomly chosen traversals at a time. This was done to diminish the influence of trial-to-trial variability on classification. Traversals including an unexpected grating in position 5 in conditions 2 and 4 were omitted from the classification. Classification of spatial position was done as above except that activity was binned into each fifth of the virtual tunnel. For both paradigms, the training set consisted of one half of the randomly interleaved traversals in the condition. The classifier was tested on the other half of traversals. Performance of the classifier was evaluated as the mean accuracy, i.e. the mean of the diagonal of the confusion matrix for each condition per animal. When determining the effect of traversal speed on classification, we classified traversals with a mean speed of 15 cm/s or below as slow, and 19 cm/s and above as fast. For trace deconvolution, traces were first smoothed (mean in a sliding window of 5 frames (333 ms)). The smoothed traces were then deconvolved using an exponential decay kernel with a time constant $\tau = 0.5$ s.

We considered neurons as having stable activity peaks if the peak of each neuron's average activity in each condition was within 5% of tunnel length (5 bins), i.e. one texture length, between conditions.

Selectivity indices for each neuron were calculated using the mean ΔF/F in the same window post-grating onset. Neurons were assigned a selectivity index for a condition if at least one of the responses to a grating (mean ***A***1 + ***A***3 or mean ***B***2 + ***B***4) throughout the condition was at or above 1.5% ΔF/F. Otherwise, selectivity for the condition was set to 0. In **Supplementary Fig. 3.4**, neurons were considered selective if their absolute selectivity index (SI) was greater than 0.5 on average across the animals' experience. In order to measure stability of selective neurons we correlated fluorescence traces for each neuron, mapped to spatial coordinates, between traversals. We only included activity in the first 85% of the tunnel, to avoid differences due to the variable grating in position 5.

Figure 3.2. Predictive and visual neurons were sorted based on the position of the peak of their average ΔF/F post grating-onset over each condition. Predictive neurons were selected as exhibiting a peak within 333ms (5 frames) of grating onset, and visual neurons were selected as having a peak after 533 ms (8 frames). The window for calculating selectivity index was 133 ms pre- to 333 ms post grating onset (-2 to 5 frames) for predictive neurons, and 533 ms to 1000 ms (8 to 15 frames) post grating onset for visual neurons. In **Fig. 3.2b** and **c**, the baseline subtraction window for both plots was -1.33 s to -1 s (-15 to -10 frames). To compute the mean of predictive or visual neurons per traversal, the mean of each predictive neuron was taken in a 7-frame window post-grating onset (0 ms to 467 ms), and the mean of each visual neuron within a 8-frame to 15-frame (533 ms to 1s) window post-grating onset. These windows were always used to compute the mean responses for the respective class of neurons in other figures. To compare visually evoked stimulus responses in trials with high predictive activity versus those with high visual activity, we chose presentations with a predictive activity in the top 20th percentile in the 10-frame window following grating onset, and compared them to presentations with predictive activity in the bottom 20th percentile. We removed outlying traversals (with average activity values above 3σ from the mean, for predictive and visual neuron activity) before making this comparison. In Figure 2j, traversals with average predictive activity below median were classified as low-predictive traversals, and those above as high-predictive traversals.

Figure 3.3. In the ACC experiments animals experienced the same tunnel for conditions 1 through 3. Imaging was only done in condition 1 and 4. To simplify comparison of **Fig. 3.2h** and **Fig. 3.3e** we use ***B*** to denote the stimulus the animal saw in position 5 in condition 4. To select for stimulus-predictive ACC axons in **Fig. 3.3d**, we selected predictive axons as in V1 but on the second half of traversals in each

condition, and then plotted the responses of the selected axons in the first half of traversals. For this analysis we excluded 2 (of 5) sites with a low number of traversals in the respective conditions. In all other aspects axon selection was identical to neuron selection in the V1 data. To calculate the mean of ***B***-predictive and ***A***-predictive axons in **Fig. 3.3e**, we first mean-subtracted as described above to select neurons, and then measured mean activity after a mean-subtraction of 1 s to 500 ms preceding onset.

Figure 3.4. Omission-selective neurons were selected as having a mean ΔF/F response larger than 10% to the omission and as having an omission selectivity index larger than 0.33. The omission selectivity index is defined as $SI_{OM} = (R_{OM} - R_{max})/(R_{OM} + R_{max})$, where R_{OM} is the mean response to the omission for each neuron and R_{max} is the largest mean response to any other grating in the tunnel. For statistical comparison of omission-selective neuron activity in traversals with high and low predictive activity (**Fig. 3.4c**), data were bootstrapped 10 times with random replacement then a Wilcoxon rank-sum test was performed on the bootstrapped data.

Code Availability. All imaging and image processing code can be found online at https://sourceforge.net/projects/iris-scanning/code (IRIS, imaging software package) and https://sourceforge.net/p/iris-scanning/calliope/HEAD/tree (Calliope, image processing software package). Code used for all data analysis is available from the corresponding author upon request.

Data Availability. The data that support the findings of this study are available from the corresponding author upon request.

Epilogue

Learning takes place constantly throughout life in the nervous system, it serves to adapt to new environmental circumstances and helps to succeed with new challenges. Learning recruits new neuronal assemblies, involves the rearrangement of subcellular components and induces gene expression (Holtmaat and Caroni, 2016). The immediate early genes Arc, c-Fos and EGR1 have been described more than twenty years ago and linked to learning related, plastic changes in the nervous system (Bramham et al., 2010; Curran and Morgan, 1995; Veyrac et al., 2014). These genes and their role during learning and plasticity have been characterized with histological methods mainly in the light of classical learning paradigms, but less so in the framework of predictive coding. With the advance of technology it is now possible to record immediate early gene expression and neuronal activity at the same time in vivo. This allows to gain deeper insight into plastic changes of neuronal activity and gene expression during sensorimotor and associative learning. This thesis is in line with the notion that the expression of immediate early genes is shaped by neuronal activity and supports the view that the expression of these genes can be linked to plastic changes in the functional type of input during learning.

Specificity of immediate early genes to functional types of neurons during learning

Chapter 1 of this thesis shows that the expression of the immediate early genes Arc and EGR1, less so c-Fos, can be correlated with the functional type of input a neuron in visual cortex layer 2/3 receives during sensorimotor-learning. By using transgenic mouse lines, which express the immediate early gene of interest either fused to GFP or drive GFP expression through the endogenous promoter, and red-shifted calcium indicator (jRGECO1a) it is possible to simultaneously record both IEG expression and neuronal activity. When stimulating visual cortex with drifting grating stimuli after an over-night dark adaptation, we find a positive correlation of IEG expression and neuronal activity (**Figure 1.1**). During sensorimotor-learning we show an increase in Arc expression and a decrease in EGR1 expression at the time of exposure to a 12/12h dark/light cycle. Such changes in average IEG expression go along with rearrangements of the IEG expression level pattern during learning (**Figure 1.2**). Additionally we find a rearrangement of the motor-related input in visual cortex during sensorimotor-learning (**Figure 1.3**). When selecting neurons with high IEG expression at the time of exposure to the 12/12h dark/light cycle, we observe a preference

for the functional type of input these high IEG neurons receive. Neurons with high Arc expression preferentially receive excitatory visual input and inhibitory motor-related input, as in contrast neurons with high EGR1 expression preferentially receive excitatory motor-related input (**Figure 1.4**). These results indicate a specificity of IEG expression for the plastic changes of the functional type of input a neuron receives in layer 2/3 of mouse visual cortex. The framework of predictive coding allows for three categories of predictions in visual cortex. Neurons in category I compute a negative prediction error and signal whenever there's too much running compared to visual flow. In contrast neurons in category II compute a positive prediction error and signal whenever there's too much visual flow compared to running, see (Attinger et al., 2017) for a detailed description. Based on the results in chapter 1 we speculate that neurons with high Arc expression might be associated with computations of category II, whereas neurons with high EGR1 expression might be associated with computation of category I. In line with such an interpretation we see a bias of high Arc/EGR1 neurons towards positive/negative mismatch signals (**Figure 1.4**)

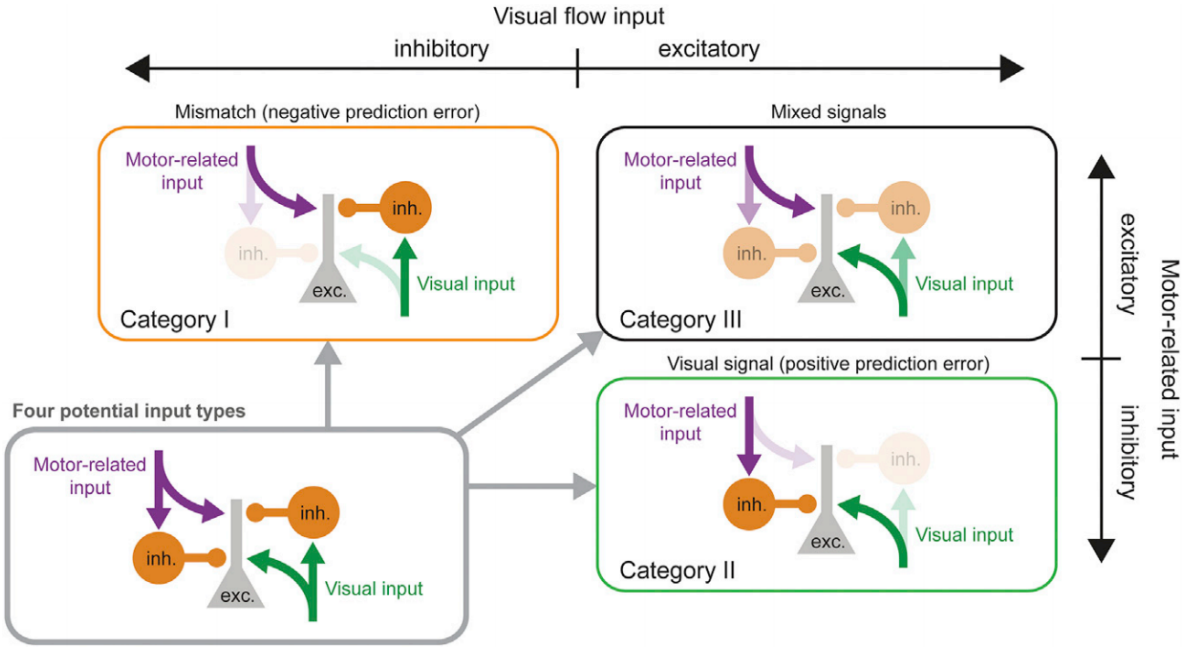

Figure 5: Three categories of circuit motifs for forming comparisons.

Visual and motor-related input can be used to from comparisons of too little visual flow (category I) or too much visual flow (category II). Note that signals of category II are indistinguishable under anesthesia from "classical" visual responses. Image from: (Attinger et al., 2017)

Such specific expression of immediate early genes might not be restricted to visual cortex. Chapter2 of this thesis shows that during associative learning both neurons with high expression of Arc and c-Fos undergo the most plastic changes to the relevant stimulus during learning. We find a positive correlation of immediate early gene expression and average neuronal activity and a stable pattern of expression of these two IEGs (**Figure 2.3**). When looking at the reward-associated stimuli in the paradigm, the tones, we observe a specific increase in the response to this stimulus of high Arc and c-Fos neurons with learning (**Figure 2.4**). These results indicate that the expression of Arc and c-Fos in the hippocampal CA1 area can be linked to specific input a neurons receives, confirming our conclusions from experiments done in visual cortex. It is interesting to note though that c-Fos might be differentially regulated and expressed across brain areas, as such a specificity to changes in the functional type of input were stronger in CA1.

Interestingly two other immediate early genes have been reported to show specificity to the input a neuron receives. The immediate early gene NARP (Tsui et al., 1996) has been described to be exclusively expressed in parvalbumin-positive (PV+) inhibitory neurons and specifically scales excitatory synapse onto these PV+ interneurons (Chang et al., 2010; Gu et al., 2013). Recently it was shown that the IEG Npas4 (Bloodgood et al., 2013) does not only regulate excitatory-inhibitory balance in a cell type specific manner (Spiegel et al., 2014), but also specifically regulates plasticity of mossy-fiber input onto neurons in the hippocampal CA3 area (Weng et al., 2018). Both studies underline the notion that immediate early genes play a critical role in plasticity and can be linked to specific functional input.

Learning shapes sensory processing

Plasticity in the nervous system is key for learning. Chapter 1 and 2 describe how plasticity-related genes influence sensory processing with learning. In Chapter 3 we show that learning about the visual environment shapes sensory processing and alters the strength of neuronal signals to identical visual stimuli based on their spatial location (**Figure 3.1**). In addition we find that V1 neurons develop predictive responses to approaching visual stimuli with experience (**Figure 3.2**). One source of such predictive responses is anterior cingulate cortex (ACC), as projections from ACC to V1 carry visual stimulus predictions (**Figure 3.3**). Intriguingly we also observe that the omission of an expected visual stimulus strongly drives activity in V1 (**Figure 3.4**). In summary we find predictive and visual signals for visual stimuli in visual cortex, which are shaped by the animal's location in space and develop plastically with learning.

Outlook and concluding remarks

While more and more pieces of the puzzle of immediate early gene expression are coming together, some open questions remain. The predictive coding theory states a comparison of top-down motor-related signals and bottom-up visual signals in visual cortex. If other brain areas use a similar mechanism of top-down and bottom-up signal comparison, it would be interesting to see evidence for the bias of EGR1 towards top-down and Arc towards bottom-up signals holds true. Somatosensory area S1 (barrel cortex) receives input from motor cortex (Pierre and Martin, 2003), providing the substrate for the testable hypothesis of a comparison of motor-related and somatosensory input. If again neurons with high EGR1/Arc expression could be correlated with the functional type of input a neuron in barrel cortex receives, it would support the notion that IEGs can be linked to a functional type of synaptic input. In general, this would lay ground for a change in the view of what triggers the expression of immediate early genes. Classically these genes have been seen as markers for average activity, in the light of new results it is worth designing experiments that address the question if the expression of these genes is more specific and related to plastic changes of a functional input neurons receive.

References

Aghajan, Z.M., Acharya, L., Moore, J.J., Cushman, J.D., Vuong, C., Mehta, M.R., 2014. Impaired spatial selectivity and intact phase precession in two-dimensional virtual reality. Nat. Neurosci. 18, 121–128. doi:10.1038/nn.3884

Alberini, C.M., 2009. Transcription factors in long-term memory and synaptic plasticity. Physiol. Rev. 89, 121–45. doi:10.1152/physrev.00017.2008

Alexander, A.S., Nitz, D.A., 2015. Retrosplenial cortex maps the conjunction of internal and external spaces. Nat. Neurosci. doi:10.1038/nn.4058

Attinger, A., Wang, B., Keller, G.B., 2017. Visuomotor Coupling Shapes the Functional Development of Mouse Visual Cortex. Cell 169, 1291–1302.e14. doi:http://dx.doi.org/10.1016/j.cell.2017.05.023

Barlow, H.B., 1953. Summation and inhibition in the frog's retina. J. Physiol. 119, 69–88.

Barth, A.L., Gerkin, R.C., Dean, K.L., 2004. Alteration of Neuronal Firing Properties after In Vivo Experience in a FosGFP Transgenic Mouse. J. Neurosci. 24, 6466–6475. doi:10.1523/JNEUROSCI.4737-03.2004

Bastos, A.M., Usrey, W.M., Adams, R.A., Mangun, G.R., Fries, P., Friston, K.J., 2012. Canonical Microcircuits for Predictive Coding. Neuron 76, 695–711. doi:10.1016/j.neuron.2012.10.038

Bell, C.C., 1982. Properties of a modifiable efference copy in an electric fish. J. Neurophysiol. 47, 1043–1056.

Bi, G.Q., Poo, M.M., 1998. Synaptic Modifications in Cultured Hippocampal Neurons: Dependence on Spike Timing, Synaptic Strength, and Postsynaptic Cell Type. J. Neurosci. 18, 10464 LP-10472.

Bliss, T.V.P., Lomo, T., Lømo, T., 1973. Long-lasting potentiation of synaptic transmission in the dentate area of the anaesthetized rabbit following stimulation of the perforant path. J. Physiol. 232, 331–356. doi:10.1113/jphysiol.1973.sp010273

Bloodgood, B.L., Sharma, N., Browne, H.A., Trepman, A.Z., Greenberg, M.E., 2013. The activity-dependent transcription factor NPAS4 regulates domain-specific inhibition. Nature 503, 121–125.

Bozon, B., Kelly, A., Josselyn, S.A., Silva, A.J., Davis, S., Laroche, S., 2003. MAPK, CREB and zif268 are all required for the consolidation of recognition memory. Philos. Trans. R. Soc. Lond. B. Biol. Sci. 358, 805–14. doi:10.1098/rstb.2002.1224

Bramham, C.R., Alme, M.N., Bittins, M., Kuipers, S.D., Nair, R.R., Pai, B., Panja, D., Schubert, M., Soule, J., Tiron, A., Wibrand, K., 2010. The Arc of synaptic memory. Exp. Brain Res. 200, 125–40. doi:10.1007/s00221-009-1959-2

Bullitt, E., 1990. Expression of C-fos-like protein as a marker for neuronal activity following noxious stimulation in the rat. J. Comp. Neurol. 296, 517–530. doi:10.1002/cne.902960402

Chang, M.C., Park, J.M., Pelkey, K.A., Grabenstatter, H.L., Xu, D., Linden, D.J., Sutula, T.P., McBain, C.J., Worley, P.F., 2010. Narp regulates homeostatic scaling of excitatory synapses on parvalbumin-expressing interneurons. Nat Neurosci 13, 1090–1097.

Chen, T.W., Wardill, T.J., Sun, Y., Pulver, S.R., Renninger, S.L., Baohan, A., Schreiter, E.R., Kerr, R.A.,

Orger, M.B., Jayaraman, V., Looger, L.L., Svoboda, K., Kim, D.S., 2013. Ultrasensitive fluorescent proteins for imaging neuronal activity. Nature 499, 295–300. doi:10.1038/nature12354

Cho, J., Sharp, P.E., 2001. Head direction, place, and movement correlates for cells in the rat retrosplenial cortex. Behav. Neurosci. 115, 3–25. doi:10.1037/0735-7044.115.1.3

Chowdhury, S., Shepherd, J.D., Okuno, H., Lyford, G., Petralia, R.S., Plath, N., Kuhl, D., Huganir, R.L., Worley, P.F., 2006. Arc/Arg3.1 Interacts with the Endocytic Machinery to Regulate AMPA Receptor Trafficking. Neuron 52, 445–459. doi:10.1016/J.NEURON.2006.08.033

Cochran, B.H., Reffel, A.C., Stiles, C.D., 1983. Molecular cloning of gene sequences regulated by platelet-derived growth factor. Cell 33, 939–947. doi:10.1016/0092-8674(83)90037-5

Cole, A.J., Saffen, D.W., Baraban, J.M., Worley, P.F., 1989. Rapid increase of an immediate early gene messenger RNA in hippocampal neurons by synaptic NMDA receptor activation. Nature 340, 474–476. doi:10.1038/340474a0

Connor, D.H., Clack, N.G., Huber, D., Komiyama, T., Myers, E.W., Svoboda, K., 2010. Vibrissa-Based Object Localization in Head-Fixed Mice. J. Neurosci. 30, 1947 LP-1967.

Curran, T., Morgan, J.I., 1995. Fos: An immediate-early transcription factor in neurons. J. Neurobiol. 26, 403–412. doi:10.1002/neu.480260312

Curran, T., Teich, N.M., 1982. Candidate product of the FBJ murine osteosarcoma virus oncogene: characterization of a 55,000-dalton phosphoprotein. J. Virol. 42, 114–122.

Dana, H., Mohar, B., Sun, Y., Narayan, S., Gordus, A., Hasseman, J.P., Tsegaye, G., Holt, G.T., Hu, A., Walpita, D., Patel, R., Macklin, J.J., Bargmann, C.I., Ahrens, M.B., Schreiter, E.R., Jayaraman, V., Looger, L.L., Svoboda, K., Kim, D.S., 2016. Sensitive red protein calcium indicators for imaging neural activity. Elife 5, e12727. doi:10.7554/eLife.12727

Denny, C.A., Kheirbek, M.A., Alba, E.L., Tanaka, K.F., Brachman, R.A., Laughman, K.B., Tomm, N.K., Turi, G.F., Losonczy, A., Hen, R., 2014. Hippocampal Memory Traces Are Differentially Modulated by Experience, Time, and Adult Neurogenesis. Neuron 83, 189–201. doi:http://dx.doi.org/10.1016/j.neuron.2014.05.018

Dombeck, D.A., Harvey, C.D., Tian, L., Looger, L.L., Tank, D.W., 2010. Functional imaging of hippocampal place cells at cellular resolution during virtual navigation. Nat. Neurosci. 13, 1433–1440. doi:10.1038/nn.2648

Dombeck, D.A., Khabbaz, A.N., Collman, F., Adelman, T.L., Tank, D.W., 2007. Imaging large-scale neural activity with cellular resolution in awake, mobile mice. Neuron 56, 43–57. doi:10.1016/j.neuron.2007.08.003

Dragunow, M., Faull, R., 1989. The use of c-fos as a metabolic marker in neuronal pathway tracing. J. Neurosci. Methods 29, 261–265. doi:http://dx.doi.org/10.1016/0165-0270(89)90150-7

Dragunow, M., Robertson, H.A., 1987. Kindling stimulation induces c-fos protein(s) in granule cells of the rat dentate gyrus. Nature 329, 441–442. doi:10.1038/329441a0

Duclot, F., Kabbaj, M., 2017. The Role of Early Growth Response 1 (EGR1) in Brain Plasticity and Neuropsychiatric Disorders . Front. Behav. Neurosci. .

Eichenbaum, H., Mathews, P., Cohen, N.J., 1989. Further studies of hippocampal representation during

odor discrimination learning. 103. doi:10.1037/0735-7044.103.6.1207

Eliades, S.J., Wang, X., 2008. Neural substrates of vocalization feedback monitoring in primate auditory cortex. Nature 453, 1102–6. doi:10.1038/nature06910

Engert, F., Bonhoeffer, T., 1999. Dendritic spine changes associated with hippocampal long-term synaptic plasticity. Nature 399, 66–70. doi:10.1038/19978

Fiser, A., Mahringer, D., Oyibo, H.K., Petersen, A. V, Leinweber, M., Keller, G.B., 2016. Experience-dependent spatial expectations in mouse visual cortex. Nat Neurosci advance on, 1658–1664. doi:10.1038/nn.4385

Flavell, S.W., Cowan, C.W., Kim, T.-K., Greer, P.L., Lin, Y., Paradis, S., Griffith, E.C., Hu, L.S., Chen, C., Greenberg, M.E., 2006. Activity-Dependent Regulation of MEF2 Transcription Factors Suppresses Excitatory Synapse Number. Science (80-.). 311, 1008 LP-1012.

Fleischmann, A., Hvalby, O., Jensen, V., Strekalova, T., Zacher, C., Layer, L.E., Kvello, A., Reschke, M., Spanagel, R., Sprengel, R., Wagner, E.F., Gass, P., 2003. Impaired Long-Term Memory and NR2A-Type NMDA Receptor-Dependent Synaptic Plasticity in Mice Lacking c-Fos in the CNS. J. Neurosci. 23, 9116 LP-9122.

Frankland, P.W., Bontempi, B., Talton, L.E., Kaczmarek, L., Silva, A.J., 2004. The Involvement of the Anterior Cingulate Cortex in Remote Contextual Fear Memory. Science (80-.). 304, 881–883. doi:10.1126/science.1094804

French, P.J., O'Connor, V., Jones, M.W., Davis, S., Errington, M.L., Voss, K., Truchet, B., Wotjak, C., Stean, T., Doyère, V., Maroun, M., Laroche, S., Bliss, T. V, 2001. Subfield-specific immediate early gene expression associated with hippocampal long-term potentiation in vivo. Eur. J. Neurosci. 13, 968–76.

Gandolfi, D., Cerri, S., Mapelli, J., Polimeni, M., Tritto, S., Fuzzati-Armentero, M.-T., Bigiani, A., Blandini, F., Mapelli, L., D'Angelo, E., 2017. Activation of the CREB/c-FosPathway during Long-Term Synaptic Plasticity in the Cerebellum Granular Layer. Front. Cell. Neurosci. 11, 184. doi:10.3389/fncel.2017.00184

Gao, M., Sossa, K., Song, L., Errington, L., Cummings, L., Hwang, H., Kuhl, D., Worley, P., Lee, H.-K., 2010. A Specific Requirement of Arc/Arg3.1 for Visual Experience-Induced Homeostatic Synaptic Plasticity in Mouse Primary Visual Cortex. J. Neurosci. 30, 7168–7178. doi:10.1523/JNEUROSCI.1067-10.2010

Garner, A.R., Rowland, D.C., Hwang, S.Y., Baumgaertel, K., Roth, B.L., Kentros, C., Mayford, M., 2012. Generation of a Synthetic Memory Trace. Science (80-.). 335, 1513 LP-1516.

Gavornik, J.P., Bear, M.F., 2014. Learned spatiotemporal sequence recognition and prediction in primary visual cortex. Nat. Neurosci. 17, 732–7. doi:10.1038/nn.3683

Greenberg, M.E., Ziff, E.B., 1984. Stimulation of 3T3 cells induces transcription of the c-fos proto-oncogene. Nature 311, 433–438.

Gu, Y., Huang, S., Chang, M.C., Worley, P., Kirkwood, A., Quinlan, E.M., 2013. Obligatory Role for the Immediate Early Gene NARP in Critical Period Plasticity. Neuron 79, 335–346. doi:https://doi.org/10.1016/j.neuron.2013.05.016

Guzowski, J.F., Lyford, G.L., Stevenson, G.D., Houston, F.P., McGaugh, J.L., Worley, P.F., Barnes, C. a, 2000. Inhibition of activity-dependent arc protein expression in the rat hippocampus impairs the maintenance of long-term potentiation and the consolidation of long-term memory. J. Neurosci. 20, 3993–4001.

Guzowski, J.F., McNaughton, B.L., Barnes, C.A., Worley, P.F., 1999. Environment-specific expression of the immediate-early gene Arc in hippocampal neuronal ensembles. Nat. Neurosci. 2, 1120–1124. doi:10.1038/16046

Guzowski, J.F., Setlow, B., Wagner, E.K., McGaugh, J.L., 2001. Experience-Dependent Gene Expression in the Rat Hippocampus after Spatial Learning: A Comparison of the Immediate-Early Genes. J. Neurosci. 21, 5089 LP-5098.

Guzowski, J.F., Timlin, J.A., Roysam, B., McNaughton, B.L., Worley, P.F., Barnes, C.A., 2005. Mapping behaviorally relevant neural circuits with immediate-early gene expression. Curr. Opin. Neurobiol. 15, 599–606. doi:http://dx.doi.org/10.1016/j.conb.2005.08.018

Hafting, T., Fyhn, M., Molden, S., Moser, M.B., Moser, E., 2005. Microstructure of a spatial map in the entorhinal cortex. Nature 436, 801–6. doi:10.1038/nature03721

Hartline, H.K., 1938. The Response of single optic nerve fibers of the vertebrate eye to illumination of the retina. Am. J. Physiol. Content 121, 400–415. doi:10.1152/ajplegacy.1938.121.2.400

Hebb, D.O., 1949. The organization of behavior: A neuropsychological approach. John Wiley & Sons.

Hess, U.S., Lynch, G., Gall, C.M., 1995a. Regional patterns of c-fos mRNA expression in rat hippocampus following exploration of a novel environment versus performance of a well-learned discrimination. J. Neurosci. 15, 7796–809.

Hess, U.S., Lynch, G., Gall, C.M., 1995b. Changes in c-fos mRNA expression in rat brain during odor discrimination learning: differential involvement of hippocampal subfields CA1 and CA3. J. Neurosci. 15, 4786–95.

Holscher, C., Schnee, A., Dahmen, H., Setia, L., Mallot, H., 2005. Rats are able to navigate in virtual environments. J. Exp. Biol. 208, 561.

Holtmaat, A., Caroni, P., 2016. Functional and structural underpinnings of neuronal assembly formation in learning. Nat Neurosci advance on.

Hubel, B.Y.D.H., Wiesel, A.D.T.N., 1962. Receptive fields, binocular interaction and fuctional architecture in the cat's visual cortex. J. Physiol. 106–154.

Inoue, M., Takeuchi, A., Horigane, S., Ohkura, M., Gengyo-Ando, K., Fujii, H., Kamijo, S., Takemoto-Kimura, S., Kano, M., Nakai, J., Kitamura, K., Bito, H., 2014. Rational design of a high-affinity, fast, red calcium indicator R-CaMP2. Nat. Methods 12, 64.

Itskov, P.M., Vinnik, E., Honey, C., Schnupp, J., Diamond, M.E., 2012. Sound sensitivity of neurons in rat hippocampus during performance of a sound-guided task. J. Neurophysiol. 107, 1822–1834. doi:10.1152/jn.00404.2011

Jenks, K.R., Kim, T., Pastuzyn, E.D., Okuno, H., Taibi, A. V, Bito, H., Bear, M.F., Shepherd, J.D., 2017. Arc restores juvenile plasticity in adult mouse visual cortex. Proc. Natl. Acad. Sci. 114, 9182–9187. doi:10.1073/pnas.1700866114

Ji, D., Wilson, M.A., 2007. Coordinated memory replay in the visual cortex and hippocampus during sleep. Nat. Neurosci. 10, 100–7. doi:10.1038/nn1825

Jorgensen, M.B., Deckert, J., Wright, D.C., Gehlert, D.R., 1989. Delayed c-fos proto-oncogene expression in the rat hippocampus induced by transient global cerebral ischemia: an in situ hybridization study. Brain Res. 484, 393–398. doi:https://doi.org/10.1016/0006-8993(89)90388-0

Kandel, E.R., 2013. Principles of Neural Science, Fifth Edition, Principles of Neural Science. McGraw-Hill Education.

Kanizsa, G., 1976. Subjective contours. Sci. Am. doi:10.1038/scientificamerican0476-48

Kawashima, T., Okuno, H., Bito, H., 2014. A new era for functional labeling of neurons: activity-dependent promoters have come of age. Front. Neural Circuits 8, 37. doi:10.3389/fncir.2014.00037

Keller, G.B., Bonhoeffer, T., Hübener, M., 2012. Sensorimotor mismatch signals in primary visual cortex of the behaving mouse. Neuron 74, 809–15. doi:10.1016/j.neuron.2012.03.040

Keller, G.B., Hahnloser, R., 2009. Neural processing of auditory feedback during vocal practice in a songbird. Nature 457, 187–90. doi:10.1038/nature07467

Kelly, M.P., Deadwyler, S.A., 2002. Acquisition of a novel behavior induces higher levels of Arc mRNA than does overtrained performance. Neuroscience 110, 617–26.

Kim, A.J., Fenk, L.M., Lyu, C., Maimon, G., 2017. Quantitative Predictions Orchestrate Visual Signaling in Drosophila. Cell 168, 280–294.e12. doi:10.1016/j.cell.2016.12.005

Kim, A.J., Fitzgerald, J.K., Maimon, G., 2015. Cellular evidence for efference copy in Drosophila visuomotor processing. Nat. Neurosci. 18, 1247–1255. doi:10.1038/nn.4083

Knapska, E., Kaczmarek, L., 2004. A gene for neuronal plasticity in the mammalian brain: Zif268/Egr-1/NGFI-A/Krox-24/TIS8/ZENK? Prog. Neurobiol. 74, 183–211. doi:http://dx.doi.org/10.1016/j.pneurobio.2004.05.007

Lau, L.F., Nathans, D., 1987. Expression of a set of growth-related immediate early genes in BALB/c 3T3 cells: coordinate regulation with c-fos or c-myc. Proc. Natl. Acad. Sci. U. S. A. 84, 1182–6.

Le Gal La Salle, G., 1988. Long-lasting and sequential increase of c-fos oncoprotein expression in kainic acid-induced status epilepticus. Neurosci. Lett. 88, 127–30.

Lee, H., Simpson, G. V, Logothetis, N.K., Rainer, G., 2005. Phase locking of single neuron activity to theta oscillations during working memory in monkey extrastriate visual cortex. Neuron 45, 147–56. doi:10.1016/j.neuron.2004.12.025

Leinweber, M., Ward, D.R., Sobczak, J.M., Attinger, A., Keller, G.B., 2017. A Sensorimotor Circuit in Mouse Cortex for Visual Flow Predictions. Neuron 95, 1420–1432.e5. doi:10.1016/J.NEURON.2017.08.036

Leinweber, M., Zmarz, P., Buchmann, P., Argast, P., Hübener, M., Bonhoeffer, T., Keller, G.B., 2014. Two-photon Calcium Imaging in Mice Navigating a Virtual Reality Environment. J. Vis. Exp. e50885. doi:10.3791/50885

Link, W., Konietzko, U., Kauselmann, G., Krug, M., Schwanke, B., Frey, U., Kuhl, D., 1995. Somatodendritic expression of an immediate early gene is regulated by synaptic activity. Proc. Natl.

Acad. Sci. U. S. A. 92, 5734–8.

Liu, X., Ramirez, S., Pang, P.T., Puryear, C.B., Govindarajan, A., Deisseroth, K., Tonegawa, S., 2012. Optogenetic stimulation of a hippocampal engram activates fear memory recall. Nature 484, 381–5. doi:10.1038/nature11028

Lyford, G.L., Yamagata, K., Kaufmann, W.E., Barnes, C. a, Sanders, L.K., Copeland, N.G., Gilbert, D.J., Jenkins, N.A., Lanahan, A.A., Worley, P.F., 1995. Arc, a growth factor and activity-regulated gene, encodes a novel cytoskeleton-associated protein that is enriched in neuronal dendrites. Neuron 14, 433–45.

Mackler, S.A., Brooks, B.P., Eberwine, J.H., 1992. Stimulus-Induced Coordinate Changes in mRNA Abundance in Single Postsynaptic Hippocampal CA1 Neurons. Neuron 9, 539–548.

Maletic-Savatic, M., Malinow, R., Svoboda, K., 1999. Rapid Dendritic Morphogenesis in CA1 Hippocampal Dendrites Induced by Synaptic Activity. Science (80-.). 283, 1923 LP-1927.

Mataga, N., Fujishima, S., Condie, B.G., Hensch, T.K., 2001. Experience-Dependent Plasticity of Mouse Visual Cortex in the Absence of the Neuronal Activity-Dependent Markeregr1/zif268 . J. Neurosci. 21, 9724–9732.

Maviel, T., Durkin, T.P., Menzaghi, F., Bontempi, B., 2004. Sites of neocortical reorganization critical for remote spatial memory. Science 305, 96–9. doi:10.1126/science.1098180

McCool, C.H., Britten, K.H., 2008. Cortical Processing of Visual Motion, in: The Senses: A Comprehensive Reference. Elsevier, pp. 157–187. doi:10.1016/B978-012370880-9.00308-X

McCurry, C.L., Shepherd, J.D., Tropea, D., Wang, K.H., Bear, M.F., Sur, M., 2010. Loss of Arc renders the visual cortex impervious to the effects of sensory experience or deprivation. Nat. Neurosci. 13, 450–7. doi:10.1038/nn.2508

Mermelstein, P.G., Bito, H., Deisseroth, K., Tsien, R.W., 2000. Critical Dependence of cAMP Response Element-Binding Protein Phosphorylation on L-Type Calcium Channels Supports a Selective Response to EPSPs in Preference to Action Potentials. J. Neurosci. 20, 266 LP-273.

Messaoudi, E., Kanhema, T., Soulé, J., Tiron, A., Dagyte, G., da Silva, B., Bramham, C.R., 2007. Sustained Arc/Arg3.1 synthesis controls long-term potentiation consolidation through regulation of local actin polymerization in the dentate gyrus in vivo. J. Neurosci. 27, 10445–55. doi:10.1523/JNEUROSCI.2883-07.2007

Milbrandt, J., 1987. A nerve growth factor-induced gene encodes a possible transcriptional regulatory factor. Science (80-.). 238, 797 LP-799.

Miller, M.W., Vogt, B.A., 1984. Direct connections of rat visual cortex with sensory, motor, and association cortices. J. Comp. Neurol. 226, 184–202. doi:10.1002/cne.902260204

Minatohara, K., Akiyoshi, M., Okuno, H., 2015. Role of Immediate-Early Genes in Synaptic Plasticity and Neuronal Ensembles Underlying the Memory Trace. Front. Mol. Neurosci. 8, 78. doi:10.3389/fnmol.2015.00078

Mower, G.D., Kaplan, I. V, 2002. Immediate early gene expression in the visual cortex of normal and dark reared cats: differences between fos and egr-1. Brain Res. Mol. Brain Res. 105, 157–60.

Mukamel, E.A., Nimmerjahn, A., Schnitzer, M.J., 2009. Automated Analysis of Cellular Signals from Large-

Scale Calcium Imaging Data. Neuron 63, 747–760. doi:http://dx.doi.org/10.1016/j.neuron.2009.08.009

Niell, C.M., Stryker, M.P., 2010. Modulation of visual responses by behavioral state in mouse visual cortex. Neuron 65, 472–9. doi:10.1016/j.neuron.2010.01.033

O'Keefe, J., Conway, D.H., 1978. Hippocampal place units in the freely moving rat: why they fire where they fire. Exp. brain Res. 31, 573–90.

O'Keefe, J., Dostrovsky, J., 1971. The hippocampus as a spatial map. Preliminary evidence from unit activity in the freely-moving rat. Brain Res. 34, 171–5.

Okuno, H., 2011. Regulation and function of immediate-early genes in the brain: Beyond neuronal activity markers. Neurosci. Res. 69, 175–186. doi:https://doi.org/10.1016/j.neures.2010.12.007

Okuno, H., Akashi, K., Ishii, Y., Yagishita-Kyo, N., Suzuki, K., Nonaka, M., Kawashima, T., Fujii, H., Takemoto-Kimura, S., Abe, M., Natsume, R., Chowdhury, S., Sakimura, K., Worley, P.F., Bito, H., 2012. Inverse synaptic tagging of inactive synapses via dynamic interaction of Arc/Arg3.1 with CaMKIIβ. Cell 149, 886–98. doi:10.1016/j.cell.2012.02.062

Paxinos, G., 2013. Paxinos and Franklin's the mouse brain in stereotaxic coordinates. Academic Press.

Pierre, V., Martin, D., 2003. Single-cell study of motor cortex projections to the barrel field in rats. J. Comp. Neurol. 464, 98–103. doi:10.1002/cne.10769

Plath, N., Ohana, O., Dammermann, B., Errington, M.L., Schmitz, D., Gross, C., Mao, X., Engelsberg, A., Mahlke, C., Welzl, H., Kobalz, U., Stawrakakis, A., Fernandez, E., Waltereit, R., Bick-Sander, A., Therstappen, E., Cooke, S.F., Blanquet, V., Wurst, W., Salmen, B., Bösl, M.R., Lipp, H.-P., Grant, S.G.N., Bliss, T.V.P.P., Wolfer, D.P., Kuhl, D., 2006. Arc/Arg3.1 Is Essential for the Consolidation of Synaptic Plasticity and Memories. Neuron 52, 437–444. doi:http://dx.doi.org/10.1016/j.neuron.2006.08.024

Poort, J., Khan, A.G., Pachitariu, M., Nemri, A., Orsolic, I., Krupic, J., Bauza, M., Sahani, M., Keller, G.B., Mrsic-Flogel, T.D., Hofer, S.B., 2015. Learning Enhances Sensory and Multiple Non-sensory Representations in Primary Visual Cortex. Neuron 86, 1478–1490. doi:http://dx.doi.org/10.1016/j.neuron.2015.05.037

Poulet, J.F.A., Hedwig, B., 2006. The Cellular Basis of a Corollary Discharge. Sci. 311, 518–522. doi:10.1126/science.1120847

Ramirez, S., Liu, X., Lin, P.-A., Suh, J., Pignatelli, M., Redondo, R.L., Ryan, T.J., Tonegawa, S., 2013. Creating a false memory in the hippocampus. Science 341, 387–91. doi:10.1126/science.1239073

Ranieri, F., Podda, M. V., Riccardi, E., Frisullo, G., Dileone, M., Profice, P., Pilato, F., Di Lazzaro, V., Grassi, C., 2012. Modulation of LTP at rat hippocampal CA3-CA1 synapses by direct current stimulation. J. Neurophysiol. 107, 1868 LP-1880. doi:10.1152/jn.00319.2011

Rao, R.P.N., Ballard, D.H., 1999. Predictive coding in the visual cortex: a functional interpretation of some extra-classical receptive-field effects. Nat. Neurosci. 2, 79–87. doi:10.1038/4580

Rial Verde, E.M., Lee-Osbourne, J., Worley, P.F., Malinow, R., Cline, H.T., 2006. Increased Expression of the Immediate-Early Gene Arc/Arg3.1 Reduces AMPA Receptor-Mediated Synaptic Transmission. Neuron 52, 461–474. doi:http://dx.doi.org/10.1016/j.neuron.2006.09.031

Rudy, J.W., Sutherland, R.J., 1989. The hippocampal formation is necessary for rats to learn and remember configural discriminations. Behav. Brain Res. 34, 97–109.

Sakurai, Y., 2002. Coding of auditory temporal and pitch information by hippocampal individual cells and cell assemblies in the rat. Neuroscience 115, 1153–63.

Sakurai, Y., 1994. Involvement of auditory cortical and hippocampal neurons in auditory working memory and reference memory in the rat. J. Neurosci. 14, 2606–23.

Saleem, A.B., Ayaz, A., Jeffery, K.J., Harris, K.D., Carandini, M., 2013. Integration of visual motion and locomotion in mouse visual cortex. Nat. Neurosci. 16, 1864–1869. doi:10.1038/nn.3567

Shen, J., Colonnese, M.T., 2016. Development of Activity in the Mouse Visual Cortex. J. Neurosci. 36, 12259 LP-12275.

Shepherd, J.D., Bear, M.F., 2011. New views of Arc, a master regulator of synaptic plasticity. Nat. Neurosci. 14, 279–84. doi:10.1038/nn.2708

Shepherd, J.D., Rumbaugh, G., Wu, J., Chowdhury, S., Plath, N., Kuhl, D., Huganir, R.L., Worley, P.F., 2006. Arc/Arg3.1 Mediates Homeostatic Synaptic Scaling of AMPA Receptors. Neuron 52, 475–484. doi:http://dx.doi.org/10.1016/j.neuron.2006.08.034

Sherrington, C.S., 1906. Observations on the scratch-reflex in the spinal dog. J. Physiol. 34, 1–50.

Shuler, M.G., Bear, M.F., 2006. Reward timing in the primary visual cortex. Science 311, 1606–9. doi:10.1126/science.1123513

Soya, H., Nakamura, T., Deocaris, C.C., Kimpara, A., Iimura, M., Fujikawa, T., Chang, H., McEwen, B.S., Nishijima, T., 2007. BDNF induction with mild exercise in the rat hippocampus. Biochem. Biophys. Res. Commun. 358, 961–967. doi:10.1016/j.bbrc.2007.04.173

Spiegel, I., Mardinly, A.R., Gabel, H.W., Bazinet, J.E., Couch, C.H., Tzeng, C.P., Harmin, D.A., Greenberg, M.E., 2014. Npas4 regulates excitatory-inhibitory balance within neural circuits through cell type-specific gene programs. Cell 157, 1216–1229. doi:10.1016/j.cell.2014.03.058

Stiles, C.D., Capone, G.T., Scher, C.D., Antoniades, H.N., Van Wyk, J.J., Pledger, W.J., 1979. Dual control of cell growth by somatomedins and platelet-derived growth factor. Proc. Natl. Acad. Sci. U. S. A. 76, 1279–83.

Tanaka, K.Z.Z., Pevzner, A., Hamidi, A.B.B., Nakazawa, Y., Graham, J., Wiltgen, B.J.J., 2014. Cortical Representations Are Reinstated by the Hippocampus during Memory Retrieval. Neuron 84, 347–354. doi:10.1016/j.neuron.2014.09.037

Teixeira, C.M., Pomedli, S.R., Maei, H.R., Kee, N., Frankland, P.W., 2006. Involvement of the anterior cingulate cortex in the expression of remote spatial memory. J. Neurosci. 26, 7555–64. doi:10.1523/JNEUROSCI.1068-06.2006

Tsien, R.Y., 1998. The Green Fluorescent Protein. Annu. Rev. Biochem. 67, 509–544. doi:10.1146/annurev.biochem.67.1.509

Tsui, C.C., Copeland, N.G., Gilbert, D.J., Jenkins, N.A., Barnes, C., Worley, P.F., 1996. Narp, a novel member of the pentraxin family, promotes neurite outgrowth and is dynamically regulated by neuronal activity. J. Neurosci. 16, 2463–78.

Tzingounis, A. V., Nicoll, R.A., 2006. Arc/Arg3.1: Linking Gene Expression to Synaptic Plasticity and Memory. Neuron 52, 403–407. doi:10.1016/J.NEURON.2006.10.016

Vann, S.D., Brown, M.W., Erichsen, J.T., Aggleton, J.P., 2000. Fos Imaging Reveals Differential Patterns of Hippocampal and Parahippocampal Subfield Activation in Rats in Response to Different Spatial Memory Tests. J. Neurosci. 20, 2711 LP-2718.

Vazdarjanova, A., Ramirez-Amaya, V., Insel, N., Plummer, T.K., Rosi, S., Chowdhury, S., Mikhael, D., Worley, P.F., Guzowski, J.F., Barnes, C.A., 2006. Spatial exploration induces ARC, a plasticity-related immediate-early gene, only in calcium/calmodulin-dependent protein kinase II-positive principal excitatory and inhibitory neurons of the rat forebrain. J. Comp. Neurol. 498, 317–329. doi:10.1002/cne.21003

Veyrac, A., Besnard, A., Caboche, J., Davis, S., Laroche, S., 2014. The Transcription Factor Zif268/Egr1, Brain Plasticity, and Memory. Prog. Mol. Biol. Transl. Sci. 122, 89–129. doi:http://dx.doi.org/10.1016/B978-0-12-420170-5.00004-0

Vitureira, N., Goda, Y., 2013. Cell biology in neuroscience: the interplay between Hebbian and homeostatic synaptic plasticity. J. Cell Biol. 203, 175–86. doi:10.1083/jcb.201306030

Vogt, B.A., Miller, M.W., 1983. Cortical connections between rat cingulate cortex and visual, motor, and postsubicular cortices. J. Comp. Neurol. 216, 192–210. doi:10.1002/cne.902160207

Von Helmholtz, H., 1867. Handbuch der physiologischen Optik. Voss.

von Holst, E., Mittelstaedt, H., 1950. Das Reafferenzprinzip. Naturwissenschaften 37, 464–476.

Wang, K.H., Majewska, A., Schummers, J., Farley, B., Hu, C., Sur, M., Tonegawa, S., 2006. In vivo two-photon imaging reveals a role of arc in enhancing orientation specificity in visual cortex. Cell 126, 389–402. doi:10.1016/j.cell.2006.06.038

Waung, M.W., Pfeiffer, B.E., Nosyreva, E.D., Ronesi, J.A., Huber, K.M., 2008. Rapid Translation of Arc/Arg3.1 Selectively Mediates mGluR-Dependent LTD through Persistent Increases in AMPAR Endocytosis Rate. Neuron 59, 84–97. doi:http://dx.doi.org/10.1016/j.neuron.2008.05.014

Weible, A.P., Rowland, D.C., Monaghan, C.K., Wolfgang, N.T., Kentros, C.G., 2012. Neural Correlates of Long-Term Object Memory in the Mouse Anterior Cingulate Cortex. J. Neurosci. 32, 5598–5608. doi:10.1523/JNEUROSCI.5265-11.2012

Weible, A.P., Rowland, D.C., Pang, R., Kentros, C., 2009. Neural correlates of novel object and novel location recognition behavior in the mouse anterior cingulate cortex. J. Neurophysiol. 102, 2055–68. doi:10.1152/jn.00214.2009

Weng, F.-J., Garcia, R.I., Lutzu, S., Alviña, K., Zhang, Y., Dushko, M., Ku, T., Zemoura, K., Rich, D., Garcia-Dominguez, D., Hung, M., Yelhekar, T.D., Sørensen, A.T., Xu, W., Chung, K., Castillo, P.E., Lin, Y., 2018. Npas4 Is a Critical Regulator of Learning-Induced Plasticity at Mossy Fiber-CA3 Synapses during Contextual Memory Formation. Neuron. doi:10.1016/j.neuron.2018.01.026

Woodruff, M.L., Isaacson, R.L., 1972. Discrimination learning in animals with lesions of hippocampus. Behav. Biol. 7, 489–501. doi:10.1016/S0091-6773(72)80211-6

Worley, P.F., Bhat, R. V, Baraban, J.M., Erickson, C.A., McNaughton, B.L., Barnes, C.A., 1993. Thresholds for synaptic activation of transcription factors in hippocampus: correlation with long-term

enhancement. J. Neurosci. 13, 4776 LP-4786.

Xie, H., Liu, Y., Zhu, Y., Ding, X., Yang, Y., Guan, J.-S., 2014. In vivo imaging of immediate early gene expression reveals layer-specific memory traces in the mammalian brain. Proc. Natl. Acad. Sci. 111, 2788–2793. doi:10.1073/pnas.1316808111

Xu, S., Jiang, W., Poo, M.M., Dan, Y., 2012. Activity recall in a visual cortical ensemble. Nat. Neurosci. 15, 449–55, S1-2. doi:10.1038/nn.3036

Yaksi, E., Friedrich, R.W., 2006. Reconstruction of firing rate changes across neuronal populations by temporally deconvolved Ca2+ imaging. Nat. Methods 3, 377–383. doi:10.1038/nmeth874

Yamada, Y., Hada, Y., Imamura, K., Mataga, N., Watanabe, Y., Yamamoto, M., 1999. Differential expression of immediate-early genes, c-fos and zif268, in the visual cortex of young rats: effects of a noradrenergic neurotoxin on their expression. Neuroscience 92, 473–484. doi:http://dx.doi.org/10.1016/S0306-4522(99)00003-2

Yassin, L., Benedetti, B.L., Jouhanneau, J.-S.S., Wen, J.A., Poulet, J.F.A., Barth, A.L., 2010. An Embedded Subnetwork of Highly Active Neurons in the Neocortex. Neuron 68, 1043–1050. doi:https://doi.org/10.1016/j.neuron.2010.11.029

Zangenehpour, S., Chaudhuri, A., 2002. Differential induction and decay curves of c-fos and zif268 revealed through dual activity maps. Mol. Brain Res. 109, 221–225. doi:http://dx.doi.org/10.1016/S0169-328X(02)00556-9

Zhang, S., Xu, M., Kamigaki, T., Hoang Do, J.P., Chang, W.C., Jenvay, S., Miyamichi, K., Luo, L., Dan, Y., 2014. Selective attention. Long-range and local circuits for top-down modulation of visual cortex processing. Science 345, 660–5. doi:10.1126/science.1254126

Ziv, Y., Burns, L.D., Cocker, E.D., Hamel, E.O., Ghosh, K.K., Kitch, L.J., El Gamal, A., Schnitzer, M.J., 2013. Long-term dynamics of CA1 hippocampal place codes. Nat. Neurosci. 16, 264–6. doi:10.1038/nn.3329

Zmarz, P., Keller, G.B., 2016. Mismatch Receptive Fields in Mouse Visual Cortex. Neuron 92, 766–772. doi:https://doi.org/10.1016/j.neuron.2016.09.057